UNIVERSITÀ DEGLI STUDI DI NAPOLI
FEDERICO II

Scuola Politecnica e
delle Scienze di Base

DI
C
Ma
PI

Dipartimento
di Ingegneria Chimica,
dei Materiali e della
Produzione Industriale
Università degli Studi
di Napoli Federico II

Università degli Studi di Napoli Federico II

Ph.D. Program in Industrial Products and Processes Engineering

XXXV Cycle

Thesis for the Degree of Doctor of Philosophy

Francesco Rusciano

Fickian non-Gaussian diffusion in glass-forming liquids

Scuola Politecnica e delle Scienze di Base

Dipartimento di Ingegneria Chimica, dei Materiali e della Produzione Industriale

Fickian non-Gaussian diffusion in glass-forming liquids

Ph.D. Thesis presented
for the fulfillment of the Degree of Doctor of Philosophy
in Industrial Products and Processes Engineering
by

Francesco Rusciano

December 2022

Approved as to style and content by

Advisor: Francesco Greco, Raffaele Pastore

Università degli Studi di Napoli Federico II
Ph.D. Program in Industrial Products and Processes Engineering
XXXV cycle - Chairman: Prof. Andrea D'Anna

Candidate's declaration

I hereby declare that this thesis submitted to obtain the academic degree of Philosophiæ Doctor (Ph.D.) in Industrial Products and Processes Engineering is my own unaided work, that I have not used other than the sources indicated, and that all direct and indirect sources are acknowledged as references.
Parts of this dissertation have been published in international journals and/or conference articles (see list of the author's publications at the end of the thesis).

Napoli, March 10, 2023

_____

Francesco Rusciano

Abstract

In 2009, ground-breaking experiments on nanometric beads in complex fluids revealed the existence of a novel type of diffusion (that is distinct from both standard and anomalous diffusion), characterized by a linear time-dependent mean square displacement and a non-Gaussian displacement distribution. In the past few years, many other examples of such a "Fickian yet non-Gaussian Diffusion", (FnGD) have been reported in literature. FnGD is generically associated to some dynamical and/or structural heterogeneity of the environment. This feature motivated us to investigate the possible occurrence of FnGD in glass-forming liquids, the epitome of dynamical heterogeneity, drawing on experiments on hard-sphere colloidal suspensions and simulations of a simple models of molecular liquid [1, 2].

We here demonstrate that FnGD "strengthens" on approaching the glass transition, by identifying distinct timescales for Fickianity, τ_F, and for restoring of Gaussianity, τ_G, as well as their associated length-scales, ξ_F and ξ_G. We find $\tau_G \propto \tau_F^{\gamma}$, with $\gamma > 1$, for all investigated systems.

In the deep FnGD regime, particle displacement distributions display exponential tails: we show that the time-dependent decay lengths $l(t)$ at different temperatures all collapse onto a power-law master-curve, $l(t)/\xi_G \propto (l(t)/\xi_G)^{\alpha}$ with $\alpha \simeq 0.33$. For the investigated glass-formers, this behaviour is independent from interaction potential and dimensionality [2]. We further discuss the connections of the time- and length-scales characterizing FnGD with structural relaxation and dynamic heterogeneity, through a complementary study of the dynamics in the reciprocal Fourier-space.

Finally, we illustrate the connections between FnGD scales and standard timescales usually considered in the late relaxation of glass-forming liquids, showing that these timescales are always related, and for whatever system, by the same power-law relations.

Overall, a number of universal scaling laws for very long-time single

particle dynamics (here reported for the first time) seem to emerge close to the glass transition, and characterize the Fickian non-Gaussian regime of glass-forming liquids.

In conclusion, this work of thesis is at the crossroads between two major issues in soft matter, namely glass transition and the recently discovered Fickian yet non-Gaussian Diffusion (FnGD), and unveils strong connections between them.

Keywords: Fickian non-Gaussian diffusion, Brownian non-Gaussian diffusion, supercooled liquids, glass-forming liquids, glass transition, Brownian motion, diffusion

Contents

List of Acronyms

The following acronyms are used throughout the thesis.

FnGD	Fickian non-Gaussian Diffusion
FnG	Fickian non-Gaussian
MSD	Mean-Square Displacement
ISSF	Intermediate Self Scattering Function
NGP	(first) Non-Gaussian Parameter
DD	Diffusing Diffusivity
SS	SuperStatistical model
KALJ	Kob-Andersen Lennard-Jones model
mKALJ	modified Kob-Andersen Lennard-Jones model
DH	Dynamical Heterogeneity

CTRW Continuous Time Random Walk

CLT Central Limit Theorem

List of Tables

AVGVSTVS FRIDERICVS ROMANORVM IMPERATOR SEMPER

List of Symbols

The following symbols are used within the thesis

α_2	Non-Gaussian Parameter
τ^*	Timescale of the maximum of NGP
τ_α	Structural relaxation time
τ_F	Fickian timescale
τ_G	Gaussian timescale
ξ_F	Fickian timescale
ξ_G	Gaussian timescale
$F_s(q,t)$	Intermediate Self Scattering Function
$g(r)$	Radial correlation function
q^*	Wave-vector of the maximum of S(q)
$S(q)$	Static structure factor

AVGVSTVS FRIDERICVS ROMANORVM IMPERATOR SEMPER

CHAPTER 1

Introduction

According to Einstein's work on Brownian motion [3], macroscopic diffusion at equilibrium corresponds to random walks of thermally agitated particles, with a *Gaussian* displacement distribution, *plus* a Mean Square Displacement (MSD), $\langle r^2(t)\rangle$, increasing linearly with time, the so-termed *Fickian* case: the diffusion constant is then obtained as $D = \langle r^2(t)\rangle/2dt$, d being the space dimensionality. In more recent years, a variety of experiments has also shown the existence of anomalous (non-Fickian) diffusion, quite often associated to correlated walks, and typically accompanied by non-Gaussian displacement distributions [4, 5]. Thus, from this double perspective, Fickian and Gaussian behaviours were thought to be biunivocally related.

In 2009, ground-breaking experiments [6] on nanometric beads in complex biological fluids broke up such scenario, revealing the existence of a novel type of diffusion that is distinct from both standard and anomalous diffusion, being simultaneously Fickian *and* non-Gaussian. In the past few years, many other examples of such a "Fickian yet non-Gaussian Diffusion", (FnGD) have been reported, mostly in soft matter and biological systems characterized by some kind of heterogeneity of the structure or in the dynamics [6, 7, 8, 9, 10, 11, 12, 13, 14]. The existence of an under-

lying heterogeneity has also been considered in various theoretical models [15, 16, 17, 18, 19] proposed to capture the main features of FnGD such as, for example, the presence of "fat tails" ("fatter than Gaussian", usually exponential) in the displacement distribution. While a full understanding of FnGD is still far from being achieved, the association between FnGD and some kind of heterogeneity generally meets a wide consensus [20, 21, 15].

Dealing with dynamical heterogeneity (DH), it comes natural to think next to glass-forming liquids. Single-particle dynamics in supercooled conditions is characterized by an intermittent motion, with a continuous alternation of localized vibrations inside the "cage" created by the surrounding particles, and sudden "jumps" to other cages [22, 23, 24]; on sufficiently large length- and time-scales, this leads to a grouping of "fast" and "slow" particles, the more so the more the glass transition is approached [25]. Thus, supercooled liquids are commonly considered the epitome of DHs. It is tempting to believe that they may also represent a paradigmatic example of FnGD.

Noticeably, exponentially-tailed displacement distributions have been reported for both experiments on colloidal systems and molecular dynamic simulations [24, 22, 26] focusing on times of the order of the structural relaxation time τ_α, related to the first jumps of the particles out of their cages, which typically falls either within the subdiffusive regime or around the subdiffusive-Fickian crossover. Deviations from Gaussianity, however, can persist even in the Fickian regime [27], corresponding to time- and length-scales where, on average, particles have performed many jumps.

Overall, several pieces of the puzzle now suggest that FnGD could be a typical feature of glass-forming liquids, but this point has not been directly addressed so far .

In this thesis we demonstrate that, on approaching glass transition, FnGD becomes more and more marked, and identify the scaling relations for its characteristic times and lengths. Further, we show the relevance of these characteristic scales in interpreting structural relaxation and dynamic heterogeneity in glass-formers. Our study draws on a combination of experiments on hard spheres colloidal glass-formers, and molecular dynamics simulations of supercooled liquid models (soft-disks and Kob-Andersen model) in equilibrium conditions. For the colloidal system, we analyzed data from previous experiments performed at Physics Department "Et-

tore Pancini" in University of Naples "Federico II"[28, 1]. Simulations and analysis of Kob-Andersen Lennard-Jones model were carried out in collaboration with Prof. Walter Kob from "Laboratoire Charles Coulomb", University of Montpellier.

The work is organised as follows. In **Chapter 2** we give a brief introduction to the dynamics of glass-forming liquids and introduce the issue of Fickian non-Gaussian dynamics in soft matter systems. Methods of our investigation are then described in **Chapter 3**. **Chapter 4** shows the results of our study concerning the characteristic features and the scaling laws characteristic of the FnGD regime in the investigated glass-formers. Finally, in **Chapter 5** we summarize our findings and make some connections with other features of microscopic dynamics near the glass-transition.

AVGVSTVS FRIDERICVS ROMANORVM IMPERATOR SEMPER

CHAPTER 2

Background on the dynamics of glass-forming liquids and on FnGD

2.1 Glass transition and the dynamics of glass-forming liquids

Glass transition is a most intriguing and long-standing open issue in the field of molecular liquids and soft matter. Its physical origin has drawn an enormous interest in the last decades, but it remains still far from being completely understood. Is it a purely dynamical crossover, or the manifestation of a true thermodynamic transition? Is there any (static or dynamical?) correlation length associated to the dramatic increase of viscosity and relaxation times? A complete, shared theory of the glass transition does not yet exist, and this topic remains largely debated.

Glassy state is reached when, under certain conditions (e.g. a fast decrease of temperature), the crystallization of the liquid is avoided, and the system acquires the mechanical rigidity typical of a solid. Colloidal and soft matter systems, and molecular liquids can reach an arrested state following different routes, such as the decrease of temperature, increase of solute volume-fraction, or imposition of a shear stresses. However, if the

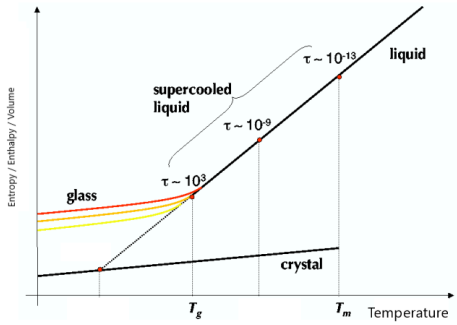

Figure 2.1. Specific entropy, enthalpy or volume as a function of temperature at the liquid-solid crossover. In the supercooled region, the relaxation time τ of the system dramatically increases as a function of temperature, with respect to the liquid phase. Adapted from Ref. [35].

degree of "supecooling" is not enough to reach the solid-like state, the liquid enters in a supercooled stable phase and is termed *supercooled liquid*(or, more generally, *glass-forming liquid*)

Glass-formers have a very rich phenomenology. From a macroscopic perspective, glass-forming systems display a dramatic slowing-down of the dynamics, with the inverse diffusion coefficient and relaxation times increasing by orders of magnitude upon even modest supercooling. At the microscopic level, single-molecule motion becomes strongly intermittent, and can indeed be conveniently described in terms of "cage-jump" events [24, 23, 29, 30, 31, 32, 33, 34]

2.1.1 Dramatic slowing down of the dynamics

Glasses are disordered materials that lack the periodical order of a crystal, though behaving mechanically like solids. When a molecular liquid is cooled sufficiently fast below its melting temperature T_m, molecules do not have enough time to rearrange in an ordered structure and crystallization is avoided [35, 36] (Fig. 2.1). Liquids in these conditions are termed *supercooled*, and show a dramatic slowing-down of the dynamics as compared to that of a standard liquid, despite poor changes in their structure [35, 37] (some structural changes can be still detected using multi-point correlation functions and percolative approaches [38, 39, 40]). An analogous

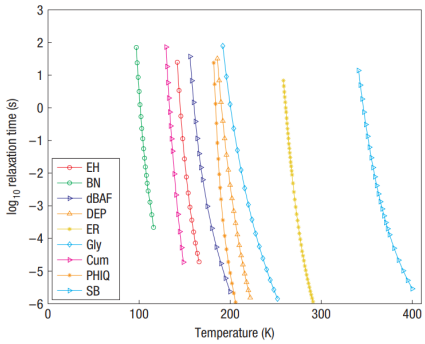

Figure 2.2. Relaxation times (determined as the inverse dielectric loss-peak frequency) as a function of temperature for typical organic liquids in the ultraviscous phase, as indicated in the legend. Image from Ref [41].

phenomenology (i.e. the colloidal glass transition) is approached by soft and hard dense colloids by increasing the volume fraction up to a critical packing fraction. As a matter of fact, two-particles static indicators, as the radial corralation function $g(r)$ or the Static Structure Factor $S(q)$, defined as (for isotropic systems)

$$S(q) = 1 + \rho \int (g(r) - 1) sin(\mathbf{q} \cdot \mathbf{r}) r^2 \, d\mathbf{r} \tag{2.1}$$

ρ being the number density and $\mathbf{q}$ the probing wavevector, do not show any marked change upon variations of the thermodynamic control parameter in the proximity of glass transition.

Conversely, macroscopic dynamical properties, such as shear viscosity and self-diffusivity, change by several orders of magnitude [41] upon supercooling (Fig. 2.2). As a matter of fact, below some conventional glass transition temperature $T_g < T_m$, the system eventually reaches a non-equilibrium disordered solid-like state, called *glass*, in which dynamics is arrested over the accessible timescales [36, 29].

2.1.2 Two-steps relaxation and the caging regime

On a microscopic level, dynamics close to glass transition shows an intermittent single-particle motion, with an alternation of localized vibrations inside the "cage" created by the surrounding particles, and sudden "jumps" to other cages[33, 30, 31, 42, 32, 23, 24]. While at high temperatures particles continuously overcome local energy barriers and smoothly change their neighbours, cage-jump dynamics becomes progressively more marked on lowering temperature, and is in fact clearly detectable in the supercooled state.

A common and simple indicator to monitor microscopic dynamics is the Mean-Square Displacement (MSD):

$$\langle r^2(t)\rangle = \frac{1}{N}\sum_i (\mathbf{r}_i(t) - \mathbf{r}_i(0))^2 \tag{2.2}$$

where $\mathbf{r}_i(t)$ is the position of the i-th particle and the sum runs over all the N particles in the system. In a standard molecular liquid, we expect the MSD to show a short-time regime in which $\langle r^2(t)\rangle \propto t^2$ (*ballistic regime*); in this regime, particles move almost freely. After many collisions with the surrounding environment, linearity of the MSD is reached $\langle r^2(t)\rangle \propto t$ (*Fickian regime*) in every fluid. This latter regime is often generically called "diffusive", and the self-diffusion coefficient (or self-diffusivity[1]) is measured through a long-time fit of the MSD, using Einstein's relation:

$$\langle r^2(t)\rangle = 2dDt \tag{2.3}$$

d being the space dimensionality. For our purposes, this relation defines *Fickian diffusion*.

However, in supercooled liquids (Fig. 2.3) these two regimes are separated by an intermediate subdiffusion in which the particle remains confined in a small region of space, termed *cage*[2]. Accordingly, this subdiffusive regime is commonly called **caging**. When the degree of supercooling is high

[1] Commonly, in literature on liquid dynamics, self diffusion is indicated as D_s. Since in this work we only deal with self-diffusion, in the text we will always use D.

[2] We notice that in a colloidal glass-former the ballistic regime is generally not observed, and a short-time linear regime, due to free Brownian diffusion, is present also before the intermediate caging.

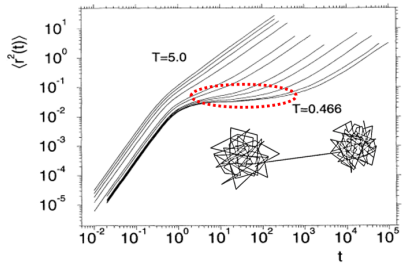

Figure 2.3. MSD as a function of time for the Kob-Andersen Lennard-Jones model of supercooled liquid, at different temperatures from hot conditions to supercooled state. A sketch of a typical trajectory of a particle in a glass-former: the exit from a caging period is linked to the occurrence of a long jump towards the successive cage. This corresponds to the exit from the MSD plateau (red dashed circle). Image adapted from Ref. [37].

enough, the caging regime corresponds to the full emergence of a plateau in the MSD. The length $\sqrt{\langle r^2(t_{DW})\rangle}$ (where t_{DW} is the time of the minimum derivative of the MSD) ideally defines to height of the plateau, and is sometimes referred to as *Debye-Waller factor*, in analogy with crystalline solids.

The behaviour of the MSD in glass-forming liquids is mirrored in the reciprocal Fourier-space by the characteristic shape of the density-density time correlation function, or Intermediate Self Scattering Function (ISSF) $F_s(\mathbf{q}, t)$, that is defined as follows:

$$F_s(\mathbf{q}, t) = \frac{1}{N} \sum_i e^{-i\mathbf{q}\cdot[\mathbf{r}_i(t) - \mathbf{r}_i(0)]} \tag{2.4}$$

In fact, the ISSF corresponds to the Fourier transform of the displacement distribution function, also termed self van Hove function $p(r, t)$[3]. For isotropic systems, like the ones that will be investigated in this work, F_s does not depend on the wave-vector direction, but only on its modulus $|\mathbf{q}| = 2\pi/\lambda$, where λ is the wave-length. Accordingly, the ISSF can be also expressed as a function of the wave-length, $F_s(\lambda, t)$. For a liquid in

[3]The self van Hove function is commonly indicated as $G_s(r, t)$ in literature on liquid dynamics. However, in this text we refer to the displacement function as $p(r, t)$ to avoid any confusion with Gaussian displacement functions, here denoted with G.

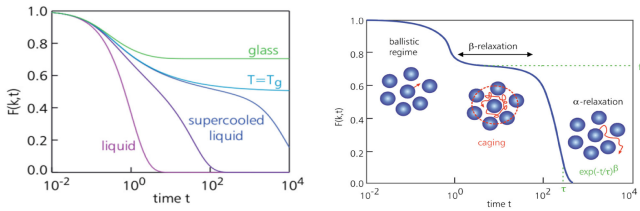

(a) **(b)**

Figure 2.4. (a) ISSFs for a system at different temperatures, from "hot" conditions to glassy state. (b) Double-steps decay of the ISSF for a glass-forming liquid. Both figures are adapted from Ref. [43]

standard conditions (sometimes pictorially termed "hot" liquid), the relaxation probed on the wavelength of a particle diameter (i.e. the *structural relaxation*)[4] is very fast, characterized by an exponential decay with a characteristic time τ_α of the order of some picoseconds (or some nanoseconds for colloidal suspensions in diluted conditions).

As glass transition is approached, the dynamics dramatically slows down: the relaxation times increase by many orders of magnitude (while diffusivity decreases similarly), and the ISSF is found to be more compatible with a stretched exponential behaviour, $\propto e^{-(t/\tau(\lambda))^\beta}$. In the deeply supercooled regime, the ISSF shows a two-steps relaxation when plotted in a semi-logarithimic chart (Fig. 2.4), with an intermediate times plateau-like regime, approximately on the timescales of the caging regime of the MSD. The first relaxation corresponds to the short-time ballistic regime and is termed β-relaxation; the late decay of the ISSF, named **α-relaxation**, shows a stretched behaviour. The height f of the ISSF plateau is often referred to as *non-ergodicity parameter*[5].

[4] Commonly, we refer to as structural relaxation when the dynamics is probed at the wavevector $q*$ corresponding to the first maximum of the static structure factor.

[5] Sometimes, the expression *Debye-Waller factor* (here in this thesis devoted to the height of the plateau of the MSD) is also common in literature.

2.1.3 Dynamical Heterogeneity

The marked increase of the relaxation time τ_α (or viscosity η[6]) is accompanied by a similar decrease of self-diffusivity D. For molecular liquids well above the melting point, in fact, the product $D\eta/T \propto D\tau_\alpha$ stays (approximately) constant on varying the temperature, which is commonly considered an extension of the celebrated Stokes-Einstein relation (SER) for the diffusion of large colloidal tracers suspended in a fluid[7]. The strong violation of such an extended SER, termed **Stokes-Einstein Breakdown** (SEB), is in fact one of the most intriguing phenomena occurring in supercooled states: typically, $D\eta/T$ is found to increase on approaching the transition [47, 48, 36, 35, 49, 50].

SEB has been interpreted in terms of the emergence of dynamical heterogeneities (DHs), i.e., roughly speaking, the coexistence of *two* dynamic populations of 'fast' and 'slow' particles [51, 52, 25, 53]. DHs emerge as dynamical clusters of particles with similar mobility whose spatial extension and duration increase on approaching glass transition, in a similar fashion to density fluctuations close to an ordinary critical point[54]. If the distinction between those populations is sufficiently sharp, a characteristic time and a diffusivity can be associated to each population (with the time being proportional to the inverse diffusivity) [55, 35]. In this simple picture, it is readily shown that the overall diffusivity D is controlled by the fast particles time, whereas slow particles time determines the overall structural relaxation time τ_α [55, 35]. SEB will then be a direct consequence of the onset of *two* characteristic times.

The presence of two populations of particles is reflected in the shape of the displacement distribution function (Fig. 2.5.a), which is clearly non-Gaussian at intermediate times, exhibiting exponential behaviour in the tails (commonly associated to fast particles) and a central Gaussian core (linked to slow, or caged particles). The (first) Non-Gaussian parameter

[6] Many observations show that $\eta/T \propto \tau_\alpha$ [44, 45, 46], with $\tau_\alpha = \tau(q^*)$ the structural relaxation time of the ISSF.

[7] Actually, the occurrence of a molecular version of SER is a non trivial fact: indeed, the original SER draws on a clear separation of length and time scales between the colloidal tracer and the molecules of the fluid, which is of course absent if the tracer itself is a tagged molecule diffusing among similar molecules.

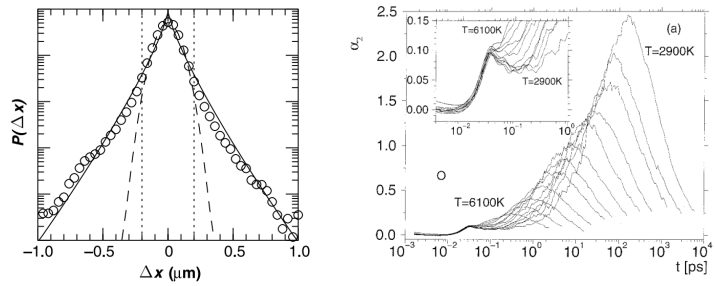

(a) **(b)**

Figure 2.5. (a) Displacement distribution function at a fixed time in the subdiffusive regime for a dense colloidal suspension at $\phi = 0.56$. Dashed line is a Gaussian fit to the core, while straight line is an exponential (also termed Laplace) distribution. Image taken from Ref. [24]. (b) NGP as a function of time for a numerical model of ultra-viscous silica melt, at different temperatures in the supercooled state. Image taken from Ref. [57].

(NGP):

$$\alpha_2(t) \equiv \frac{d}{d+2} \frac{\langle \boldsymbol{r}^4 \rangle}{\langle \boldsymbol{r}^2 \rangle^2} - 1 \tag{2.5}$$

is a simple and popular way to quantify non-Gaussian deviations of the displacement distribution and to monitor their temporal evolution. In systems approaching the glass transition, the NGP is exploited as a proxy for quantifying DHs [24], as its behaviour (Fig. 2.5.b) indeed closely resembles more direct (and less easily obtained) indicators of DHs, such as the dynamic susceptibility [56]. The NGP of a glass-former shows a non monotonic time-evolution, with a maximum at intermediate times, corresponding to the subdiffusive regime, and a subsequent decrease to zero at longer times. As glass transition is approached, the NGP reaches higher peaks, indicating stronger deviations from gaussianity of the van Hove function.

Summing up, in the proximity of the glass transition, the dynamics dramatically slows down upon tiny modifications of the thermodynamic control parameter (temperature, volume fraction, shear stress), without any easily detectable variation of the microscopic structure. Thus, the dynamics of glass-forming liquids is characterized by

- the intermittency of single-particle trajectories, resulting in a cage-jump motion.
- an increase of structural relaxation times (and viscosity), or decrease in diffusivity, by orders of magnitude;
- the emergence of a two-steps dynamics through an intermediate caging regime, that can be visualized, for example, in the ISSF and in the MSD;
- the presence of dynamical heterogeneities, signalled by non-Gaussianity of the displacement function and by the presence of correlations among particles' mobilities.

2.2 Fickian non-Gaussian Diffusion in soft-matter systems

In section 2.2.1 we introduce the issue of Fickian non-Gaussian dynamics and then review some of the occurrences found in literature of this novel phenomenology in different types of soft meterials (Sec. 2.2.2). Finally, we present in Sec. 2.2.3 some models available in literature to describe the fundamental features of FnGD.

2.2.1 The strike of a new paradigm in Brownian motion: FnGD, a *hybrid* diffusion

Fickian diffusion, in which the Mean Square Displacement (MSD) grows linearly with time, represents the most common form of diffusive transport both at the molecular and supramolecular level. In the case of colloidal particles, this kind of diffusion was first predicted by Einstein in its celebrated description of Brownian motion [58] assuming that the particle's motion is caused by a stochastic succession of collisions with the solvent molecules that are characterized by a timescale which is much smaller than the one of the colloidal particle. In a wider context than the colloidal one, Fickian diffusion can be interpreted with a simple random walk model [59, 60, 61] in which the particle performs a sequence of uncorrelated steps. In this type of models the linear growth of the MSD is accompanied by a Gaussian

displacement distribution function. These two properties, linearity of the MSD (i.e. Fickianity) and Gaussianity of the displacement distribution, together characterize what we define **standard diffusion** (FGD) in what follows.

On the other hand, for example in the presence of correlations among steps, the existence of **anomalous diffusion** (nFnGD) processes, with a non linear MSD paired with a non-Gaussian displacement distribution, is well kwnon and studied both on experimental and theoretical grounds.

Based on this scenario and on experimental observations, the linearity of the MSD and the Gaussianity of the displacement distribution function have been believed to be intrisincally related and concomitant until very recent years: the expressions *Fickian diffusion* and *Gaussian diffusion* started to be implicitly considered as synonyms almost everywhere in scientific literature.

However, in the last ten years, an ever increasing number of experimental evidences, above all in Soft Matter systems, demonstrated the existence of *Fickian non-Gaussian diffusion* (FnGD) with the consequent breakdown of the well established dychotomy of Standard-Anomalous diffusion (Fig. 2.6).

The intense although recent research on FnGD (Fig. 2.7), which we also term "**hybrid diffusion**" in what follows, allowed to observe this phenomenon in a great variety of systems including colloidal suspensions [62, 63, 64, 1, 7] supercooled liquids [1, 65, 66], active systems [67, 68, 9], biochemical and cellular environments [6, 69, 70, 11], polymer matrices [71, 72, 73], confined media [74, 75, 12] and diffusion on liquid-solid interfaces [76, 77, 78], and even on very long timescales. It is also worth to be mentioned that this dynamical behaviour was even recognized as a model to map economic and social dynamics such as the fluctuations in stock-exchange [79]. In particular, it is due to the great recent advances of computer simulations, imaging techniques and single particle tracking that it is now possible to measure, with a high level of accuracy, the entire displacement distribution function (also with a focus on the tails corresponding to rare-events), instead of simply measure macroscopic quantities (averages) as the diffusion constant which, of course, bring only cumulative information. These practical considerations help to understand why why such a peculiar dynamics has remained unveiled until recent times.

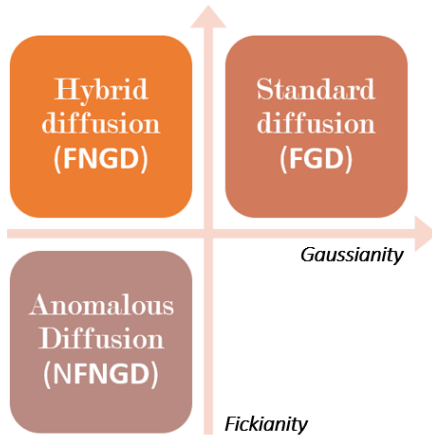

Figure 2.6. *The diffusion paradigm.* Schematic representation of diffusion processes on a Fickian-Gaussian 2d-plane. In the bottom right corner we expect non-Fickian Gaussian diffusion to be placed. This condition is found, for example, in the short time β-relaxation of glassy liquids where a Gaussian ballistic regime is present before the subdiffusive caging regime.

Hybrid diffusion represents today and intriguing puzzle that is still unsolved: from one side the non-Gaussianity of the displacements suggests the presence of spatio-temporal correlations, either related to heterogeneous interactions between the particles and the environment in which they diffuse, or among particles themselves, just like in anomalous diffusion. On the other hand these correlations must be small enough and/or balanced somehow in order to preserve the linearity of the MSD, as it happens in standard diffusion.

2.2.2 Experimental and numerical evidences

In this section we briefly review the main occurrences, present in scientific literature, of Fickian non-Gaussian behaviour both in experiments on real systems and in numerical simulations. We limit our analysis to the soft matter context that represents the largest field in which evidences of this phenomenology have been collected, both in numerical and experimental studies (Figs. 2.7, 2.8, 2.9). Obviously, the here presented list is not meant to be fully exhaustive, also due to the continuous discovery of

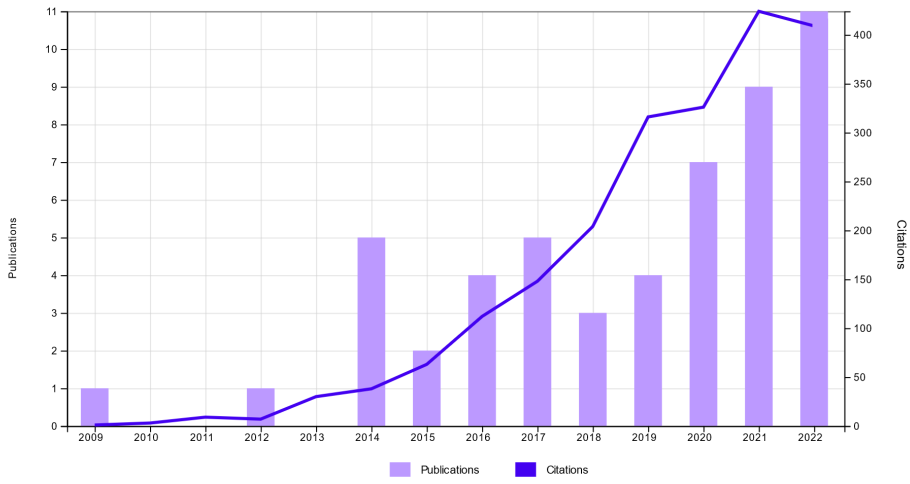

Figure 2.7. Number of scientific papers published every year on Fickian non-Gaussian Diffusion (with a reference in their title or abstract) and yearly citations to these publications. Raw data are provided by Web of Science - Clarivate^{TM} and updated to January 2023. There are no data before 2009, when Hapca and Granick published their seminal works.

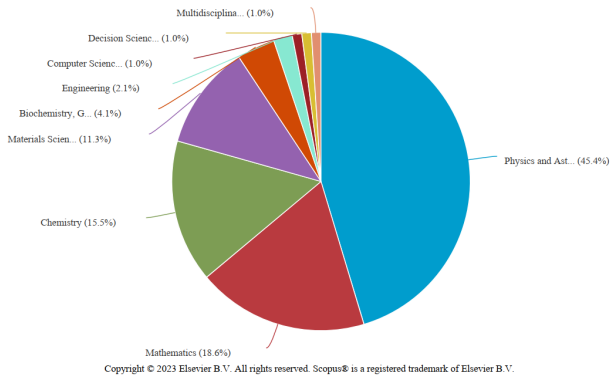

Figure 2.8. Main subject areas of the publications with an explicit reference to FnGD in title or abstract. Raw data are provided by Scopus ® 2023 Elsevier B.V.

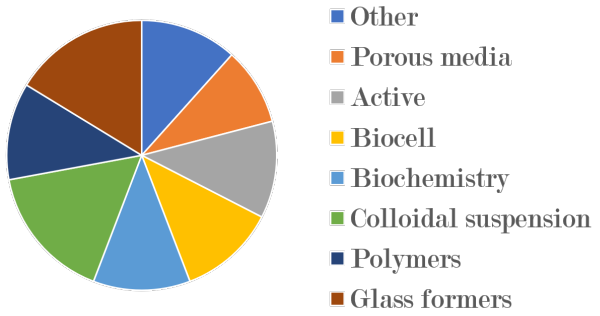

Figure 2.9. Types of systems in which we have found clear evidences of Fickian non-Gaussian dynamics.

this phenomenon in new systems.

We start our review with a description of the first two works (both appeared in 2009) in which, to the best of our knowledge, the existence of a Fickian non-Gaussian diffusion was explicitly recognized: *Anomalous diffusion of heterogeneous populations characterized by normal diffusion at the individual level* by Hapca et al. [67], and *Anomalous, but Brownian* [6] (Wang et al.) by the Granick's group.

Hapca et al. 2009

The diffusive dynamics of active particles is intrinsically heterogenous as a consequence of the individual variavility of the microorganisms in a population. Moreover, even the cell itself at different times, corresponding to different stages of its life, shows great alterations of its mobility due to the changes of life habits. Hapca et al. [67] first reported that populations of the parasitic nematode *Phasmarhabditis hermaphrodita*, a microorganism with characteristic size of 1 mm, show a great heterogeneity of mobilities and display FnGD. To the best of our knowledge, along with Granick's *Anomalous, but Brownian* (2009), this article was the first work in which Fickian non-Gaussian dynamics was explicitly recognized. The authors show that a correlated random walk model can be used to correctly predict the single particle diffusivity, while the superstatistical

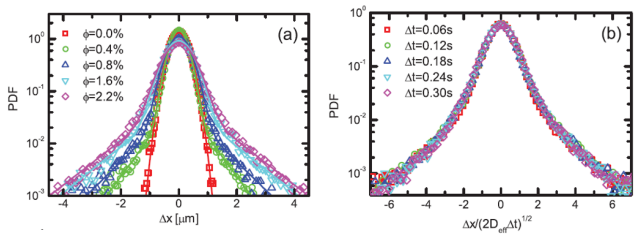

Figure 2.10. (a) Displacement distributions of passive tracers for systems in [9] at various concentrations of microswimmers, observed at the same time. Exponential deviations from the Gaussian curve, which is present only in absence of swimmers (red line), become stronger as concentration increases. (b) Van Hove function at a fixed concentration of swimmers $\Phi = 2.2\%$, as a function of the displacement divided by the root-MSD, shows a self-similar behaviour as time goes on.

model (See. 2.2.3), lately also applied by Granick's group, is presented for the first time in order to capture the fundamental features of the dynamics of the whole population.

Further evidences of FnGD in active matter In [9] hybrid diffusion in an active environment is instead studied from the point of view of a passive 1-micron sized tracer. It was found that tracers in a suspension of about 10 μm sized eukaryotic swimmers (the biflagellated algae *Chlamydomonas reinhardtii*) behave diffusively, with a time-dependent but self-similar displacement distribution function consisting of a Gaussian core with robust exponential tails (Fig. 2.10). The role of flagellar beating in creating oscillatory flows is central and the complex interplay between Brownian motion and advection seems to be the origin of FnGD in this context. Different models for this kind of advection-diffusion processes have been proposed (see 2.2.3). Examination of 3d trajectories of the tracers close to the algae shows the presence of complex loops, consistently with recent findings on hydrodynamics at zero Reynolds number [80].

A later work by Kurtuldu et al. [68] on dynamics in two dimensions of tracers in *Chlamydomonas* suspensions confined to thin films revealed even stronger deviations from Gaussianity, compared to that in three dimensions. In this case, the displacement distribution function shows power-law

tails ($\sim \Delta x^4$), instead of the typical exponential ones, which progressively turn to a Gaussian as time goes on.

Also simulations of self-propelled Brownian particles in 2d geometry performed at different concentrations [81] show the presence of FnGD. In this system, as in molecular liquids, it was found that particle diffusion is superdiffusive at short-time and Fickian at longer times, with an effective diffusion coefficient decreasing as concentration grows. Exponential tails are clearly visible in the self van Hove function at any time, and Gaussianity is never restored within the simulated time window.

Anomalous, but Brownian, Wang et al., 2009

The cell environment and, in general, all biochemical systems are characterized by a high level of complexity of the microstructure. In this kind of systems many examples of FnG dynamics were reported. The non-Gaussianity in these environments directly stems from the complexity of the system. In many cases the heterogeneity of the dynamics is suggested to arise from the coupling between the relaxation of the environment and diffusion of the tracer. As a matter of fact, it is not really surprising that FnGD was explicitly recognized for the first time in this kind of highly complex system [6]. Precisely, Granick's group performed single particle tracking experiments in two biochemical systems:

a) colloidal beads diffusing along linear phospholipid bilayer tubes whose radius is as that of the beads;

b) colloidal beads diffusing in entangled F-actin networks with a characteristic mesh size which is 3 to 6 times the diameter of the bead.

In both cases the MSD is found to be a linear function of time and the displacement distribution is exponential-shaped (Laplace distribution) ore clearly shows exponential tails In (a) it is shown that at long times the distribution becomes Gaussian, while for the second system Gaussianity is never restored. However, it is somehow expected since, as underlined by the authors, the experiments in (b) were carried on within a time window which is much smaller than the structural relaxation time of the system, obtained separately via rheological measurements. In a following commentary by the same authors [20], a Superstatistical Model (See. 2.2.3) was

Ref.	Year	Type of analysis	Type of system	System details
[6, 20]	2009	Exp.	Biochemistry	1D/2d - Beads in entangled network and beads on a surface
[82]	2015	Exp.	Biochemistry	2d - Diffusion on a membrane
[69]	2016	Exp.	Biochemistry	2d - Chemical diffusive transport in a cell
[11]	2019	Exp.	Cell biology	2d - Cell migration
[70]	2022	Exp.	Cell biology	2d - Migration of nanodomains in lipid monolayers
[67]	2009	Exp.	Active matter	2d - Migration of $1mm$-sized microorganisms
[9]	2009	Exp.	Active matter	3d - Passive tracers diffusion enanched by microswimmers
[68]	2011	Exp.	Active matter	2d - Passive tracers diffusion enanched by microswimmers
[7]	2014	Exp.	Colloidal suspension	3d - Hard sphere concentrated suspension at $\phi = [0 - 0.55]$
[83]	2016	Exp.	Colloidal suspension	2d - Hard sphere concentrated suspension at $\phi = [0.08 - 0.66]$
[1]	2022	Exp.	Colloidal suspension	2d - Hard sphere concentrated suspension at $\phi = [0.63 - 0.77]$
[84]	2018	Exp.	Supercooled liquid	3d - Neutron scattering on a molecular and an ionic liquid.
[62, 85]	2020	Exp.	Colloidal suspension	2d - Hard sphere suspension at $\phi = [0]$
[63]	2017	Exp.	Colloidal suspension	2d - Diffusion of a sigle particle in a liquid near a wall.
[64]	2022	Exp.	Colloidal suspension	2d - Diffusion of diluted particles in a glassy matrix.
[76]	2010	Exp.	Colloidal suspension	2d - Diffusion on a surface
[12]	2013	Exp.	Confined media	2d - Nanoparticles in microfabricated arrays
[86]	2015	Exp.	Confined media	2d - Nanoparticles in microfabricated arrays
[74]	2019	Exp.	Confined media	2d - Nanoparticles in microfabricated arrays
[75]	2020	Exp.	Confined media	2d - Anisotropic nanoparticles in microfabricated arrays
[71]	2016	Exp.	Polymer system	2d - Nanoparticles in entangled network
[72]	2016	Exp.	Polymer system	2d - Nanoparticles in entangled network
[73]	2013	Exp.	Polymer system	2d - Nanoparticles in entangled network
[77]	2013	Exp.	Liquid-solid interface	2d - Mocromolecule adsorption from a liquid bulk
[78]	2013	Exp.	Liquid-solid interface	2d - Mocromolecule adsorption from a liquid bulk
[87]	2017	Sim.	Colloidal suspension	3d - WCA, 3d-LJ
[8]	2013	Sim.	Colloidal suspension	2d - Hard sphere suspension at $\phi = [0.664 - 0.754]$
[88]	2014	Sim.	Colloidal suspension	2d - Dumbells in percolating media
[89]	2018	Sim.	Liquid crystal	3d - 12,6 Kihara-LJ for rods
[90]	2014	Sim.	Colloidal suspension	3d - HI+LJ
[66]	2018	Sim.	Supercooled liquid	3d - KALJ, 3d-IPL, 3d-R10
[10]	2019	Sim.	Colloidal suspension	2d - Yukawa potential
[91]	2016	Sim.	Colloidal suspension	3d - Non-equilibrium dynamics of charged binary colloid
[1]	2022	Sim.	Supercooled liquid	2d - 50:50 binary mixture harmonic disks
[65]	2019	Sim.	Supercooled liquid	2d - LJ, 3d-LJ, 3d-patchy
[92]	2019	Sim.	Liquid crystal	3d - KALJ, 3d-R10
[93]	2018	Sim.	Polymer system	3d - Bead-spring polymer + chemical heterogeneous NP
[94]	2017	Sim.	Biochemical system	2d - Protein diffusion on binding-membrane
[81]	2019	Sim.	Active matter	2d - Active chiral particles
[95]	2016	Sim.	Lattice model	1D - Energy diffusion
[96, 97]	2021	Sim.	Numerical simulation	1D - Diffusion in presence of non-Gaussian noise
[98]	2021	Exp + Sim.	Colloidal suspension	1D - Diffusion in presence of non-Gaussian optical trap $\phi = [0]$
[99]	2020	Sim.	Numerical simulation	1D - Diffusion with evaporation model

Table 2.1. Main evidences of Fickian non-Gaussian dynamics in literature.

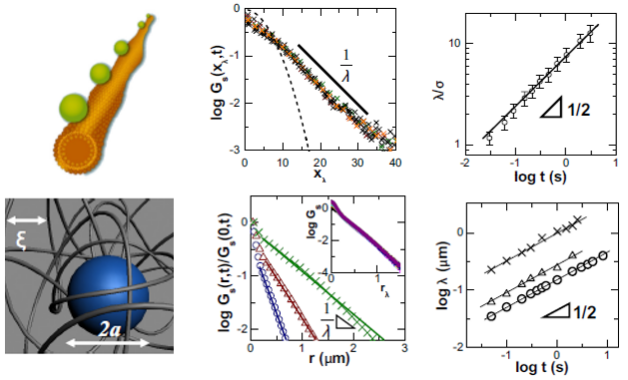

Figure 2.11. Top panels refer to system (a) and bottom to system (b) in [6]. (Left) sketches of the investigated systems. (Centre) Exponential tails of the van Hove functions as a function of the displacement, which have been divided by the root-MSD in top panel and in the inset of bottom panel. (Right) Characteristic length of the exponential tails as a function of time. The different data sets in right-bottom panel correspond to various combination of the mesh-size ξ and bead diameter a: $a = 50, \xi = 300$; $a = 100, \xi = 450$; $a = 100, \xi = 300$ (top-down). Diffusive scaling of the tails $\sim \sqrt{t}$ is always present.

tested by using an iterative algorithm [100] in order to measure the distribution of diffusion constants among the experimental sample and it is found to be bimodal shaped.

Further evidences of FnGD in biochemical systems A similar approach has been followed by [82] in single-particle tracking experiments on a quantum dot labeled molecule of the biochemical receptor (DC-SIGN) with unique pathogen-recognition capabilities for pathogens such as HIV-1, Ebola virus, hepatitis C and tubercolosis viruses inside dorsal membranes of Chinese hamster ovary living cell. The dynamics of the receptor is subdiffusive in the short times and shows a weak ergodicity breaking and aging[8], indicating that the system is out of equilibrium. It is also shown

[8]The non-equivalence between time-averaged and ensemble-averaged dynamical indicators is indicated as a *weak ergodicity breaking*. The dependence of statistical quantities on the observation time is termed *aging*.

that the dramatic instantaneous changes in the magnitude of single particle displacements can be interpreted in terms of stochastic fluctuations of diffusivity, in agreement with *diffusing diffusivity (DD) model* (See 2.2.3). Simulations of the DD model, using as an input a so computed distribution of diffusivities, reproduce many features of the dynamics.

Also the lateral motion[9] of acetylcholine [69], another biochemical receptor present on muscle cell membranes, shows FnGD with Laplace displacement distribution. The authors of this study further speculate that the observed non-Gaussian statistics is inherently linked to the slow-active remodelling process of the underlying cortical actin network.

Hybdrid dynamics has also been found in two-dimensional diffusion of lung cancer cells [11] and, more recently, experiments on the diffusion of nanodomains in lipid monolayers [70] have pointed out that the FnGD diffusion in these membranes is peculiarly accompanied by the presence of a double-peak in the of the displacement distribution function, with a minimum at the centre.

Although many examples of hybrid diffusion come from experiments on biochemical systems, these complex environments are not equally easy to be investigated through simulations, as they require high computer performaces. All-atoms dynamic simulation of DAPP1 PH gene domains bound on a lipid cell membrane surface [94] unveiled remarkable heterogeneous dynamics. The magnitude of the fluctionations of mobility of the particles is quantified using the relative standard deviation of the time averaged mean square displacement (RSD) which is a power-law function of time with an exponent $b = -0.5$. This result is consistent with some predictions obtained in the framework of Diffusing Diffusivity model (See. 2.2.3).

Towards simpler systems: FnGD of colloidal particles

In more recent years, Granick's group [7] focused on the motion of small tracers in a colloidal suspension of eight times larger hard spheres submerged in a simple liquid solvent. This work represents a turning point in FnGD field, as it clearly demonstrated that even a system of simple

[9] Hop-like movement of lipids within each leaflet of the lipid bilayer, due to membrane "fluidity".

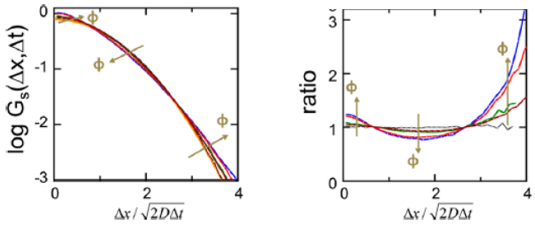

Figure 2.12. Left panel: normalized van Hove function for various concentration of hard spheres ϕ in [7] at a fixed time lag. The distributions cross the Gaussian fit (orange curve) twice seemingly at the same distances from the origin for every system. This interesting feature is much clearer on the right panel, where the ratio between expected Gaussian and actual distribution is plotted against the normalized displacement. The ratio strongly increases in the tails where non-Gaussian deviations are at their most. The same phenomenology was reported in different systems [62, 1].

particles (in a simple liquid), can display hybrid dynamics. In this case the heterogeneity of the dynamics must have an entropic origin since all interactions are negligible. In this work, a wide range of volume fractions is investigated, from dilute conditions to the proximity of cristallization (55% nominal) and, even at relatively low concentration (15%), deviations from gaussianity can be noticed in the Fickian regime (Fig. 2.12). Gaussianity is never restored on the experimental time window, but the non-Gaussian parameter approaches a decreasing trend at long times. The tails here are not exponential as in other systems; anyway, displacement distributions are self similar and they all collapse into a mastercurve when plotted against the displacement rescaled on the square root of the MSD.

Molecular dynamics simulations are suited to study the impact of different interaction potentials on the microscopic dynamics and over a wide range of timescales.

Above all, Lennard Jones (LJ) potential is the most popular among simple yet realistic models. Lots of variants of this potential have been proposed and have been extensively used both in materials modelling and fundamental studies. For example, studies of small WCA/LJ solute particles in a solvent medium, where the solute particle is much smaller in size than the solvent, are used to mimic the diffusion of small particles in crowded

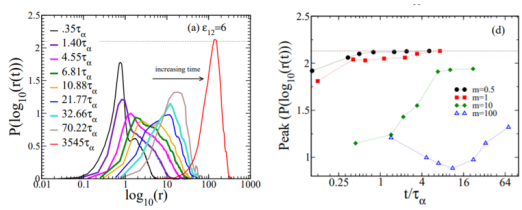

Figure 2.13. (Left panel) Rescaled $2\pi r G_s(r,t)$ at several times for one system in [87]. A Gaussian distribution of $G_(r,t)$ of the above distributions should result in a unimodal function with height indicated by the horizontal line. (Right panel) Peak of the rescaled self van Hove distribution as a function of time rescaled on the structural relaxation time for systems with different mass of the solute particles $m = 0.5 - 100$. Horizontal line represents the expected value for normalized Gaussian function. It is clear from this picture that the restore of Gaussian diffusion largely exceed the structural relaxation time of the system as particle mass increases and structural relaxation and Gaussian diffusion are decoupled phoenomena.

environments [87]. In this case, the solute was proved to exhibit Fickian diffusion arising from non-Gaussian van Hove function (Fig. 2.13)for several values of the potential energy scale, solvent particle mass and solvent-solute diffusivities ratio. Dynamics eventually becomes Gaussian for every system at longer times; however, in some cases FnGD is still present even at times much larger than the structural relaxation timescale of the system. Results also show an interesting feature: as the mass of the solute particle increases, the degree of non-Gaussianity of the displacement distribution also increases, even if the Fickian regime is achieved at earlier times compared with systems with smaller solute particles. Two possible reasons can be proposed to rationalize the presence FnGD in this system: the decoupling of the solute-solvent dynamics, which becomes stronger as the mass of the solvent particles increases, and intermittency that, according to the authors, can be also recognized by the emergence of a secondary peak in the radial displacement distribution function.

Similar results come from studies on rotational diffusion of dumbells in a porous percolating medium [88] investigated through molecular dynamics. The single molecule shows Gaussian diffusion, but all the dumbells have different mobilities. The result is a non-Gaussian total distribution.

This result well fits the picture of the Superstatistical model (See 2.2.3).

However, it is not true that the presence of more complex interactions in the system generally leads to more marked hybrid features. Indeed, a generalization of LJ potential for non-spherical particles (12-6 Kihara potential) has been used in Brownian simulations of oblate and prolate colloidal particles in the nematic phase [89] to prove that in this anisotropic system a FnGD regime is not present: dynamics is standard both at short and long times, while on the intermediate timescale the diffusion is non-Fickian and non-Gaussian. This proves that FnGD is not an ubiquitous phenomenon.

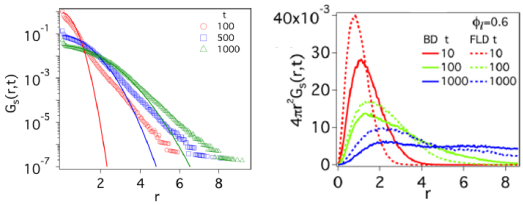

Figure 2.14. In [90] spectacular deviations from Gaussian displacement distribution are reported for LJ solute particles in Fickian regime (left panel) although $2\pi r G_s(r,t)$ shows only one peak (right panel), as in contrast to other systems that show bimodal shaped functions.

Also the influence of hydrodynamics in a LJ system has been investigated numerically. The dynamics of a dilute colloidal tracer ($\phi = 0.2\%$) immersed in a concentrated solution ($\phi = 20-60\%$) of much larger spheres (from 3 to 5 times larger) was studied for the first time [90] in simulations with and without hydrodynamic interactions (HI) through simple Brownian dynamics in the fast lubrication approximation of the full Stokesian dynamics. FnGD is present (Fig. 2.14) with and without HI for both small and big particles, implying that this behavior is a general feature of colloidal dynamics. Although HI affects the specific value of the diffusion constant, generally resulting in a lower diffusivity with respect to the case without HI, the displacement distribution is found to be very similar in both cases, provided that they are compared at the same value of the mean-square displacement.

Performing experiments on colloids at higher concentration and, hence, closer to the dynamical arrest, is much more complicated. In this case,

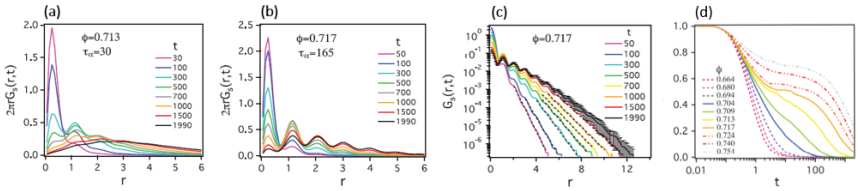

Figure 2.15. Exceptional heterogeneous dynamics in 2d hard disks hexatic phase [8]. $2\pi r G_s(r,t)$ demonstates the presense of multiple peaks at different area fractions (a) $\phi = 0.713$, (b) $\phi = 0.717$. The presence of peaks is also recognizable in the Self van Hove function (c) which also shows exponential tails. non-Gaussianity is also related to the non-exponential decay of the self scattering function in the proximity of the relaxation time (d).

numerical simulations may come back into play and aid in studying the dynamics even on very long time-scale. Simulations of a two dimensional suspension of hard discs [8] were studied in a wide range of area fractions and showed that FnGD is present even in the hexatic phase. Dynamics is massively heterogeneous, as shown by the displacement function that is exponential at large r and oscillatory with multiple peaks on intermediate length-scales (Fig. 2.15). The existence of such several peaks is attributed to the presence of clusters of discs with discretized mobility. Investigations on clusters of marginally mobile discs reveal that the size of the cluster increases in time and begin to percolate at the relaxation time. A recent work [10] showed that also Yukawa colloids exhibit FnGD, and the degree of non-Gaussianity increases as temperature is decreased. Both the two latter systems indeed shares some similarities with glass-forming systems and eventually reach an arrested state, as some thermodynamic parameter is properly varied.

As a matter of fact, many experiments on real systems are performed using scattering techniques that provide results in the reciprocal Fourier-space. However, the equivalent of the features of FnGD (that is precisely defined through real space quantities) in Fourier space is non-trivial and the exact relation remains unclarified. A first step in this direction has been recently provided in [64]. Using confocal differential dynamic microscopy (ConDDM) on diluted tracers diffusing in a glassy matrix of larger hard spheres, it was shown that the experimentally determined ISSF can be

well fitted by diffusing diffusivity model, whose analytical predictions are available only in reciprocal space. [64] explicitly propose that the reciprocal space counter-part of FnG fundamental features are a q^2-scaling of the structural relaxation time (Fickianity) in presence of a non-exponential decay of ISSF (non-Gaussianity). However, the connection between FnGD and reciprocal-space dynamics remains subtle and needs to be further clarified. In next chapters we will further address this point.

The dynamics of a single colloidal tracer in a simple molecular solvent cannot give rise to FnGD unless some kind of heterogeneity is superimposed. A study [62, 85] on an extremely dilute colloidal suspension has demonstrated that FnGD could arise also in a very simple system without long range correlations. A stationary random field of optical forces (speckle pattern) with tunable features is used in order to reproduce an environment for the colloidal tracers that mimics the heterogeneous energy landscape of a typical soft matter matrix. This optimal experimental system displays all the main benchmarks of FnGD and makes it possible to investigate this phenomenon over a wide range of time and length-scales. The experiments also pointed out that the hybrid diffusion regime is closely tangled to the temporary anomalous diffusion occurring at shorter time, suggesting a causal connection between anomalous and hybrid dynamics [1].

Also other experiments on dilute colloidal suspensions under particular conditions reported the occurence of FnGD. In [63] a test particle with $2.5\mu m$ diameter is placed in the vicinity of a wall where edge effects are not negligible on the hydrodynamics of the colloidal particle. In this way the diffusivity of the colloid can be regarded as a function of space and the Diffusing Diffusivity model (See 2.2.3) can be tested.

Conceptually, a similar situation is presented in [76], a study of the diffusive motion of a small object ($45\mu m$ placed on a solid support using an inertial tribometer. With an external bias and a Gaussian noise, the object slides accompanied by a fluctuation of displacements that exhibits unique characteristics at different powers of the noise. While the particle motion is fluid-like at high powers, a stick-slip motion occurs at lower powers. Below a critical power, no motion is observed anymore. As the power of the noise increases, the effect of the non-linearity appears to play a lesser role, and the displacement fluctuation becomes more Gaussian. When the distribution is exponential, it also exhibits an asymmetry with

its skewness increasing with the applied bias.

Many experiments on the diffusive dynamics of diluted nanoparticles in confined conditions have been carried out in recent years. Dispersions of nanoparticles in microfabricated arrays of nanoposts in a square lattice has been systematically investigated both for simmetric [12, 86, 74] and anisotropic objects [75] and a FnG regime is detectable. As the spacing between posts is decreased, the dynamics slows down and self scattering function is well represented by a stretched exponential rather than a simple exponential at all length-scales. Both the diffusivity and the stretching exponent decrease with increased confinement or, equivalently, with decreased void volume. Both MSD and the structural relaxation time show Fickian scaling. The slowing down of the dynamics and the broadening of the distribution of nanoparticles' displacements with increased confinement anticipate a confinement-induced vitrification. The degree of order/disorder of the environment in which the nanoparticles diffuse was instead taken into account in [74]. Several structural configurations of micropillars, acting as obstacles for the free diffusion process, are investigated, from perfect order to completely disordered. The dynamics slows with increasing the degree of order and going from diluted to concentrated conditions. Furthermore, the degree of randomness and the concentration increase the non-Gaussianity of the van Hove function. The MSD is always found linear and the NGP seems to reach a plateau at a non-zero value: the Gaussianity is never restored.

Evidences of FnGD have also been found in confined diffusion of particles in entangled network. Diffusion of polystyrene nanoparticles in polyethyleneoxide (PEO) solutions is investigated in [71]. Experiments are performed by controlling the particles' diameter (from 40 to 200 nm), PEO molecular weight (0.6 to 8M) and also PEO concentration. Their findings suggest that the non-Gaussianity of the van Hove can be explained only at short time by invoking the local heterogeneity of the environment. At long times the main source of non-Gaussianity is attributed to the hopping dynamics of the nanoparticles between the pores of the polymer mesh.

An extensive study on the diffusion of fluorescent tracers in agarose and dextran polymer gels is carried out in [72]. Experiments are carried out by using variable-lengthscale fluorescence correlation spectroscopy (VLS-FCS) that allows to directly track the dynamics over five decades. It is

worth noticing that the dynamics in this system is very fast if compared with other crowded environments (as colloidal glass-formers), hence the detection of a transient hybrid diffusion is remarkable. Results show that not all dense cross-linked polymer solutions display FnGD.

An intriguing experimental work [73] on the dynamics of tracers in polymer matrices with different degrees of humidity (mimicing the stages of a plasticization process) suggests that FnGD could be a microscopic hallmark also in system of great pratical interest that are generally investigated at a mesoscopic level. Experiments on PVP, a high T_g amorphous polymer, which is often used as coatings on pharmaceuticals, are carried out in a wide range of temperatures from far above the glass transition to lower than T_g. Also anomalous and confined diffusion can be observed in this system. However, non-Gaussianity of the van Hove function remains a common feature of the microscopic dynamics.

As a matter of fact, studies on solid nanoparticles in polymeric materials are very common because of their wide range of technological applications. However, from a theoretical point of view, the diffusion of particles of characteristic size comparable to the structural correlation length of the environment has not yet been fully rationalized. In [101] the dynamics of weakly interacting mixtures of nanoparticles in an entangled polymer melt is studied through large-scale molecular dynamics simulations. The particle size is varied from 1 to 15 times the characteristic size of the monomers. However, in this simple system the dynamics of the nanoparticle is found to be Fickian and Gaussian, while the chains of the polymer shows non-Gaussian dynamics.

FnGD in peculiar conditions

In the context of polymer physics, also the mechanism of adsorption of polymer chains on a solid interface from a dilute solution is reported to be FnG and different from what expected [77]: the molecules do not localize immediately after attaching on the surface and then crawl on it towards adsorption sites. On the contrary, particles adsorb (forming weak bonds with the surface) and then diffuse back to solution, and then again they adsorb until they reach the site (with a permanent bonding). This mechanism is faster than expected and is modelled by CTRW as a Levy process.

The effects of the heterogeneity of the interface between polymer and nanostructured solids can instead introduce intriguing dynamical effects as shown in MD simulations [102], inspired by the experiments of Ref.[77], where chemical heterogeneity is introduced by placing strongly and weakly attractive sites at variable relative compositions. In this case, the heterogeneous interaction leads to FnG dynamics that is reflected in a stretched exponential decay of the ISSF and is inconsistent with Rouse model of polymer dynamics that predicts a simple exponential relaxation for each single mode; also the single-mode relaxation time shows an unexpected wave-vector scaling.

Similar results [78] were found for Atto6G, a fluorescent rhodamine derivative dye. Trajectories of the molecules were segmented in order to extract a waiting time distribution. Predictions of the CTRW model agree with the experimental van Hove and a power law waiting time distribution $\psi(\tau) \sim \tau^{-2.5}$ is found. However, we notice as an aside that for this kind of power-law lag time distribution, the expected MSD in the CTRW formalism cannot be Fickian (as instead visible in experimental data), but anomalous. This point should be further clarified.

As a final remark, we note that some interest is found in literature for showing that FnG dynamics is a common feature in models and experiments on particles diffusing in the presence of non-equilibrium conditions, such as equilibrium noise [96, 97, 98], evaporation model [99] and diffusion of charged colloids in an electric field.

Finally, in Table 2.2 we have summarized the dynamical features which found in systems displaying FnGD and described in this section.

Ref.s	Type of "non-standard" dyamical feature
[70, 87]	Multiple peaked $r^n G_s(r,t), n = 0, 1, 2...$
[6, 20, 69, 11, 9, 68, 1, 62, 85, 71, 73, 88, 90, 65, 92]	Exponential tails
[68, 77]	Power-law tails
[1, 64, 8, 10, 93]	Stretched exponential ISSF's decay
[1, 93]	Non-q^2 scaling of structural relaxation time
[6, 20, 1, 64, 8, 92]	Presence of long-time Gaussian restore
[69, 70, 68, 1, 62, 85, 71, 77, 8, 90, 65, 92, 93, 94]	Pre-Fickian subdiffusion
[87, 10]	Pre-Fickian superdiffusion
[69, 70, 1, 62, 85, 76, 77, 78, 8, 65, 92, 94]	Intermittent single-particle trajectories
[6, 20, 9, 7]	Self-similar displacement distribution

Table 2.2. Main dynamical features related to systems with Fickian non-Gaussian dynamics found in literature.

2.2.3 Models of FnG dynamics

Currently, no specific model is present in literature proved to be able to catch all the features of Fickian non-Gaussian diffusion. Moreover, there is not an intuitive statistical explanation to fully rationalize the rise of this phenomenology in a variety of different systems.

However, there seems to be a general agreement of the scientific community that a certain degree of heterogeneity in the mobilitiy of the diffusing particle, over different time and length-scales, is the key element to unfold hybrid diffusion. This heterogeneity can have different origins, for example:

- the environment in which the particle is moving is heterogeneous from a morphological point of view (e.g. in structural heterogeous systems or in isotropic suspension with a decoupling of solvent-solute relaxation times);
- there is a morphological or chemical heterogeneity in the ensemble of diffusing particles;
- the dynamics self-induces dynamical heterogeneities on certain scales, as it happens in strongly interacting systems, such as crowded media and glassy systems [103];

Identifying and isolating the different possible causes of heterogeneity is a challenging issue, as they appear to be often linked to each other and coexist in the same environment. Just few studies have shown how hybrid diffusion is directly induced from a recognized and controlled source of heterogeneity [62, 85, 63, 96, 97, 98]. Anyway, the heterogeneity of the dynamics is the fundamental ingredient of Fickian non-Gaussian diffusion, either if it is induced by correlations in multibody systems, or if it is a consequence of a real structural rearrangement of the environment on different timescales.

Statistical mechanism: *delaying* the Central Limit Theorem.

At a fixed time t, the displacement $x(t)$ of a Brownian particle is a random variable and corresponds to the sum of all displacements performed

by the walker up to time $t = t_N = N\delta t$, δt being an elementary timescale and $N \in \aleph$:

$$x(t) = \sum_{t_i=0}^{t} x(t_i) \tag{2.6}$$

Hence, the probability distribution function $p(x,t)$ of the random variable $x(t)$ is a distribution of summed random variables. If all elementary displacements are independent and identically distributed, the distribution of the summed variables converges to a Gaussian function as long as the number of summands is large *enough* (i.e. for sufficiently long time): this is the essence of the so-called *Central Limit Theorem* (CLT).

The statistical foundation of anomalous diffusion is nowadays clearer and has been rationalized to a certain extent: everything comes from the fact that the Central Limit Theorem for particle displacements does not hold in its usual form, either because the distribution of summed variable is *too broad*, or because the random variables are somehow *long-range correlated* [103].

While in the case of strong correlations there is no general understanding on the limit distribution of dependent summed random variables, a general extension of the CLT in the case of broad displacement distributions was given by Levy, Khintchine, Gnedenko and Kolmogorov [104]. If the distribution of displacements' lengths decays more slowly than l^{-3} for large l, then the limit distribution of $x(t)$ must be a *stable distribution* (also called $\alpha-$*stable Levy distribution*). These distributions represent attractors in the space of probability distributions of independent summed variables, towards which any distribution must converge as time goes on (and the number of summed variables grows to infinity). Stable distributions are in general leptokurtic and heavy-tailed, fully characterized by two parameters (unless translations).

Actually, only few cases of completely analytic stable distributions are known, and the Gaussian function is just a special case among possible stable distributions, being characterized just by one parameter (its variance) and mesokurtic. Stable non-Gaussian distributions (such as Cauchy, Laplace or Levy distributions) are very common in soft matter physics. For example, they play a fundamental role in glassy dynamics as pointed

out in the Mode Coupling Theory [105] and experiments on structural glasses [106].

However, it is not clear whether and to what extent the current understanding on the statistical mechanisms of subdiffusion will be fruitful to catch the origin of hybdrid diffusion. We also report that in the case of the usual Central Limit Theorem, the convergence of the probability function towards the Gaussianity was characterized by Chebyshev [103] through a systematic expansion in time.

It is important to stress that standard diffusion and anomalous diffusion are generally present on different time-scales in the same system: standard diffusion represents the asymptotic diffusive behaviour and it is preceded by an anomalous regime. However, in many cases, tipically when the dynamics is pretty fast (e.g. in molecular simple liquids or diluted colloidal suspensions), non-Fickian diffusion concerns timescales that are simply too short to be observed.

An intriguing hypothesis connecting FnGD and subdiffusion [1, 62] lies in the fact that FnGD could be intrinsically related to the pre-Fickian regime, and considered as a long-time *memory effect* of the anomalous regime. This could be applied also in cases in which Gaussian diffusion is never restored, even in the long time regime (See Table 2.2). As a matter of fact, it is very common that the experimental observation time is too short for the system to reach the standard diffusive asymptote. (This latter being a universal feature of equilibrium fluid-like matter since the CLT must be finally fulfilled, in the thermodynamic limit).

As a direct consequence, the establishment of a permanent long-time hybrid regime must be intepreted as a (weak) ergodicity breaking. On the other hand, for out of equilibrium systems the Central Limit Theorem simply is not strictly required to be suited and standard diffusion is not necessarily expected to take place. non-Gaussianity of the van Hove function as a proxy of ergodicity break was also investigated in heuristic trap models for diffusion in supercooled liquids [107, 108, 109, 110].

Back to the past, reset the clock to 1905. Before going on and present the models of hybrid diffusion found in literature, we believe that it could be very useful to stress the range of validity and the assumptions lying behind the theory of standard diffusion. We take Einstein's theory

of Brownian motion as an instructive example.

Einstein's model of standard diffusion and heat equation In [58] Einstein gave the first microscopic statistical foundation of the macroscopic diffusion (or heat) equation

$$\frac{\partial p(x,t)}{\partial t} = D\frac{\partial^2 p(x,t)}{\partial x^2} \tag{2.7}$$

empirically found by Fick precisely 50 years before [111]. This linear parabolic equation is uniquely solved by the standard Fickian-Gaussian solution when accompanied by a delta-distribution initial condition (which is an intuitive condition in diffusion processes). Einstein's derivation consists of a microscopic detailed balance for the 1-particle displacement distribution function under the following assumptions:

1. Mass conservation law $\Longleftrightarrow$ Normalized probability density function $\int_{-\infty}^{\infty} p(x,t)dx = 1 \quad \forall t$;
2. Isotropic system $\Longleftrightarrow$ Spatially simmetric distribution function $p(x,t) = p(-x,t)$;
3. Equivalence between the time-independent displacement distribution function $\phi(\Delta x)$ and the position distribution function $p(x,t)$ in an appropriate frame of reference;
4. Existence of a well defined unique timescale that is short enough to allow one to neglect higher order time derivatives;
5. All non-zero terms after the first one in series expansions are neglected;

As a matter of fact, Einstein model leads rigourously to uncontrolled power-series expansions of the displacement function $p(x,t)$ if only Hp.1, 2 are invoked. Precisely

$$\Delta t\frac{\partial p(x,t)}{\partial t} + \frac{\Delta t^2}{2}\frac{\partial^2 p(x,t)}{\partial^2 t} + ... + \frac{\Delta t^n}{n!}\frac{\partial^n p(x,t)}{\partial^n t} =$$

$$\frac{\partial^2 p(x,t)}{\partial x^2}\int_{-\infty}^{+\infty}\frac{\Delta x^2}{2}\phi(\Delta x)d\Delta x$$

$$+\frac{\partial^4 p(x,t)}{\partial x^4}\int_{-\infty}^{+\infty}\frac{\Delta x^4}{24}\phi(\Delta x)d\Delta x+\frac{\partial^{2m} p(x,t)}{\partial x^{2m}}\int_{-\infty}^{+\infty}\frac{\Delta x^{2m}}{2m!}\phi(\Delta x)d\Delta x \tag{2.8}$$

which can be rewritten in a more compact form:

$$\Delta t\frac{\partial p(x,t)}{\partial t}+\frac{\Delta t^2}{2}\frac{\partial^2 p(x,t)}{\partial^2 t}+...+\frac{\Delta t^n}{n!}\frac{\partial^n p(x,t)}{\partial^n t}= \tag{2.9}$$
$$\frac{\langle x^2(t)\rangle}{2}\frac{\partial^2 p(x,t)}{\partial x^2}+\frac{\langle x^4(t)\rangle}{24}\frac{\partial^4 p(x,t)}{\partial x^4(t)}+...+\frac{\langle x^{2m}(t)\rangle}{2m!}\frac{\partial^{2m} p(x,t)}{\partial x^{2m}}$$

Expansions in Eq. 2.9 are arrested to the first non-zero derivative order (Hp.4,5):

$$\frac{\partial p(x,t)}{\partial t}=\frac{\langle x^2(t)\rangle}{2\Delta t}\frac{\partial^2 p(x,t)}{\partial x^2} \tag{2.10}$$

By comparing this microscopic equation with the macroscopic phenomenological law, we get Einstein's relation for the MSD

$$\langle x^2\rangle = 2D\Delta t \quad \Longleftrightarrow \quad D=\frac{\langle x^2\rangle}{2\Delta t} \tag{2.11}$$

which also identifies the microscopic meaning of the diffusion constant in a Fickian process.

Einstein's model indicates the existence of a timescale over which (at equilibrium) Brownian dynamics can be modeled as a standard stochastic process, *the same as that of fortuitous errors, which was to be expected* [58].

However, Gaussianity and Fickianity do not explicitly arise from Hp. 4, 5 in a distinct way, so that it is not clear, a priori, the physical meaning of those approximations taken separately.

Higher order expansion of the standard limit Einstein model does not offer an accurate physical description of Brownian dynamics in general, but it is a universal asymptotic theory, derived heuristically. The model is forced to self-reduce to heat equation through Hp.4 and 5. Therefore, one could conjecture that the hybrid regime is somehow encoded in the general equation Eq.2.9 taking the expansions to the $2m$-th order in

space and the n-th order in time $n, m \in \mathbb{N}$. However, there is no a priori statistical justification at the moment for choosing any values of (n, m) different from the standard case $(n, m) = (1, 1)$. Furthermore, a closure relation would be probably needed anyway, in order to practically solve the model because of its integro-differential nature, that naturally fades away when dealing with the standard diffusion asymptote. We note that this procedure corresponds to the Kramers-Moyal expansion of a generic master-equation [112, 113]

Literature models of FnG dynamics

In this section we briefly review the main mathematical approaches presented in literature to model Fickian non-Gaussian dynamics. Table 4.1 presents a brief summary of the peculiar features of the models described in what follows.

Model	Eqs.	Inputs	Gaussian restoring	Pre-Fickian regime	Characteristic timescales	Ref.
Superstatistics	Eq. 2.13	p_D	No	No	None	[6, 20, 67, 17]
Diffusing Diffusivity	Eqs. 2.18, 2.19	τ, σ, n or p_D	Yes	Yes	τ	[114, 16, 115, 116, 17]
Mora-Pomeau trap model	Eq. 2.23	λ	Yes	No	τ_{tr}	[15]
Ideal CTRW	Eqs. 2.24, 2.25	$P(l)$, $\psi(\tau)$	Yes	No	Unknown	[117]

Table 2.3. Peculiar dynamical features of the main models of FnGD present in literature.

Superstatistical Approach Both the superstatistical (and, later, diffusing diffusivity models, 2.2.3) are concerned with the possibility of introducing correlations between subsequent length-steps in a random walk without triggering anomalous diffusion. This point can be readily shown by considering the MSD of a 1D random walker:

$$\langle x^2(t)\rangle = \sum_{i=1}^{N}\langle x_i^2(t)\rangle + \sum_{i\neq j}^{N}\langle x_i x_j\rangle \tag{2.12}$$

we can neglect correlations in the different directions of motion (that are present when anomalous diffusion is originated from having a preferred direction on certain scales) still keeping correlations among lengths of subsequent steps. The idea that long steps (in any direction) follow from long

steps (and, conversely, for small steps) can be represented by introducing a distribution of diffusion coefficients.

The superstatistical approach (SS) was first proposed in modern days by Granick and Hapca in their 2009 seminal papers to rationalize Fickian non-Gaussian behaviour[6, 20, 67]. This naming traces back to the works of Cohen and Beck [118] on thermodynamics of non-linear systems. In the SS framework, the overall diffusion process is modeled as a result of independent standard Brownian trajectories of particles with different mobilities, i.e. a distribution of diffusion coefficients $p_D(D)$ is defined. Therefore the overall distribution function is a *super*-position (hence the name of the model) of two different distributions: the single particle Gaussian displacement distribution and the distribution of diffusivities:

$$p(x,t) = \int_0^{+\infty} p_D(D) \frac{1}{\sqrt{4\pi D t}} e^{-\frac{x^2}{4Dt}} dD \tag{2.13}$$

Fickian diffusion is clearly obtained for every choice of the (time-independent) distribution of diffusivity. On the other hand, the displacement distribution is Gaussian only in the case of a unique diffusivity $p_D(D) = \delta(D - D_0)$.

The main lack of this picture is that it cannot predict a restore of standard Gaussian diffusion at long times, and the distribution function remains timescale-invariant [17]. Furthermore, the model can only be reasonably applied in scenarios in which there is a clear distribution of mobilities among diffusing objects, e.g. the diffusion of microorganisms in a solvent. Otherwise, the physical meaning of the distribution of diffusivities is lost.

Role of initial conditions in the standard model In this paragraph we give a possible interpretation of the superstatistical formula from the point of view of Einstein's standard model. Heat equation (Eq.2.7) is uniquely solved by a standard Gaussian process as long as the initial condition is chosen as a Dirac delta function centered in the origin of the frame of reference [119]. In the case of a generic initial distribution $p(x, t = 0) = p_0(x)$, the solution is a convolution

$$p(x,t) = \int G(x - x', t) p_0(x') dx' \tag{2.14}$$

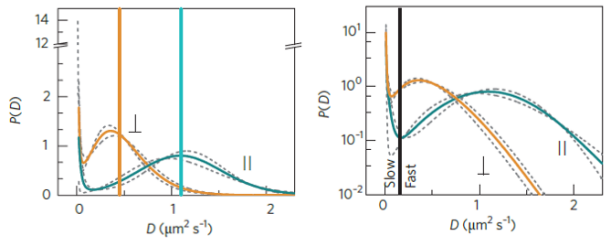

Figure 2.16. Diffusivity probability distribution for parallel and orthogonal component computed through inversion of Eq. 2.13 for system (b) in [6]. Vertical lines represent the macroscopic diffusion coefficient obtained from MSD linear fits. Both curves show bimodal shape, which can be interpreted as slow particles and fast particles clusters (separated by a vertical black line on the right panel).

of the initial distribution $p_0(x)$ and the fundamental heat kernel $G(x,t) = \frac{e^{-\frac{x^2}{4Dt}}}{\sqrt{4\pi Dt}}$. This formula indeed shares some similarities with Eq.2.13. This suggests the possibility of interpreting the distribution of diffusivities as a way to incorporate a non-delta initial distribution in a process which is still described by the heat equation.

Delta distribution at time zero represents the initial configuration in a radially simmetric diffusion process from a point source. However, in the case of FnGD it seems that the common belief that all particles can be thought as concentrated in the origin at time zero is not so obvious. In a Fickian non-Gaussian process described by diffusion equation there must be an initial condition that takes into account the correlations between particles, that can be present in the short time regime. In this case, the initial condition might encode a second timescale different from the one enclosed in the diffusion constant.

However, we stress that not all initial conditions may lead to standard diffusion in the long time regime and a bifurcation analysis is needed[119, 120]. This speculation suggests another point of view to connect structural information, Hybrid Brownian dynamics and departure from ergodicity.

Diffusing Diffusivity Model

The Diffusing Diffusivity model (DD) is probably the most cited in FnGD literature and represents, as we will demonstrate, a generalisation of the superstatistical approach. Although a very similar model had already been introduced by Harrowell and Hurley [114] to catch some features of supercooled liquid dynamics many years before the discovery of Fickian non-Gaussian diffusion, it was more recently shown by Chubynsky and Slater [16] that this model gives an intuitive explanation of hybrid diffusion, also giving the current name to this model. Although there have been a lot of contributions and modifications to this model, the essence of this model has not really changed from its original formulation given in [16].

The model describes the heterogeneity of the dynamics by representing the diffusivity itself of the random walker as a stochastic process in a mean-field framework. The expression *diffusing diffusivity* is not completely justified as it is not linked to a purely diffusive dynamics since the fundamental equation proposed for the dynamics of the diffusivity is always not only diffusive (which would merely reproduce the *superstatistical limit*), but it must have an "elastic" term which generates a memory effect on the displacement distribution function. That is why it could be suggested to prefer the more generic expression *fluctuating diffusivity* [115, 121, 122] .

A simple introductory case First, we will consider the simple case of a 1D random walker with time lags and displacement moves taken as discrete variables. Let $p(\Delta x_i, t)$ be the displacement distribution of the the i-th particle with diffusivity D_i, or, equivalently, the displacement distribution in the i-th region in which all the particles have the same local diffusivity D_i. The physical origin of the mobility heterogeneity is irrelevant in the DD model, since diffusivity and displacement are not coupled nor they are necessary linked to real space features. Now, we assume that $p(x_i, t)$ is a standard Brownian process (i.e. Fickian and Gaussian process):

$$p(\Delta x_i, \Delta t) = \frac{1}{\sqrt{4\pi D_i \Delta t}} e^{-\frac{\Delta x^2}{4D_i \Delta t}} \tag{2.15}$$

and we can compute the MSD of all particles assuming that the time steps Δt are evenly distributed ($t = N\Delta t$):

$$\langle x^2(t)\rangle = \sum_{i=1}^{N} \langle \Delta x_i^2 \rangle = 2\langle D_i \rangle N \Delta t \tag{2.16}$$

By comparing Eq. 2.16 with the usual definition of a Fickian process given by Einstein $\langle x^2 \rangle = 2Dt$, we conclude that *the macroscopic diffusion constant is the average of the diffusivities of the single trajectories in a DD framework, regardless of the distribution given for the diffusivities.*
At this stage we do not have any information on the shape of the overall displacement distribution function. However, we can already measure the intensity of the deviations from Gaussianity for this random walk, by computing the excess kurtosis of the displacement distribution for all the trajectories, averaging both over the distribution $p(\Delta x_i, t)$ of different particles' displacements and the unknown distribution of diffusivities [114]:

$$\begin{aligned} \langle x^4(t)\rangle - 3\langle x^2(t)\rangle^2 = 12(\langle D^2(t)\rangle - \langle D(t)\rangle^2)t + \\ +24 \sum_{i=1}^{N-1} \sum_{j=i+1}^{N} \Big(\langle D(t_i)D(t_j)\rangle - \langle D(t_i)\rangle\langle D(t_j)\rangle \Big) \end{aligned} \tag{2.17}$$

Now, to have more information on the time evolution of non-Gaussian deviations, it is necessary to know how diffusivities are distributed among trajectories. It is evident that in the case of a unique diffusivity $p_D(D) = \delta(D - D_0)$, the standard diffusion is regained.

Interestingly, some features can be estimated also without having the complete shape of the diffusivity distribution, since it happens that some dynamical features are shared by diffusivity distributions pertaining to a same *class*. As an example, we can define a **correlation timescale for the diffusivities** τ_D, which can be seen as the longest relaxation time of the two-times correlator $\phi_D(|t_i - t_j|) = \langle D(t_i)D(t_j)\rangle - \langle D(t_i)\rangle\langle D(t_j)\rangle$, considered as a function of $|t_i - t_j|$. If $\tau_D \longrightarrow \infty$ the environment is slowly varying and D experiences very small changes from step to step, hence the double sum in Eq.(2.17) dominates. By taking $\langle D^2\rangle - \langle D\rangle^2 \sim \langle D\rangle^2$, the first non-Gaussian parameter $\alpha_2 = \langle x^4\rangle/3\langle x^2\rangle^2 - 1 \sim 1$ for $t \lesssim \tau_D$, while $\alpha_2 \sim \tau_D/t$ for $t \gg \tau_D$. This very slow decay of the NGP in the long time regime agrees with idealized Mode Coupling Theory [123] and

CTRW [124].

Since the NGP only decays as $1/t$, deviations from Gaussianity can be appreciated even at times larger than τ_D. We will come back later to the possible central role of the correlator ϕ_D to explain the Fickian-Gaussian decoupling. Different shapes of the diffusivity distribution function have been proposed in literature. It was first shown using Monte Carlo simulations [16] that by sorting a diffusivity from an expontial distribution and then a displacement from Eq.(2.15), we obtain a total displacement distribution which changes from an exponential-like to a Gaussian curve as time goes on, with a linear MSD at any time.

General formulation Some authors have shown that it is possible to represent the algorithimic procedure described at the end of the previous paragraph, with an analytical model that gives the complete shape of the Fourier transform of the displacement distribution at any time, namely the Self Intermediate Scattering Function, also using different types of $p(D)$, such as power-law [125], exponential [17, 126] or, more generally, a Gamma function [19].

In order to get more general analytical insights, it is useful to present the DD model as a set of coupled stochastic/Fokker-Planck equations ((2.18) and (2.19)):

$$\frac{dx(t)}{dt} = \sqrt{2D(t)}\xi_1(t) \iff \frac{\partial p(x,t)}{\partial t} = D(t)\frac{\partial^2 p(x,t)}{\partial x^2} \tag{2.18}$$

$$\begin{aligned} \frac{dD(t)}{dt} &= f(D(t),t) + \sigma(D(t),t)\xi_2(t) \iff \\ \iff \frac{\partial p_D(D,t)}{\partial t} &= \frac{\partial}{\partial D}\left(f(D,t)p_D(D,t) + \frac{1}{2}\sigma^2(D,t)\frac{\partial p_D(D,t)}{\partial D} \right) \end{aligned} \tag{2.19}$$

where $\xi_1(t), \xi_1(t)$ are Gaussian white noises and f, σ are generic deterministic functions. Eq. 2.18 is a truly diffusive dynamics which formally agrees with mass conservation law. All the deviations from standard diffusion due to the complex interactions between the particle and the environment are enclosed in the stochastic diffusivity $D(t)$ which coarse-grains the

dynamics and colours the white noise through eq.2.19. As already shown for the introductory model, it is possible to prove the general relation between the distribution of the diffusivities and the macroscopic diffusion constant. Using Green-Kubo relation [13]:

$$D(t) = \int_0^{+\infty} \langle v(t)v(0)\rangle dt = \int_0^{+\infty} \left\langle \sqrt{2d(t)}\xi_1(t)\sqrt{2d(0)}\xi_1(0) \right\rangle dt = \\ = 2\langle D\rangle = 2\int_0^{+\infty} D p_D(D,t) dD \tag{2.20}$$

We notice as an aside that some authors [115] have also suggested the possibility of extending the model of the Langevin equation with fluctuating diffusivity to a tensorial form, in order to take into account other kinds of heterogeneity.

The possibility of a time-dependent distribution of the diffusivity has also been considered [125, 19, 127] to obtain a diffusing-diffusivity model also for the pre-Fickian anomalous dynamics. However, the linear relation between time and MSD is ensured by any $p(D,t)$ which has a stationary mean value.

Solving the DD model A complete solution for the model in the simplest non-trivial case of an Ornstein-Uhlenbeck modulated white noise[10] was provided by Chechkin et al. [17] in terms of the Fourier-transform of the displacement distribution functions $F(q,t)$ using a subordination scheme [34]. Jain and Sebastian [116] demonstrated that the model with $f(D,t) \propto D(t)$ and $\sigma(D,t) \simeq const.$ is equivalent to Brownian motion in the presence of a sink and provided a similar solution by means of phase space path integral. A similar approach was proposed by [128] and extended to the case of a memory kernel in the diffusivity dynamics [129].

Analytical solutions in the asymptotic cases of very short and very long times show that a slow convergence from a Laplace distribution ($t \longrightarrow 0$) to a Gaussian ($t \longrightarrow \infty$) is a common feature of DD models. In particular,

[10] We notice as an aside that in [17] the proposed Ornstein-Uhlenbeck model is not for the stochastic diffusivity, but for its square-root $Y(t)$, $D(t) = Y^2(t)$.

at short time the DD model is equivalent to SS model since a particle experiences only a certain value of diffusivity and memory effects are not yet at play. Conversely, in the long time regime every particle has sampled all the diffusivity distribution and memory has faded away.

As previously noticed, it is possible to derive direct relations between the correlation function of the diffusivities and some dynamical properties, such as the relative fluctuation of the time averaged MSD or the NGP [115, 121, 32, 114], regardless of the details of the dynamics of the diffusivity and without explicitly solving the model. In particular, we can prove that as long as $\phi_D(t)$ is fastly decaying (faster than $1/t$) we expect the NGP to decay as $1/t$ in the long time regime. Some examples (such as exponential decay) can be recognized in different models. It can be further conjectured that a slower decay of ϕ_D leads, in turn, to a slower decay of the NGP. This is point is crucial since the seemingly power-law decay of the NGP in the asymptotic regime seems to be a common feature of the FnGD regime of glass-formers [1, 123], as we will demonstrate in next chapters.

Some considerations on the fluctuating diffusivity model The main issue concering the DD model is that it does not present any physical justification for the form of the drifting term of Eq.(2.19), which is directly linked to the form of the auto-correlation function of the diffusivity ϕ_D.

Moreover, from an experimental point of view, there are some problems in measuring a fluctuating diffusivity, since diffusion constant is a well defined observable only for the ensemble or long-time dynamics. Hence, any effort to determine a fluctuating diffusion constant from single trajectories must rely on some ad hoc criterion. However, some attempts in this regard have been made with encouraging partial results [82].

Finally, we note that the DD model seems to be intrinsically unable to give any information on the relation between the fundamental dynamical timescales: it is not a microscopic theory, but a dynamical model lacking a clear link to thermodynamic control parameters.

Trap model

Recently [15], it was demonstrated that Fickian non-Gaussian diffusion is also expected in a very simple model of an isolated Brownian particle diffusing among a dilute field of randomly located traps. The proposed

model relies on a clearcut and simple microscopic mechanism without ad hoc laws for mobility fluctuations, which in principle could be valid even in homogeneous media. At variance with diffusing-diffusivity scenarios, which rely on the presence of diffusivity fluctuations, the trap model describes the random motion in a heterogeneous medium, characterized by a non trivial energy landscape.

The microscopic dynamics of the center of mass of a Brownian particle with characteristic size r_0 is governed by an overdamped Langevin equation

$$\frac{d\mathbf{r}}{dt} = -\frac{1}{\zeta}\nabla\Phi + \xi(t) \tag{2.21}$$

where Φ is the potential energy due to the presence of random traps, and $\xi(t)$ is a Gaussian white noise. Dynamics inside the cage is corse-grained since the complete form of the potential is not given. Therefore any potential (and noise) which does not contrast with the microscopic constraint of reversibility and that satisfies a proper form of the Fluctuation - Dissipation Theorem (in order to ensure thermodynamic consistency) can be chosen. The total potential energy of a particle is a linear superposition of single traps potentials:

$$\Phi = -\sum_i w_i(\mathbf{r} - \mathbf{r}_i^{tr}) \tag{2.22}$$

Two main simplifications are made at this stage: *(i)* all traps are isotropically distribututed, (ii) each trap is isotopic $w(\mathbf{r}) = w(r)$ and *(iii)* they all have same depth w_0 larger than kT. Therefore, all the traps are characterized by a unique trapping time τ_{tr} that represents the long timescale needed to have non-Gaussian fluctuations, even if the dynamics is Fickian from time $t = 0$. Dynamics in the trap is thus coarse-grained and the whole system can be described by a set of mass balances for the density of the particles inside the trap $p_{tr}(r,t)$ and outside $p_{out}(r,t)$:

$$\begin{cases} \frac{\partial p_{tr}}{\partial t} = p_{out} - p_{tr} \\ \frac{\partial p_{out}}{\partial t} = \nabla^2 p_{out} - \lambda(p_{out} - p_{tr}) \end{cases} \tag{2.23}$$

The Markovian form of the model holds because of dilution hypotheses, therefore memory effects due to previously visited traps are neglected. This

mean field model describes an equilibrium dynamics since time-translatian invariance is ensured by the conservation of the total 1-particle displacement probability $P(x;t)$.

The theory presents just one non-dimensional parameter $\lambda = \frac{4\pi\nu r_o^3 \tau_{tr}}{3\tau_F}$ with ν being the volume fraction of traps in the environment. This parameter represents a balance between the time spent outside the trap and the total time inside the trap. Conceptually, two contributions to the latter are present: the density of traps ν, and the strength of the trap through the trapping time. However, the model is reliable in the $\nu \to 0$ limit, thus only one contribution really plays a role.

The total probability density function $p(x;t)$ is of course the weighted sum of the one outside and inside the trap and can be analytically evaluated by Laplace-Fourier transform of Eq. 2.23 in the small and large λ regimes. In both cases exponential tails of the distribution are present with a charachteristic length described by a power law $\propto t^\alpha$, with an exponent α depending on λ. The diffusion is Fickian for all values of λ and over all time-scale and Gaussianity is always recovered at long times, as the NGP decreses as $1/t$ in the long time regime.

We notice tha the presented model, in spite of its simplicity, was found to be qualitatively in agreement with some experimental results [1, 6, 20, 65].

Continuous Time Random Walk Approch

In the ideal Continuous Time Random Walk (CTRW) a random walker performs a stationary process with distributed step-sizes and waiting times taken from two indipendent distributions. It could be considered as the most simple extension of the classic random walk model that is obtained as a special case of CTRW by taking a delta distrbuted (*constant*) time lags and a Gaussian distribution for the steps length. CTRW model was successfully applied to model microscopic dynamics in a great variety of systems, including polymer systems and supercooled liquids [102, 51, 130, 131].

In the case of decoupled CTRW, the displacement distribution function of a single particle can be splitted in the two separate contributions from the input distributions of step lengths $p_n(x)$ and time lags $\psi(t)$. In particular, if $\chi_n(t)$ is the probability of taking exactly n steps up to the

time t, then the subordination formula

$$p(x,t) = \sum_{n=0}^{+\infty} p_n(x)\chi_n(t) \tag{2.24}$$

takes into account that the total probability of having a step x at time t comes from all the combinations of precisely n steps until time t which gives as total displacement x. Eq. 2.24 is equivalent to the celebrated Montroll and Weiss formula [132] in the Laplace-Fourier domain:

$$F(q,s) = \frac{1-\psi(s)}{1-\lambda(q)\psi(s)}\frac{1}{s} \tag{2.25}$$

Recently [117, 133], it was demonstrated that for a large class of systems where CTRW description is applicable, exponential tails are expected independently from the shape of the second moment of the van Hove distribution. However, strict assumptions must be required:

- waiting times distribution must be not too broad in order to be analytic in the vicinity $s = 0$;
- step-size distribution must not be too-broad.

The first property is enough to ensure that the mean waiting time is finite, which is a necessary condition not to have anomalous diffusion.

Finally, we note that the link between non-Gaussian dynamics (also in the long time regime) and the shape of waiting time distributions was studied in a semi-quantitative way in [107, 108, 109, 110] at least in some cases of practical interest for structural glassformers.

Other models

In the last decades, many advances have been made in particle tracking and our understanding of the behaviour of microswimmers such as bacteria or algae in dilute and concentrated suspension has advanced greatly. For this kind of mesoscopic systems, specific arguments can be brought to explain the rise of non-Gaussian displacement distribution in the Fickian regime. In particular, hydrodynamic considerations can be made to explain the peculiar characteristics of the motion of flagellated microorgan-

isms [134]. Through a scaling argument one can prove that the velocity distribution function has the power law form

$$p(v) \propto v^{-(1+3/n)} \tag{2.26}$$

To ensure the validity of the central limit theorem, the second moment must be finite, which is true for $n < 3/2$. This condition is satisfied in the case of Stokeslets ($n = 1$), but it is not in the case of stresslets ($n = 2$)[11].

The displacement PDF is linked to the velocity PDF trough the hydrodynamic decay law r^{-n}. In the spatial point in which we have a variation of this law, we also have a deviation from the gaussianity of $p(x)$ in the case $n > 3/2$. In this way, we can infer the shape of the near-field velocity around a particle from the displacement distribution and demonstrate the presence or absence of Stokeslet contributions on the fluctuation spectrum.

A complete model for the motion of self-propelled particles was developed by [135] starting from a set of two stochastic equations describing the motion of an active brownian particle in the general case of a chiral (rotating) particle. The complete equations of motion which are derived are equivalent, under certain conditions, to the simple Smoluchowski-like equation for the one-particle distribution function:

$$\frac{\partial^2 p(x,t)}{\partial t^2} + 2D\frac{\partial p(x,t)}{\partial t} = \frac{v_0^2}{3}\frac{\partial^2 p(x,t)}{\partial x^2} \tag{2.27}$$

D being the rotational diffusivity of the particle and v_0 the modulus of the average rotational velocity. This *telegrapher's equation* generalizes the diffusion equation [136, 137, 138] and provides also a model for the crossover from anomalous to Fickian diffusion.

2.3 FnGD in glass-forming systems?

Four are the main motivations that justify the scope of the present work, namely the quantitative search and characterization of Fickian non-Gaussian diffusion in supercooled liquids:

[11] A fundamental solution of Stokes equations in the presence of a point-like force, or dipolar force in the origin are termed *stokeslet* and *stresslet*, respectively.

1. As pointed out in previous sections, the heterogeneity of the dynamics is a fundamental ingredient of all systems displaying FnGD; as indicated in Section 2.1, glass-forming liquids, in fact, can be considered the epitome of soft-matter systems with dynamical heterogeneity [25];

2. Hybrid diffusion is accompanied in many systems by intermittency of single-particle trajectory; cage-jump motion is considered hallmark of feature of glassy dynamics [28];

3. FnGD has been suggested [62, 139] to be present in systems with a subdiffusive pre-Fickian regime, which is also present and particularly extended in glass-formers;

4. The dynamics close to glassy state is extremely slow, hence a complete characterization of an intermediate-time regime (as FnGD is expected to be in equilibrium systems) is likely easier.

We now review some previous results on dynamics of glass-forming liquids to show that, although it was never claimed, the the presence of a FnG regime in these systems was already detectable by examining retrospectively some previous findings present in literature.

Noticeably, exponentially-tailed displacement distributions had been reported for both experiments on colloidal systems and molecular dynamic simulations [24, 22, 26, 140] focusing on times of the order of the structural relaxation time τ_α (related to the first jumps of the particles out of their cages) which typically falls either within the subdiffusive regime or around the subdiffusive-Fickian crossover. For example, in [141] it was found that τ_α and a so-called "Fickian time", which is in fact defined from the restoring of Gaussianity (with no reference to the restoring of linearity in the MSD) show different temperature dependence, the latter being larger than the structural relaxation time. Interestingly, the authors of that article declare [141]: "*The probability distribution* $P(log\Delta r; t)$ *is a convenient indicator of Fickian diffusion, because if particles move via Fickian diffusion, then the self-part of the van Hove function is Gaussian*". As a matter of fact, with *Fickian diffusion* they meant *Fickian and Gaussian diffusion*. This latter naming mirrors the belief in a coincidence of Fickian and Gaussian diffusion, as it was widespread before the discovery of FnGD.

It is also very intersting to note that in [141] it is also hinted that the onset time of Gaussian diffusion "*occurs well within the regime of apparent linear time dependence of the mean-squared displacement*", but, nevertheless, no quantitative analysis of this issue (primarily, the time needed to recover the linearity in the MSD) had been provided in [141].

This point has never been fully clarified [142]. Indeed, it was also speculated [143, 144] that the structural relaxation time is expected to increase at least as fast as the time needed for the restoring of van Hove Gaussianity as glass transition is approached.

Only very recently, some studies have shown how different inter-particle potentials can give rise to non-Gaussianity in supercooled liquids is presented in [66, 1, 65, 92]. An interesting result of [66] is that the length-scale of dynamical heterogeneity, computed through finite-size scaling, is proportional to the length-scale which can be measured through a coarse-graining of the displacement distribution function using a binning size for which the distribution appears Gaussian. This result further strengthens the idea that non-Gaussianity of the van Hove (a single-particle indicator) and DHs in glassy liquids (stemming from multi-particle correlations) are connected to each other, as originally suggested in the seminal work by Weeks et al. [24], and lately largely remarked in literature of glassy dynamics [145, 49, 106].

Some deviations from Gaussianity, however, do persist even in the Fickian regime of glass-formers, as clearly demonstrated in [92, 1].

A fundamental work on FnGD in this model-system of supercooled liquid, carried out very recently by [65], focuses on the time-dependence of the characteristic length of the exponential tails of the van Hove function in 2d and 3d. Furthermore, a comparison with results of simulations on systems with anisotropic interaction (3d tethraedral patchy particles) is also provided. The main results of this work will be further discussed in next chapters and compared with our results presented in Chapter 4.

Concentrated colloidal suspensions are often regarded as good proxies for glass forming liquids, which can be easily studied via experiments, at odds with their supercooled counterpart. For example, the 2d hard sphere suspension case was investigated by [83] in a wide range of volume fractions. The authors specifically focus their analysis on testing the validity of the so-called Gaussian approximation of the ISSF, without a specific con-

nection to the concomitant achievement of the linearity in the MSD. As also suggested by [146], the unsuitability of the Gaussian approximation in most complex fluid should strongly suggest to reconsider the interpretation of many findings on diffusion on colloidal systems (and soft matter in general). However, the departure from the Gaussian behaviour is not dramatic at this (not too high) concentrations. In fact, only small deviations are visible in the tails of the van Hove distribution and a first-order correction to the Gaussian approximation of the self-scattering function already gives excellent agreement with the experimental correlation functions computed from single-particles' trajectories. Of course, the persistence of these small non-Gaussian deviations in the long-time Fickian regime is not readily assessed. However, a short-lived FnG regime seems detectable at the highest concentrations ($\phi = 0.66$) at intermediate times, although not explicitly noted by the authors.

Experiments on real supercooled liquids remain way harder to be carried out, so they are not as popular as their colloidal counterpart for studying self diffusion processes. In line of principle, FnGD is not detectable as long as a real space analysis is not performed with non scattering tecniques.

However, if we consider (as elsewhere proposed [64]) the co-existence of a so-called "Fickian" scaling of the structural relaxation time ($\tau_\alpha \propto q^2$) with a stretched exponential decay of the ISSF as the Fourier-space counterpart of FnGD, it becomes evident that many known results on glassy dynamics should be re-examined on a different perspective, as also suggested in [64]. For example, incoherent quasielastic neutron scattering measurements carried out on two types of glass-forming liquids revealed the possible presence of FnGD both in a molecular and an ionic liquid [84]. From the combined analysis of the dependence on the probing wavevector both of the stretching exponent of intensity correlation function and of its relaxation time, a crossover was found between a short wave-vector regime (in which the exponent is nearly 1 and the relaxation time has a diffusive scaling with the wavector) and a long wave-vector regime (characterized by a constant beta at 0.5 and a diffusive scaling). The crossover regime is bounded between two conventional critical values of the wavevector: the first threshold is defined as the *Fickian crossover* and the second *Gaussian crossover*. However, it would be very interesting to understand the physical meaning of these scalings in real-space, and the connection with anomalous

and hybrid diffusion time windows.

In conclusion, we think that the here presented framework fully supports the motivation of the present thesis, namely the characterization of the peculiar features of Fickian non-Gaussian regime in the proximity of the glass transition.

AVGVSTVS FRIDERICVS ROMANORVM IMPERATOR SEMPER

CHAPTER 3

Methods

3.1 Investigated systems

In this chapter we describe the methods of our analysis, consisting in numerical simulations on 2d and 3d models of supercooled molecular liquids, and experiments on a quasi-2d hard-sphere colloidal suspension at high area fractions. While in the numerical systems glass transition is approached by decreasing the temperature below the crystallization (or melting) point, in the experiments the dynamic slows down with increasing concentration. Since the present thesis aims at a novel characterization of the effects of the dynamical heterogeneity of glass-forming liquids (in which dynamical behaviours are not necessarily related to evident structural changes), we chose very simple model-systems of glass-formers, namely crowded binary mixtures of spherical particles with pair-additive and isotropic interactions. Hence, the impact of different polydispersities on the dynamics is not considered in this work, while the possible role of spatial dimensionality and type of inter-particle potential is instead taken into account.

3.1.1 Experiments on 2d Hard colloidal Disks binary mixture (2HD)

We analyzed data from previous experiments performed at Physics Department "Ettore Pancini" in University of Naples "Federico II"[28, 1]. Quasi-two dimensional hard-sphere-like colloidal suspensions at different area fractions, ϕ, were obtained by using a 50:50 binary mixture of silica beads dispersed in a water. Surfactant (Triton X-100, 0.2% v/v) was added to the solution to avoid particle sticking through van der Waals forces. Large and small beads diameters measure $\sigma_L = 3.16\ \mu m$ and $\sigma_S = 2.31\ \mu m$, respectively, resulting in an average particle diameter $\sigma = 2.7\ \mu m$ and in an 1.4 ratio known to prevent crystallization. We focused on a area fraction range where the samples can be equilibrated on the experimental time scale, and monitored the dynamics after thermal equilibrium is attained. Digital videos of the samples were obtained using a standard microscope equipped with a 40x objective (OlympusUPLAPO 40XS) and a fast digital camera (Prosilica GE680). At the highest area fraction, roughly a thousand particles in the field of view of the microscope were imaged. At each area fraction, the video duration, t_v, was several times larger than the structural relaxation time, τ_α, while the interval between subsequent frames, t_f, was much smaller than τ_α. In particular, t_v ranged in $[10^3 s, 10^5 s]$ and t_f in $[0.2s, 2s]$, respectively, depending on the area fraction, i.e., larger times at larger area fraction. Particle tracking was performed through a Python based implementation of the Crocker-Grier algorithm [147]. Data analysis was performed using Matlab and different SciPy libraries in Python [148]. Interactive data exploration and visualization was performed using IPython and Jupyter notebooks [149]. All dynamic observables are computed averaging over all particles and over the time origin, since the system is time-translation invariant. When not explicitly stated, results on this system are expressed in time units of seconds and length units of micrometers.

3.1.2 Simulations of 2d Soft Disks binary mixture (2SD)

NVT molecular dynamics simulations were performed (with the standard Noseé-Hoover thermostat implemented in LAMMPS [150, 151]) of a two dimensional binary (50 : 50) mixture of disks with diameter σ_L and

σ_S for large and small disks, respectively, and size ratio $\frac{\sigma_L}{\sigma_S} = 1.4$, which is known to avoid long-range crystallization[102, 1]. The total number of particles is $2N = 10^3$ at constant area fraction $\phi = 1$. Particles interact through harmonic soft pair potential

$$V(r_{ij}) = \epsilon\left(\frac{\sigma_{ij} - r_{ij}}{\sigma_L}\right)^2 \Theta(\sigma_{ij} - r_{ij}) \tag{3.1}$$

with r_{ij} the inter-particle separation and $\sigma_{ij} = \frac{\sigma_i + \sigma_j}{2}$ the average diameter of the interacting particles and Θ the Heavyside function, ϵ a characteristic energy scale. We adopt reduced units $\sigma_L = m = \epsilon = k_B = 1$, with m being the mass of both particle species and k_B the Boltzmann constant. Thus, temperatures displayed in the text are measured in units of the interaction energy scale ϵ. Periodic boundary conditions are applied in two dimensions. The dynamics is monitored after fully equilibrating the system. While the two species generally show a qualitatively similar behaviour, in what follows we solely focus on the smallest component. All dynamic observables are computed averaging over all particles of the selected species and over the time origin, since the system is time-translation invariant.

3.1.3 Simulations of 3d Kob-Andersen Lennard-Jones binary mixture (3KALJ)

Three-dimensional (3d) NVT molecular dynamics simulations, using the standard Noseé-Hoover thermostat, are performed in LAMMPS of a 80:20 (A:B) binary mixture of particles interacting via a shifted and truncated version of the LJ interaction potential

$$V^{LJ} = V_{\alpha,\beta}(r_{ij}) = 4\epsilon_{\alpha\beta}\left[\left(\frac{\sigma_{\alpha\beta}}{r_{ij}}\right)^{12} - \left(\frac{\sigma_{\alpha\beta}}{r_{ij}}\right)^{6}\right] \tag{3.2}$$

where $\alpha, \beta \in A, B$, r_{ij} is the distance between the centres of mass of particles i and j, $\sigma_{AA} = 1$, $\sigma_{AB} = 0.8$, $\sigma_{BB} = 0.88$, $\epsilon_{AA} = 1$, $\epsilon_{AB} = 1.5$, $\epsilon_{BB} = 0.5$; precisely, the potential is (i) truncated at $r = r_c = 2.5\sigma_{AB}$ in order to save unessential computer time (at the cutoff the potential is 1.6% of its minimum value $-\epsilon$); (ii) a constant term $V'_{LJ}(r_c)$ is subtracted in the force in order to have the force continuously go to zero at the cutoff

distance. Modifications (i) and (ii) corresponds to the following implementation of the potential:

$$\begin{cases} V(r) = V_{LJ}(r) - (r - r_c)V'_{LJ}(r) - V_{LJ}(r_c) & r < r_c \\ V(r) = 0 & r > r_c. \end{cases} \tag{3.3}$$

Hence, this model is a modification, introduced in [152, 153], of the standard Kob-Andersen Lennard Jones (KALJ) model of supercooled liquid[154], in order to prevent crystallization at very low temperatures. This modification is essential for the scope of our study (i.e. the rare event statistics occurring in the long time dynamics close to the glass transition). For the standard KALJ model at standard density 1.2, crystallization unavoidably occurs [155, 156, 152] for lengthy simulations starting from $T \sim 0.45$ by phase separating into a pure A phase, and it is anticipated for larger samples [157]. In our study, the so-modified KALJ model (mKALJ) did not present crystallization for every run and simulated temperature. Moreover, dynamics and structure of mKALJ were tested to be equivalent to those of the standard model as far as a comparison was feasible.

All results are given in reduced units, where σ_{AA} is the unit of length, ϵ_{AA} the unit of energy and $\sqrt{m\sigma_{AA}^2/\epsilon_{AA}}$ the unit of time (being $m = 1$ the mass of the particles). For argon these units correspond to a length of 3.4Å, an energy of $120k_BK$ and time of $2.1\times10^{-12}s$. Notice that the here adopted unit of time differs from the original $\sqrt{m\sigma_{AA}^2/(48\epsilon_{AA})}$ convention by a factor $\sqrt{48}$ [37]. The total number of particles is $N = 32.000$ at constant density $\rho = 1.2$, and temperature was varied in the range $T = 5.000-0.380$.

The dynamics is monitored after fully equilibrating the system (i.e. no drift in temperature, pressure or potential energy is observed). The system is initially prepared and equilibrated at high temperatures, where relaxation times are shorter. Temperature in the high-T equilibrated configuration is then lowered to a desidered value and the system is re-equlibrated.

The integration time-step is $dt = 0.003$ for $T > 1$ and $dt = 0.005$ for $T \leq 1$. At the lowest temperatures, the maximum run length extends up to 2×10^9 integration time steps, i.e. a time duration of 1×10^7 time units. While the two species generally show a qualitatively similar behaviour, in what follows we solely focus on the largest component (particles A).

Unless otherwise explicitly indicated, dynamic observables are computed averaging over all particles of the selected species and over 100 different runs of simulation at $T > 0.550$, 200 runs for $0.550 \geq T \geq 0.400$ and 400 runs fot $T < 0.4$

Simulations and analysis of this system were carried out in collaboration with Prof. Walter Kob from Laboratoire Charles Coulomb, University of Montpellier.

AVGVSTVS FRIDERICVS ROMANORVM IMPERATOR SEMPER

CHAPTER 4

Results

4.1 Characteristic scales of the FnG regime

In this section we show that all the glass-formers investigated in our study (3KALJ, 2SD, 2HD) show Fickian non-Gaussian dynamics and identify the fundamental timescales (as well as the corresponding length-scales) that characterize this regime.

For the estimate of the Fickian onset τ_F, we will demonstrate that, in the investigated systems, the standard diffusion timescale marks the onset of linearity in the MSD, while Gaussianity is still far from being reached, the timescale of the onset of Gaussianity τ_G systematically being larger than τ_F.

We anticipate that our approach to define Fickian and Gaussian onsets robustly draws on "time-temperature/concentration" superpositions, in analogy with other characteristic scales defined in a variety of systems [158, 49, 159].

We also remark that in molecular supercooled liquids (2SD and 3KALJ), the glassy state is approached by decreasing temperature, while in the experimental colloidal system (2HD) glass transition is is the area fraction of colloidal particles. We will generally refer either to temperature or area

fraction as *thermodynamic control parameter*, in the following.

Results on 2SD and 2HD systems have been recently published in [1], while the publication of results on 3KALJ is still in preparation.

4.1.1 The Fickian onset

The estimate of the time- and length-scales, τ_F and ξ_F, for restoring the Fickian behaviour after the subdiffusive regime draws on the MSD data (Fig. 4.1). While subdiffusion becomes more marked and persistent on approaching the glass-transition, the length-scales for attaining the Fickian regime seem instead to remain constant (as the thermodynamic parameter is varied) and of the order of the particle diameter, σ[1].

Thus, we assume as an ansatz $\xi_F = \sigma$ (whose effectiveness will be verified a posteriori, in the following). Accordingly, the corresponding time τ_F is defined through the relation $\langle r^2(\tau_F)\rangle = 2dD\tau_F = \xi_F^2$, d being the spatial dimensionality, and therefore coincides with the standard diffusion time. Hence, the Fickian length is constant, while the Fickian time, τ_F (that is also a broad estimate of the duration of subdiffusion), scales as the inverse of the diffusion coefficient, consistently with theoretical predictions for diffusion in a heterogeneous energy landscape [160] and previous numerical results on glass-formers [27].

The effectiveness of the just discussed estimation of τ_F and ξ_F is fully demonstrated by the data collapse reported in Fig. 4.2. The adopted shifting factors are $\xi_F = \sigma$ and τ_F: all MSD datasets collapse on a linear master curve starting from the point of coordinates $(1, 1)$ (Fig. 4.3).

We also notice that, in fact, the adopted rescaling leads data to collapse even before the Fickian regime (Fig. 4.4), consistently with Mode Coupling predictions and previous numerical results on glass-forming systems [161, 49, 37]. Collapse at short time becomes less effective for all systems around $t \lesssim 0.1\tau_F$.

We further checked the effectiveness of τ_F and ξ_F. Fig. 4.5 shows the time evolution of the logarithmic derivative of the MSD $a = \frac{d\log\langle r^2(t)\rangle}{d\log t}$.

[1] For molecular systems with soft interactions, σ is here defined as the length-scale corresponding to the first peak of the radial correlation function. Another common way to determine σ is to consider the length $\lambda^* = 2\pi/q^*$ corresponding to the first peak of the static structure factor. However, the two methods provide similar estimates of σ, both independent on variations of thermodynamic parameters close to glass transition.

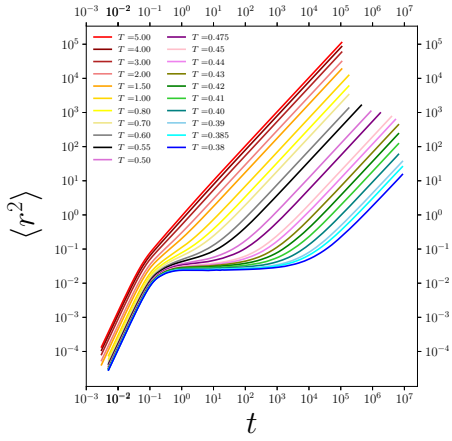

(a) 3KALJ

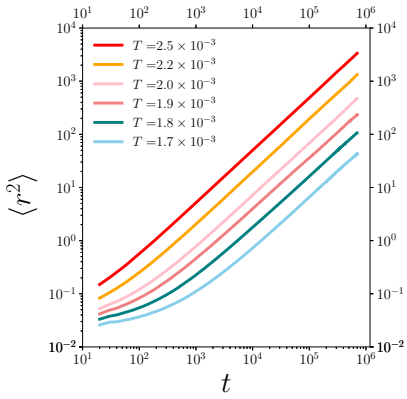

(b) 2SD

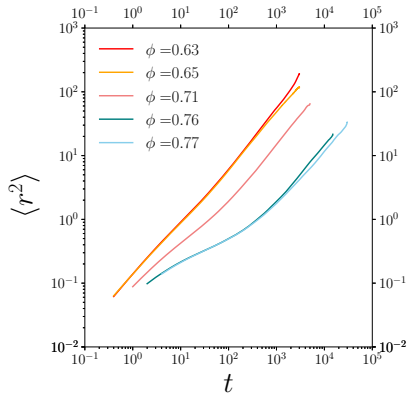

(c) 2HD

Figure 4.1. MSD as a function of time for the three systems at different values of the thermodynamic control parameters.

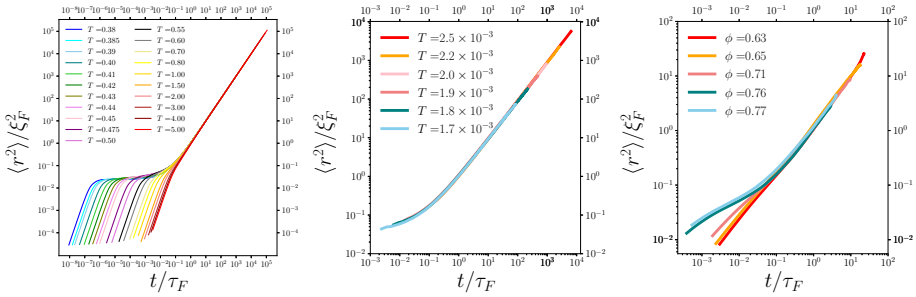

(a) 3KALJ **(b)** 2SD **(c)** 2HD

Figure 4.2. MSD as a function of the rescaled time t/τ_F for the three systems at different values of the thermodynamic control parameters.

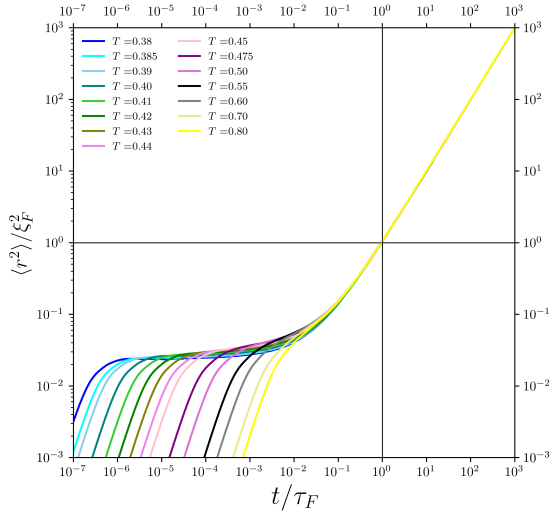

(a) 3KALJ

Figure 4.3. MSD as a function of the rescaled time t/τ_F for KALJ system within the supercooled temperature-window.

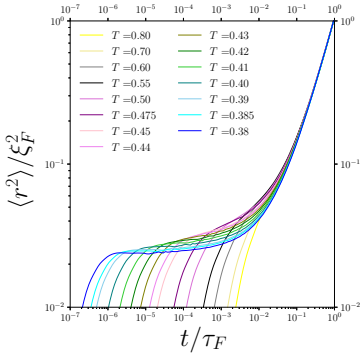

(a) 3KALJ

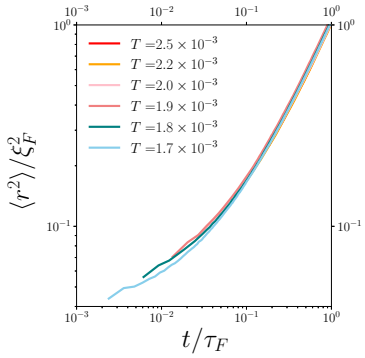

(b) 2SD

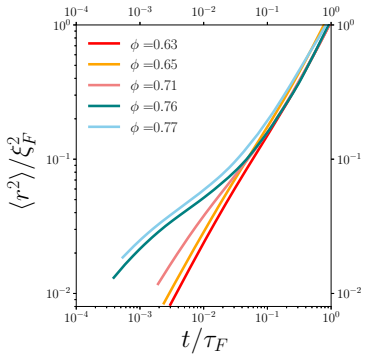

(c) 2HD

Figure 4.4. MSD as a function of the rescaled time t/τ_F in the pre-Fickian regime for the three systems at different values of the thermodynamic control parameters.

Simulations of the KALJ system, in particular, provide an illustrative example of the evolution of the MSD over more than ten decades in time. At very short time, single-particle motion is ballistic and $a = 2$; KALJ system in the supercooled temperature-window ($T \lesssim 0.8$) show a clear subdiffusive regime ($a < 1$) at intermediate times, which becomes more marked as temperature is decreased. At very low temperature ($T \lesssim 0.42$), the system enters a temperature regime in which the minimum value of the derivative, $a_{min} = a(t_{DW})$ (t_{DW} being the Debye-Waller time, Fig. 4.6.a), remains almost constant and close to zero as temperature is decreased. This corresponds to the appearance of a plateau-like regime in the MSD. Interestingly, the Debye-Waller factor $\sqrt{\langle r^2(t = t_{DW})\rangle}$, (i.e. the length-scale of the inflection of the MSD), is not constant, but keeps decreasing as temperature is lowered (Fig. 4.6.b). This can be intuitively interpreted as a small shrinking of the particle cage as the system approaches glass transition [33].

Figure 4.7 further confirms the effectiveness of the Fickian timescale τ_F, obtained from the long-time collapse of the MSD: indeed, it is found that all $a(t)$ datasets in the supercooled regime now collapse onto a unique mastercurve for any $t > t_{DW}$, and approach the asymptotic value $a = 1$ around $t/\tau_F = 1$. (Precisely, all curves are around a value of 0.95 at the Fickian onset.)

4.1.2 The Gaussian onset

The (first) Non-Gaussian Parameter (NGP) α_2 is the simplest and most common indicator to monitor the time evolution of non-Gaussian deviations of the displacement distribution function. In the systems here investigated, $\alpha_2(t)$ displays an increasing maximum, on approaching glass transition, at times around τ_F, and vanishes in the long-time limit, as typically reported for glass-forming liquids [26] (Fig. 4.8).

Our approach to identify the timescale τ_G characteristic of the onset of Gaussian diffusion, and the associated length-scale $\xi_G = (4D\tau_G)^{1/2}$, draws on a visual inspection of NGP data in double logarithmic plot, as shown in Fig. 4.9. We define τ_G as the time where $\alpha_2(t)$ reaches an arbitrarily chosen (low) threshold $\alpha_{2\infty} = 0.05$ (shortly, we will come back to the choice of this threshold). As a matter of fact, the displacement distribution for $t \geq \tau_G$ is indistinguishable from the Gaussian distribution of standard Brownian

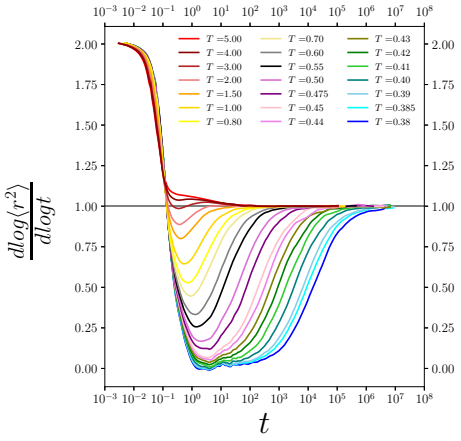

(a) 3KALJ

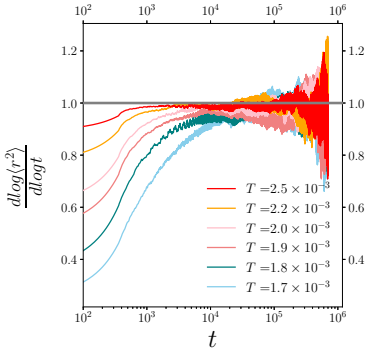

(b) 2SD

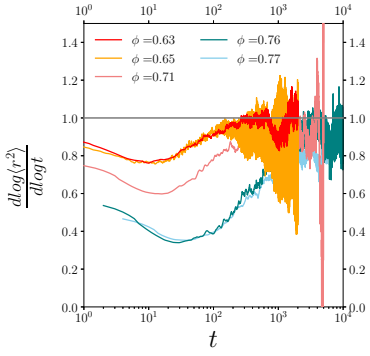

(c) 2HD

Figure 4.5. Log-derivative of the MSD as a function of time for the three systems at different values of the thermodynamic control parameters.

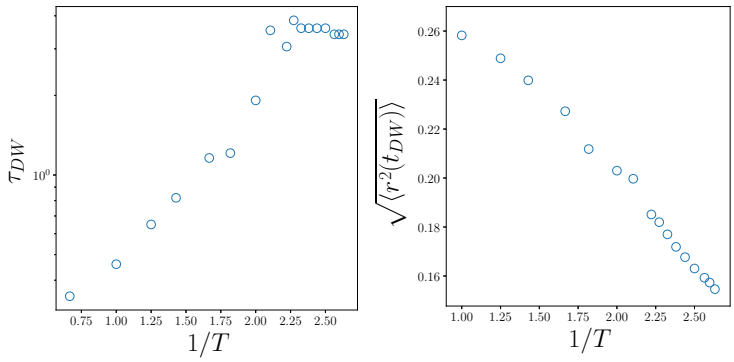

(a) 3KALJ **(b)** 3KALJ

Figure 4.6. (a) Debye-Waller time and (b) Debye-Waller factor as a function of temperature for KALJ system.

motion, as it will be shown in Section 4.3.

Figure 4.10 shows a striking result of our definition of τ_G. By plotting the NGPs as a function of t/τ_G, we succeed in collapsing all the long-time tails over well defined mastercurves. The collapse works quite well within the Fickian time-window (Fig. 4.11). At high-ϕ/very low-T conditions, where the adopted low threshold $\alpha_{2\infty}$ is not attained within the monitored time window, we estimate τ_G as the appropriate shifting factor to obtain the aforementioned data collapse.

Fig. 4.12 (b-c) shows that, in the long-time, $\alpha_2(t)$ seemingly shows a power-law tail $\propto t^{-\delta}$ with exponent $\delta = 0.55$ for experiments on hard spheres and $\delta = 0.7$ for simulations on soft disks. In KALJ system (panel a) the behaviour of the mastercurve does not seem to be compatible with a unique power-law function of time. The curve apparently shows a crossover from a power-law with an exponent $\delta < 1$ to $\delta = 1$ (at very long times).

We notice that several theories, including Mode Coupling Theory for hard-spheres [161], some Diffusing Diffusivity [16, 17] and Continuous Time Random Walk models [124] predict power-law tails of the NGP with an exponent 1. Other models, such as [162, 110], predict however power-law tails, with an exponent that can differ from unity, consistently with our results here and with some previous numerical simulations of glass-

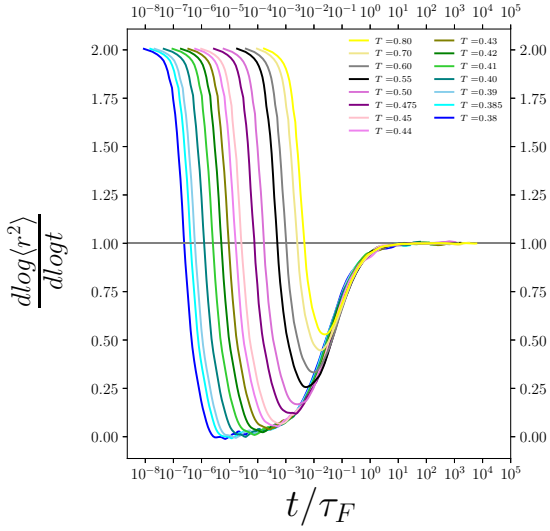

(a) 3KALJ

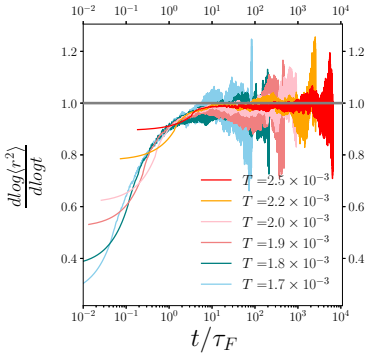

(b) 2SD

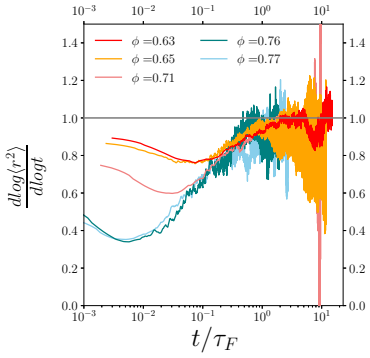

(c) 2HD

Figure 4.7. Log-derivative of the MSD as a function of the rescaled time t/τ_F for the three systems at different values of the thermodynamic control parameter.

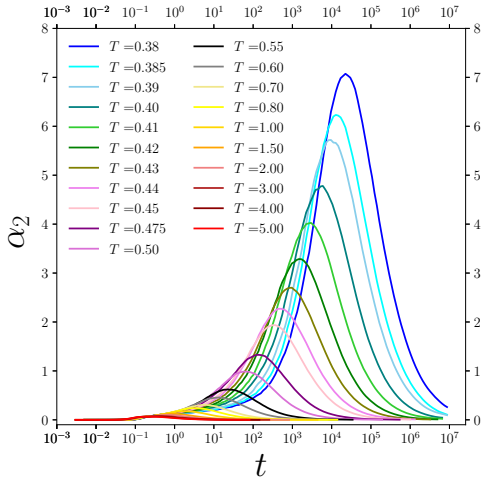

(a) 3KALJ

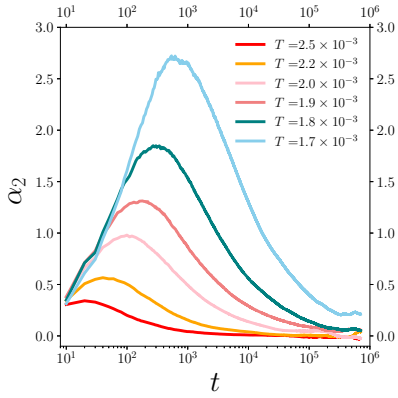

(b) 2SD

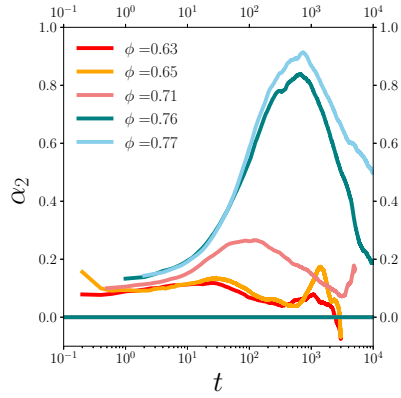

(c) 2HD

Figure 4.8. NGP as a function of time for the three systems at different values of the thermodynamic control parameters.

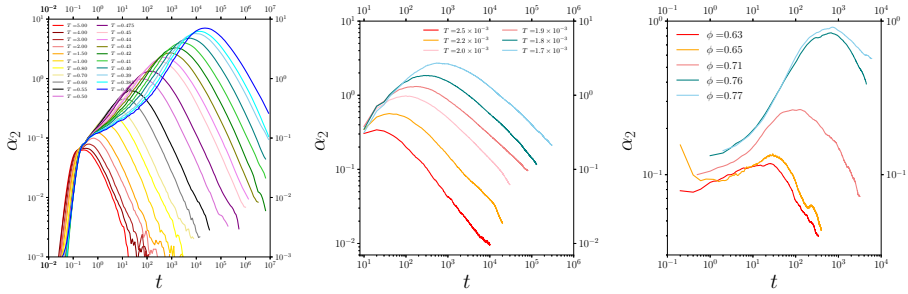

(a) 3KALJ **(b)** 2SD **(c)** 2HD

Figure 4.9. Same data of Fig. 4.8 on a double logarithmic scales.

formers [163, 124, 164]. As a matter of fact, failures of MCT in predicting the NGP behaviour in numerical glass-forming models are reported also in other works [165, 166, 29].

Notice that the existence of the data collapse (whether it is a power-law or not) ensures that the choice of the threshold $\alpha_{2\infty}$ does not affect the volume-fraction or temperature dependence of the estimated τ_G. Indeed, on changing the threshold, τ_G would merely change by a constant factor, provided that the NGP has reached its asymptotic behaviour. This is readily demonstrated in Fig. 4.13.a that shows a data collapse equivalent to that in Fig. 4.10.a, obtained with a different definition of the threshold. In this case $\tau'_G \equiv t(\alpha_2 = \alpha'_{2\infty} = 0.1)$. In panel b we compare τ'_G with a τ'''_G defined with a very small threshold, $\alpha'''_{2\infty} = 0.01$: Fig.4.13.b definitely demonstrates that even if $\alpha_{2\infty}$ is varied by a factor 10, the measured timescales are linearly related.

Finally, it is worth noticing that the NGP also provides another characteristic timescale, τ^* ($< \tau_F$), related to the presence of a maximum ${\alpha_2}^*$. As demonstrated by Fig. 4.14, this time scale is not relevant for our study and further investigations on τ^* are not necessary.

Of course, it is likely that stronger displacementS correlationS at short times (signalled by the presence of higher peaks of the NGP) are also more persistent in the long-times. However, the absence of a collapse in Fig. 4.14 suggests that the connection between long-time behaviour of the NGP and non-Gaussianity in the caging regime is not trivial. However, this timescale

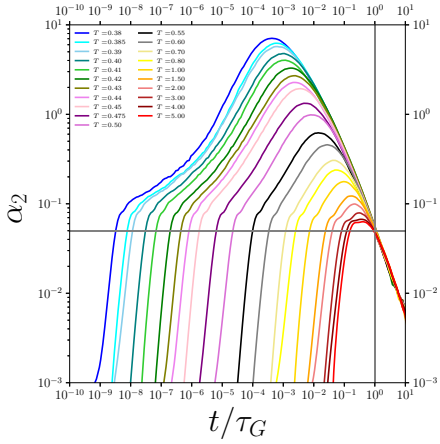

(a) 3KALJ

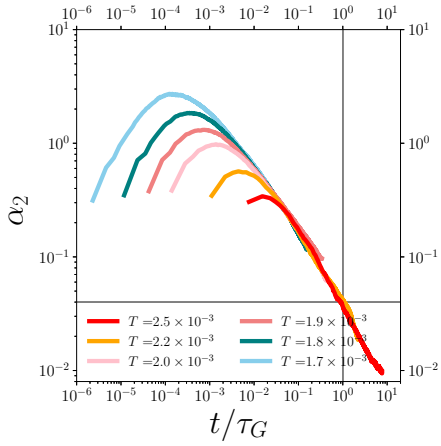

(b) 2SD

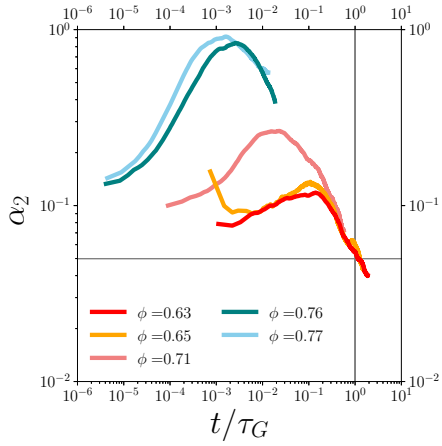

(c) 2HD

Figure 4.10. NGP as a function of the rescaled time t/τ_G for the three systems at different values of the thermodynamic control parameters.

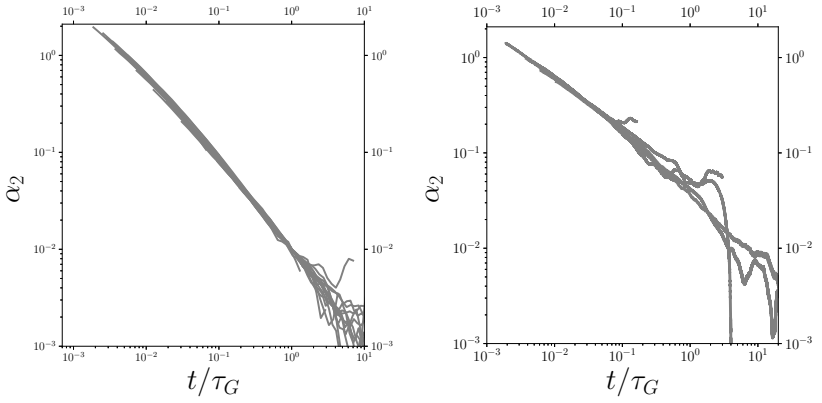

(a) 3KALJ **(b)** 2SD

Figure 4.11. NGP mastercurves as a function of the rescaled time t/τ_G in the range $t > \tau_F$ for the numerical systems.

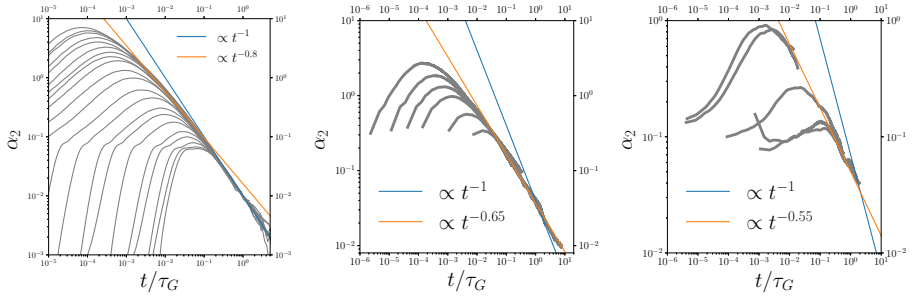

(a) 3KALJ **(b)** 2SD **(c)** 2HD

Figure 4.12. (a-c) NGP as a function of the rescaled time t/τ_G for the numerical systems, at different values of the thermodynamic control parameters. Solid lines are power-law function of the rescaled time.

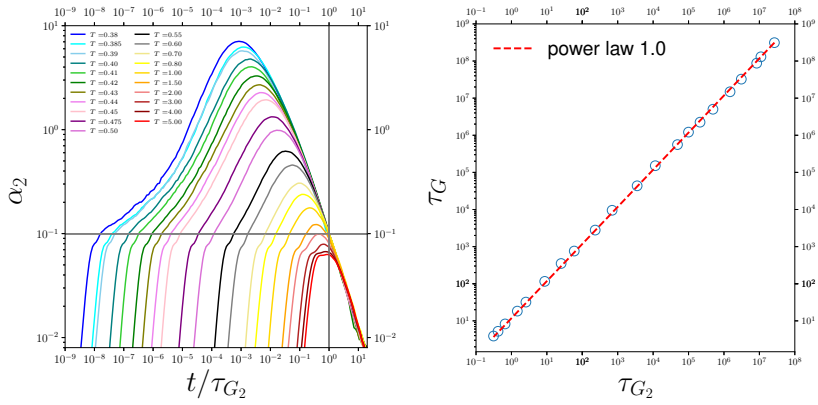

(a) 3KALJ **(b)** 3KALJ

Figure 4.13. (a) NGP as a function of the rescaled time t/τ_{G2} for KALJ system. (b) Scatter plot of τ_G vs τ_{G2}.

is out of the central scope of our investigation, being definitely not referring to *very* long time dynamics.

4.1.3 The Fickian non-Gaussian window

Figure 4.15 shows the area-fraction/temperature dependence of τ_F and τ_G, as measured trough the just described approaches, for experiments and simulations. For each 2d-system, the two timescales are well fitted by the same functional form: a power-law $A(\phi_c - \phi)^b$ (with a unique $\phi_c = 0.81$) for experiments, and an Arrhenius law $Be^{\frac{E}{T}}$ for simulations. In both systems, τ_G is always larger and increases faster than τ_F on approaching the glass transition, as indicated by the power-law exponents (in experiments) and the activation energies (in simulations) of τ_G being roughly twice those estimated for τ_F.

In the Kob-Andersen mixture, data cover a much wider range, from hot to highly supercooled conditions, and a crossover between two (approximately exponential) behaviours for both timescales is seemingly present (See Section 4.4 for further analysis). Hence, a single Arrhenius fit is not suited to fit data in the whole investigated range of investigate tempera-

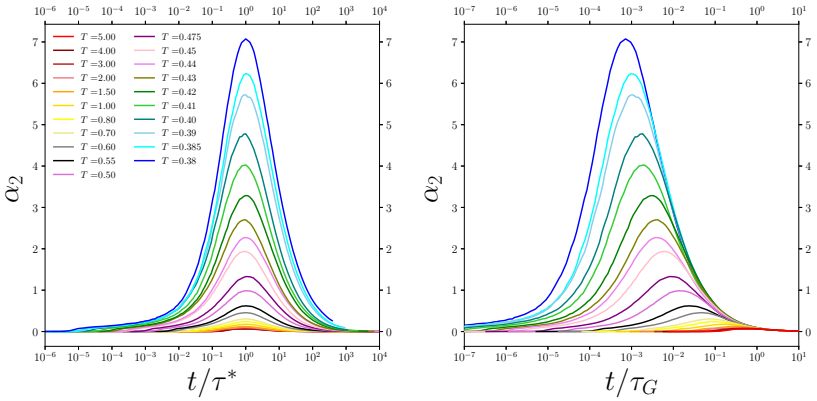

(a) 3KALJ **(b)** 3KALJ

Figure 4.14. NGP rescaled as a function of the rescaled time t/τ^* (a) and as a function of t/τ_G (b) in KALJ system at different values of the thermodynamic control parameters.

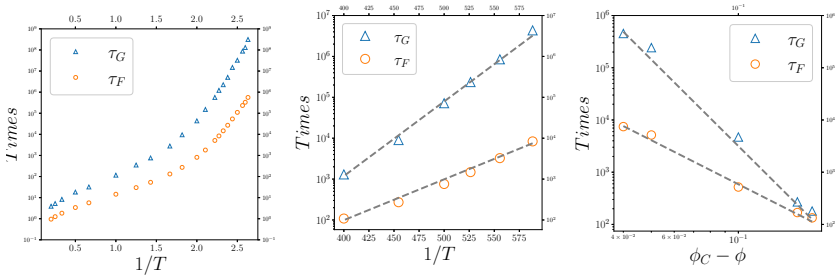

(a) 3KALJ **(b)** 2SD **(c)** 2HD

Figure 4.15. Gaussian τ_G and Fickian τ_F timescales as a function of the thermodynamic control parameter for the three systems. Dashed lines in panel (b) are Arrhenius fits $e^{\frac{E}{T}}$ with $E_F = 2.3 \times 10^{-2} \pm 3 \times 10^{-3}$ for τ_F and $E_G = 4.2 \times 10^{-2} \pm 3 \times 10^{-3}$ for τ_G. Dashed lines in panel (c) are fits through power-laws of $(\phi_c - \phi)$, with exponent $b_F = -2.8 \pm 0.2$ for τ_F and $b_G = -5.5 \pm 0.2$ for τ_G, and with a unique $\phi_c = 0.81 \pm 0.01$.

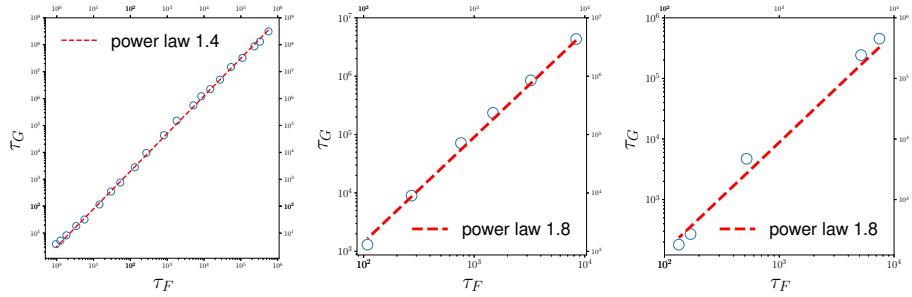

(a) 3KALJ **(b)** 2SD **(c)** 2HD

Figure 4.16. Scatter plot of τ_F VS τ_G for the three systems. Dashed lines are power-law fits.

tures. However, also in this case we confirm that τ_G is markedly larger and more steeply increasing than τ_F.

In both two-dimensional systems, the just presented behaviour implies that the two timescales are directly connected by a power-law relation, $\tau_G \propto \tau_F^{\gamma}$ (as demonstrated in Fig. 4.16.b-c). In fact, a unique value of the exponent, $\gamma = 1.8$, is found for both 2-dimensional systems. Surprisingly, also in KALJ system, in which a crossover in the dynamics seems to be present, τ_G and τ_F are connected by a unique power law relation, with an exponent $\gamma = 1.4$ (Fig. 4.16.a).

Figure 4.17 shows that the Gaussian length ξ_G markedly grows on approaching the glass transition (while the Fickian length, ξ_F, is constant).

Overall, figures 4.16 and 4.17 clearly demonstrate that FnGD exists in all the examined systems, and spans increasingly larger time- and length-scales on approaching the glass transition.

4.2 FnGD and dynamics in reciprocal Fourier-space

To have a complementary perspective on FnGD, we probe the dynamics through the Intermediate Self Scattering Function (ISSF) $F_s(\lambda, t)$ at different wave-lengths λ.

In Fourier space, the hallmarks of standard Brownian diffusion (both Fickian and Gaussian) are a pure exponential shape of the ISSF, i.e.

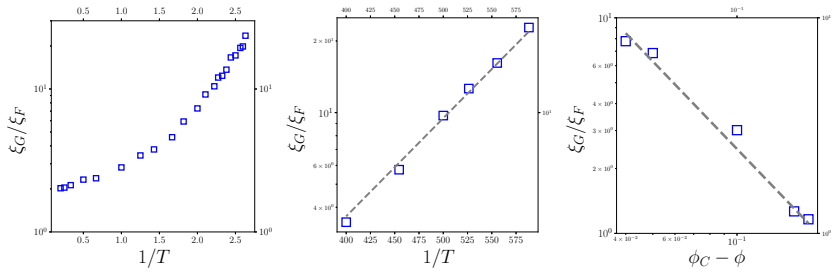

(a) 3KALJ **(b)** 2SD **(c)** 2HD

Figure 4.17. Gaussian length-scale ξ_G rescaled by the Fickian length ξ_F as a function of the thermodynamic control parameters for the three systems. Dashed line in panel (b) is an Arrhenius law $\xi_G \propto e^{\frac{E_G - E_F}{2T}}$. Dashed line in panel (c) is a power-law $\xi_G \propto (\phi_c - \phi)^{\frac{b_G - b_F}{2}}$.

$F_s(\lambda, t) = e^{-t/\tau_B(\lambda)}$[83] and a wavelength-dependent relaxation time given by $\tau_B(\lambda) = \frac{\lambda^2}{4\pi^2 D}$. It is interesting to check how these features change and/or decouple when FnGD is present.

We report in Fig 4.18 the ISSFs for both experimental and numerical systems computed at the Fickian length-scale, $\lambda = \xi_F \simeq \lambda^*$, as a function of the non-dimensional time $\frac{t}{\tau(\xi_F)}$, $\tau(\xi_F)$ being the ISSF relaxation time at the probing length ξ_F[2]. In the linear-log representation (Fig. 4.19, a and b) a straight line corresponds to an exponential decay $e^{-\frac{t}{\tau}}$, which should be expected for $t > \tau_G$. For $\tau(\lambda) < \tau_G$, conversely, the observed non-Gaussian shape of the displacement distribution turns out to be mirrored into a stretched exponential ISSF decay, $e^{-(\frac{t}{\tau(\lambda)})^{\beta(\lambda)}}$, with $\beta(\lambda) < 1$.

ISSFs clearly show stretched behaviour for $\tau(\lambda = \xi_F) < \tau_G$ (and in particular for $t \simeq \tau$)[3]. Data clearly indicate that the degree of non-exponentiality (and, hence, non-Gaussianity in the van Hove) increases

[2]For all systems, we fitted the late-time decay of the ISSF computed at a fixed wave-length λ with a Kohlrausch-Williams-Watts stretched exponential law $e^{(\frac{t}{\tau(\lambda)})^{\beta(\lambda)}}$ and extracted the relaxation time $\tau(\lambda)$ and the stretching exponent β. The so obtained relaxation time closely coincides with the value $\tau_e(\lambda)$ obtained from the relation $F_s(\lambda, \tau_e(\lambda)) = 1/e$.

[3]β exponents computed via stretched exponential fits lie in the range $0.5 - 0.75$ for 2DS and 2HS systems and $0.5 - 0.95$ for KALJ system.

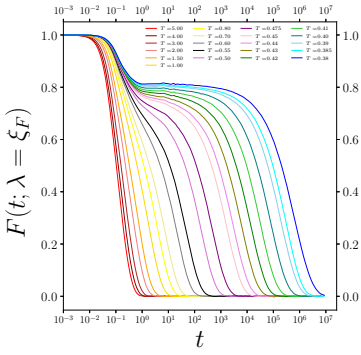

(a) 3KALJ

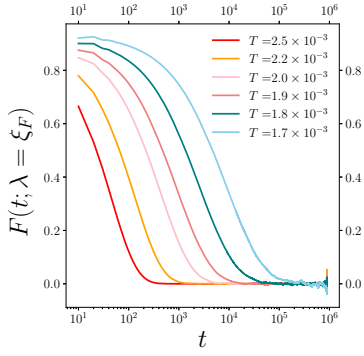

(b) 2SD

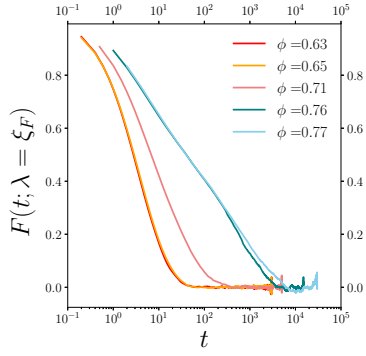

(c) 2HD

Figure 4.18. ISSF computed at wavelength $\lambda = \xi_F$ as a function of time for the three systems at different values of the thermodynamic control parameters.

as glass transition is approached.

Hereafter, we will focus on the wavelength-dependence of the relaxation time $\tau(\lambda)$ for wavelengths $\lambda \geq \xi_F$ only, i.e. where Fickian behaviour is at play in the real-space. We further stress that, since in our systems $\xi_F \simeq \lambda^*$, $\tau_\alpha \equiv \tau(\lambda^*)$ is around the lower boundary of the $\tau(\lambda)$-range investigated here.

In order to clarify the effect of increasing the wavelength λ, Fig. 4.20.a, shows the ISSFs for KALJ system at $T = 0.45$ and for different values of λ. The figure clarifies that, for very large λ's, the relaxation becomes less stretched, the plateau disappears, and pure exponentiality is gained on the Gaussian probe length (i.e., at $\lambda \simeq \xi_G$). Of course, for $\lambda < \xi_F$ dynamics becomes even more heterogeneous[4].

For any λ value, in principle, relaxation must eventually revert to a simple exponential at very large times, ($t > \tau_G$). However, for small λ, such transition to a pure exponential occurs at very low values of the correlation function. For small enough λ (i.e. when $\tau(\lambda) \ll \tau_G$), the transition, in fact, becomes no more detectable, since it occurs when the ISSF has already vanished within the statistical noise. Figure 4.20.b should help clarify this point: the figure shows the ISSF for $\lambda = \xi_F$ as a function of t/τ_G. At relatively short times, the relaxation is clearly non-exponential (panel a). The restoring of exponentiality should be observed on a longer timescale ($t/\tau_G = 1$), but it is, in fact, completely masked by the noise (panel b). Indeed, the ISSF has vanished within the noise already for $t/\tau_G = 0.2$ for $\lambda = \xi_F$, hence the transition towards exponentiality cannot be detected. In our systems, in fact, we confirmed the occurrence of a simple exponential decay of the ISSF as far as $\tau(\lambda) > \tau_G$.

Fig. 4.21 shows $\tau(\lambda)/\tau_B(\lambda)$ vs λ/ξ_G for 2D simulations and experiments. We find all datasets to collapse onto a single master-curve which smoothly decreases on increasing λ/ξ_G, and attains a unitary plateau, corresponding to standard-Brownian scaling, just around $\lambda/\xi_G = 1$. Notice that small λ/ξ_G values hint at a strong FnGD regime[5]: in fact, the range $\lambda/\xi_G < 0.5$ is covered by simulations only, whereas experimental data start

[4]Notice that an apparent purely exponential eventually sets in also at very small λ, $\lambda \gg \xi_F$. This limit corresponds to the very short-time ballistic dynamics (β-relaxation). In this case α-relaxation is shifted on very low values of the correlation function, and, in fact, not visible in semilog-scale.

[5]The existence of small values λ/ξ_G implies $\xi_G \gg \xi_F$.

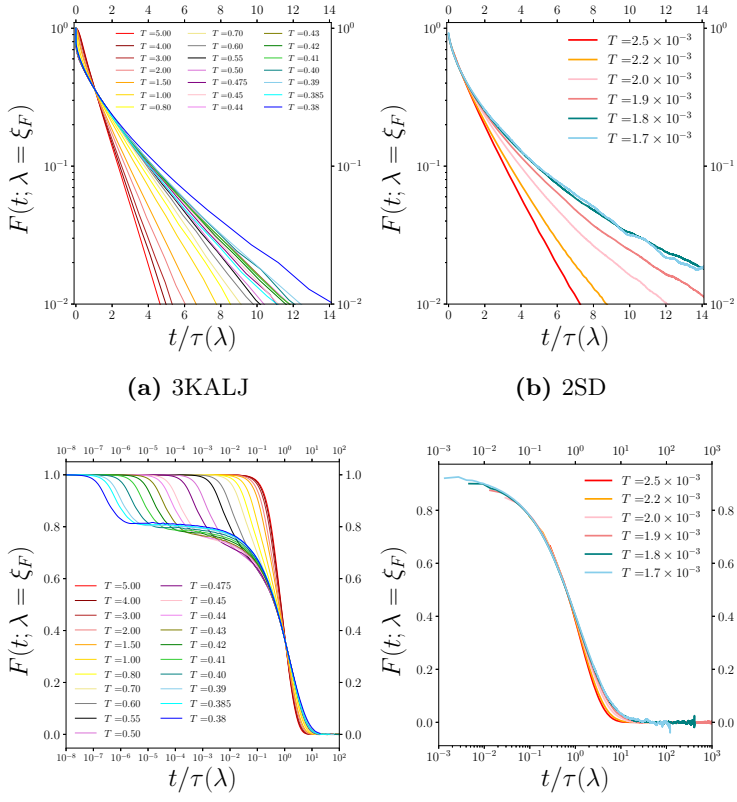

(a) 3KALJ **(b)** 2SD

(c) 3KALJ **(d)** 2SD

Figure 4.19. ISSF computed at wavelength $\lambda = \xi_F$, plotted as a function of the rescaled time $t/\tau(\lambda)$ for numerical systems.

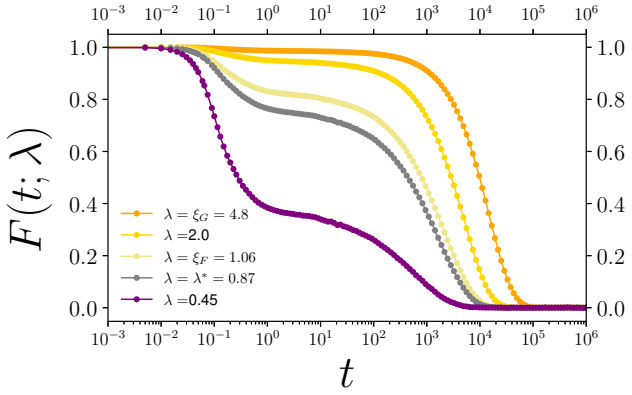

(a) 3KALJ

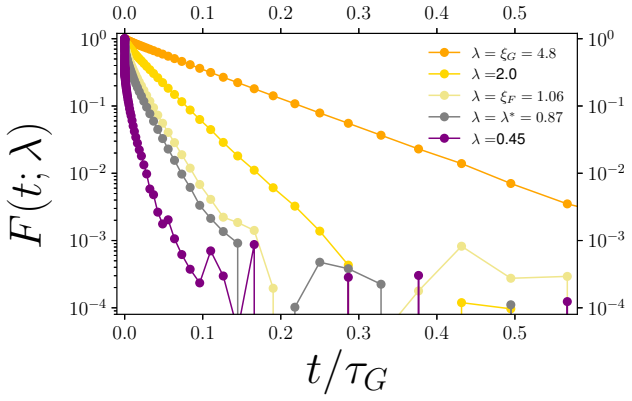

(b) 3KALJ

Figure 4.20. (a) ISSF computed at different wavelengths λ as a function of time, for KALJ sytem at temperature $T = 0.450$. (b) ISSF computed at different wavelengths λ, as a function of the rescaled time t/τ_G for KALJ sytem at temperature $T = 0.450$.

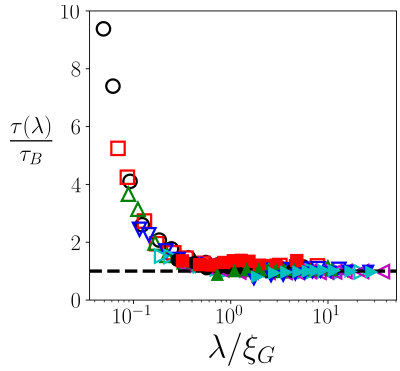

(a) 2DS+2HS

Figure 4.21. $\tau(\lambda)/\tau_B(\lambda)$ as a function of λ/ξ_G for 2DS (empty symbols) and 2HS (full symbols) systems at different values of the thermodynamic control parameter.

close to the plateau.

It should be remarked that the behaviour of τ/τ_B at small λ/ξ_G implies that the product $D\tau(\lambda)$ does depend on temperature. Such a Stokes-Einstein Breakdown (SEB) is commonly reported in systems approaching the glass-transiton, for wavelengths close to the first peak of the static structure factor, and is ascribed to the presence of marked DHs [35]. Fig. 4.22 shows that, in soft disks simulations, SEB is about a factor 7 at the lowest temperature and for $\lambda = \xi_F$, indicating that DHs are strongly at play when the dynamics is probed at the Fickian length-scales. Conversely, at a wavelength corresponding to the lowest-temperature Gaussian length, $\xi_G(T_{min})$, the Stokes-Einstein behaviour is fully recovered over the whole temperature range, suggesting that DHs are averaged out on this probe-length. We will further discuss the analysis of the Stokes-Einstein breakdown in all three investigated systems in Section 4.4.

Overall, we can conclude that the recovery of *both* the standard-Brownian features in Fourier space is *solely* ruled by the Gaussian scale: the stretched-exponentiality of ISSF and the λ-dependence of its relaxation time remain coupled throughout FnGD.

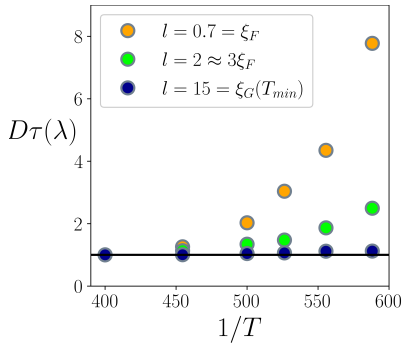

(a) 2SD

Figure 4.22. Product $D\tau(\lambda)$ for three values of the probing length λ in soft disks simulations. Data have been rescaled for the values at the highest temperature.

4.3 Characterization of the deviations from Gaussianity

Figure 4.23 show the displacement distributions[6] for all the investigated systems at representative values of the thermodynamic control parameter and for many non-dimensional times t/τ_G with $t \geq \tau_F$, i.e. within the FnGD regime. To properly compare the distributions at different times, we have rescaled the axes as follows: $x \to X = \frac{x}{\sqrt{\langle x^2(t)\rangle}}$, and $p(x,t) \to P(X,t) = p(x,t)\sqrt{\langle x^2(t)\rangle}$, thus preserving normalization. It is worth noticing that the standard Gaussian distribution $g(x,t) = \frac{e^{-\frac{x^2}{4Dt}}}{\sqrt{4\pi Dt}}$ becomes, after this rescaling, a universal time-independent master-curve: $G(X) = \sqrt{\frac{2}{\pi}} e^{-\frac{X^2}{2}}$.

The distributions in Fig. 4.23 always display an excess probability with respect to $G(X)$ both at small and large values of X, 'compensated' by a defect probability at intermediate displacements. At large displacements and short times ($t/\tau_G < 0.1$), tails are well fitted by exponential decays

[6] $p(x,t)$ is computed over both the $x-$ and $y-$ and $z-$ component of displacements, since systems are isotropic.

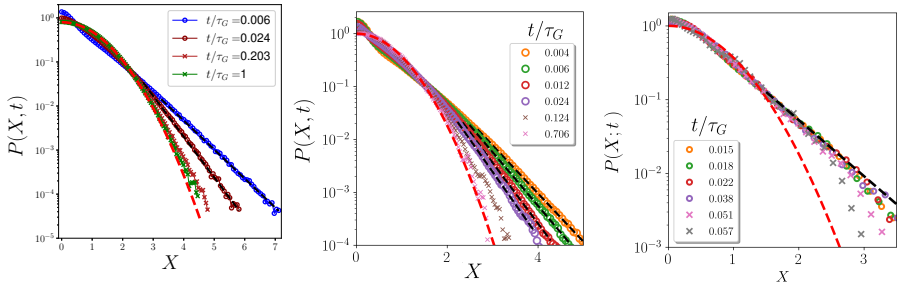

(a) 3KALJ **(b)** 2SD **(c)** 2HD

Figure 4.23. Rescaled van Hove function $P(X,t)$ as a function of X at different times for KALJ system at $T = 0.43$ (a), for 2DS system at $T = 0.0018$ (b) and for 2HS experiments at $\phi = 0.77$ (c). The red dashed lines are the universal Gaussian distribution $G(X)$.

$\simeq e^{-\frac{X}{L(t)}}$ over at least two orders of magnitude of probability values; the non-dimensional decay length L shows a continuous decrease within this time-range. Such an initial smooth change in L is then followed by the restoring of Gaussianity for the distribution function, which is fully attained in the numerical examples, consistently with the simulations time eventually reaching the estimated τ_G at those temperatures.

4.3.1 Exponential decay of the displacement distribution tails

We monitored the temporal evolution (withn the FnG window) of the non-dimensional exponential decay length L, and the corresponding dimensional length $l = L\sqrt{2dDt}$, in all the investigated systems and for all choices of the thermodynamic control parameters (e.g. Fig. 4.24). This type of analysis is commonly reported in literature on FnGD [6, 7, 9, 65].

Let us now separately discuss numerical and experimental systems. It proves convenient here to start from simulations. Figures 4.25.a and b show the non-dimensional length L in the FnGD regime at all temperatures, in the time-range where exponential fits to the tails are reliable. L data at

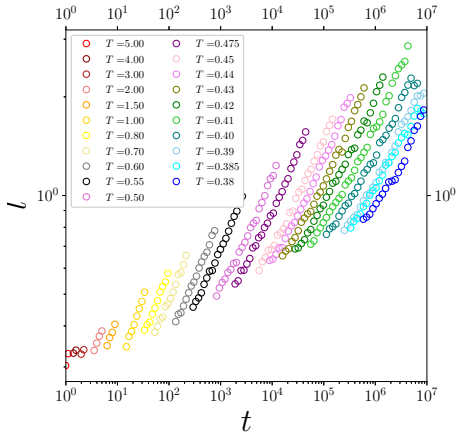

(a) 3KALJ

Figure 4.24. The exponential decay length l as function of time in the range $\tau_F(T) \leq t \geq 0.3\tau_G(T)$, for KALJ system at different temperatures.

all temperatures do collapse onto a power-law decrease:

$$L = C\left(\frac{t}{\tau_G}\right)^{-\zeta}, \tag{4.1}$$

C being a unique constant and $\zeta = 0.17 \pm 0.02$. Some deviations from this collapse are only observed at the highest temperature and large times, where, however, the fits to the distribution tails are less robust. Notice that, at high temperature, the recovery of Gaussianity is relatively rapid and exponential tails become quickly limited to a small X-range (see Fig. 4.26.a). The occurrence of this master-curve not only points out the power-law dependence of L upon time t/τ_G, but also highlights that the effect of changing temperature is fully captured by the T-dependence of τ_G. Notice that the first point in each dataset in Fig.d corresponds to the ratio τ_F/τ_G as its abscissa. Since such ratio decreases on lowering the temperature (see Fig. 4.16), $L(\tau_F/\tau_G)$ is larger at lower temperatures, i.e. the exponential tails are more extended. In other words, on approaching the glass transition, FnGD becomes not only more time-persistent, but also more marked.

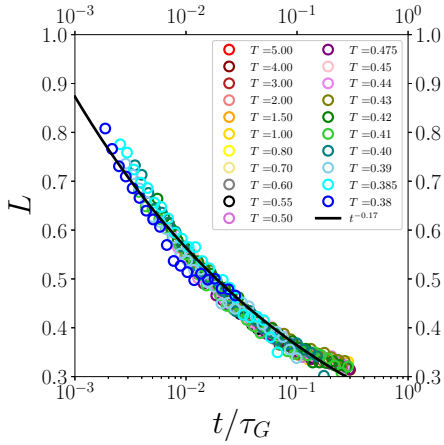

(a) 3KALJ

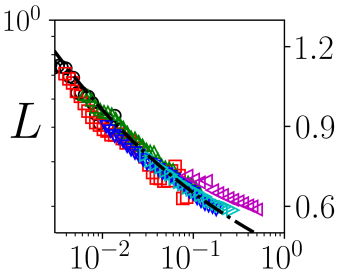

(b) 2SD

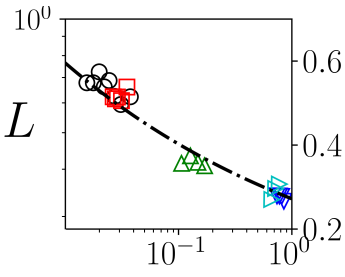

(c) 2HD

Figure 4.25. The rescaled exponential decay length L as function of t/τ_G (starting from $t = \tau_F$), for the three systems at different values of the thermodynamic control parameters. The black dashed line is a power law $\propto (t/\tau_G)^{-0.67}$.

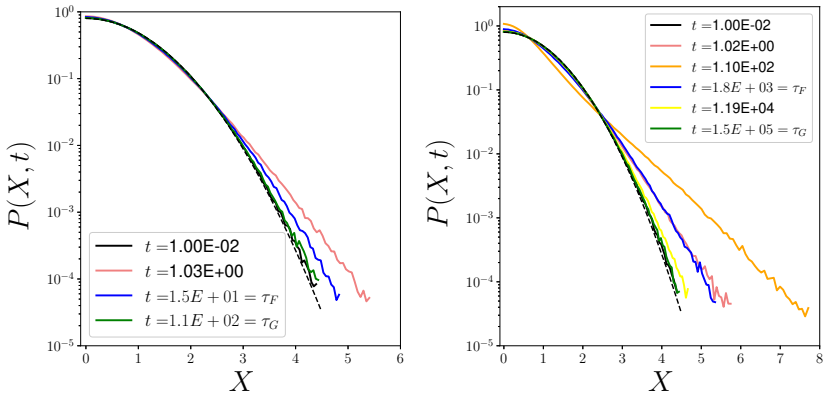

(a) 3KALJ **(b)** 3KALJ

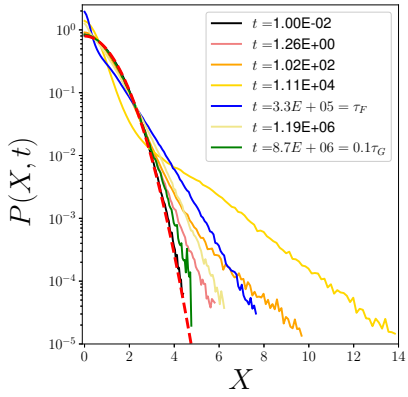

(c) 3KALJ

Figure 4.26. Rescaled van Hove function $P(X,t)$, as a function of X at different times for KALJ system at $T = 1.00$ (a), $T = 0.50$ (b), $T = 0.39$ (c). The red dashed lines are the universal Gaussian distribution $G(X)$.

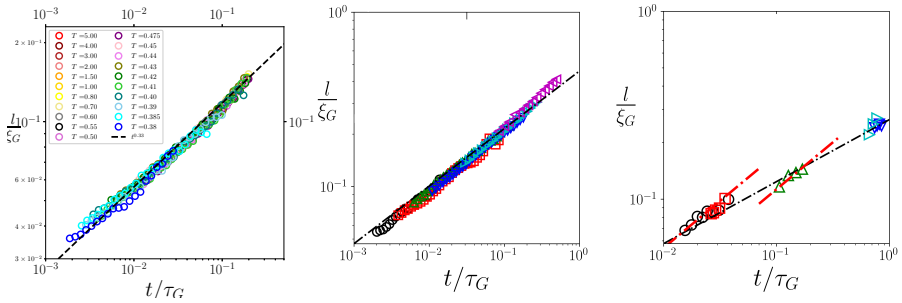

(a) 3KALJ **(b)** 2SD **(c)** 2HD

Figure 4.27. The rescaled dimensional exponential decay length l/ξ_G as function of t/τ_G (starting from $t = \tau_F$), for all systems, at different values of the thermodynamic control parameters. The black dashed line is a power law $\propto (t/\tau_G)^{0.33}$. Red dashed lines are $\propto (t/\tau_G)^{0.5}$.

Let us now separately discuss numerical and experimental systems. It proves convenient here to start from simulations. The just found behaviour for L implies that, at any temperature, the dimensional decay length l increases as a power-law of time with an exponent $\alpha = 0.5-\zeta = 0.33\pm0.02$, which is different from the value 0.5 commonly reported in FnGD [6, 7, 9]. In addition, from Eq.4.1, data corresponding to different temperatures will of course collapse onto a single power-law, when plotted as $l(t)/\xi_G$ versus t/τ_G (Fig. 4.27).

We now turn to experimental distributions, as the ones shown in Fig. 4.25 and Fig. 4.27. Seemingly, here, at small t/τ_G, the tails of the distributions nearly collapse onto an exponential decay with a unique L; for larger t/τ_G, evolution towards the Gaussian mastercurve is observed. Full restoring of Gaussianity is however far from being attained here, consistently with the fact that the estimated $\tau_G \approx 5 \times 10^5 s$ at this area fraction is significantly larger than the total observation time $t = 3 \times 10^4 s$. At lower area fractions, we find the same qualitative scenario, with less persistent and weaker deviations from $G(X)$, consistently with the behaviour of the NGP (Fig. 4.10).

A comparison of Fig. 4.27 a-b and c may suggest a different behaviour of the exponential decay length, with $L \simeq const$ for experiments, but

depending on time in simulations (see Eq.4.1). Such difference should be carefully reconsidered, however, in the light of the relatively narrow ranges of times and probability available for the colloidal system. Indeed, in our experiments, t/τ_G for each concentration spans less than a decade, and probabilities are reliable down to 10^{-3}, at most. In simulations, by contrast, the range of t/τ_G for each temperature exceeds two decades, and probabilities are fairly-well sampled down to 10^{-4}. Thus, our observation of a nearly constant L may simply be due to limited experimental data. As a matter of fact, experimental data for L and l/ξ_G as functions of t/τ_G, reported in Fig., display collapses and scaling exponents that are compatible (at least) with those found in our simulations.

However, the limited experimental datasets leave open the possibility that these scalings may be system-dependent, as suggested in a recent study [65], whose results are analyzed in details and questioned in next Section 4.3.2. In this perspective, we notice that, at a single area fraction, data can be described equally well by "local fits" with exponents $\alpha = 0.33$ or $\alpha = 0.5$ (Fig. 4.28), but a "global fit", i.e. for all area fractions, with this latter power-law will patently fail, at variance with what is found for the exponent $\alpha = 0.33$. In Fig. 4.27 we have made a comparison between a "global" fit (i.e. for experiments at all area fractions) with $\alpha = 0.33$ vs two "local fits" (i.e. for single area fractions) with $\alpha = 0.5$. In order to make a "homogeneous comparison" between the two power laws, we also report in 4.28 the results for local fits with $\alpha = 0.33$. Indeed, we fit two of our datasets (with different prefactors for different area fractions) with 0.33 and 0.5 power-laws. We do find a very similar quality of the fittings. Precisely, the R-squared values are as follows: i) $\phi = 0.71$, $R^2 = 0.905$ and 0.890 for $\alpha = 0.5$ and 0.33, respectively; ii) $\phi = 0.77$, $R^2 = 0.931$ and 0.936 for $\alpha = 0.5$ and 0.33, respectively. Thus, from a single set of our experimental data, no sharp conclusion concerning the exponent can in fact be drawn. The global fitting, as reported in Fig. 4.27.c, is instead evidently in favour of the $\alpha = 0.33$ power-law.

4.3.2 Does tails behaviour depend on dimensionality?

In a recent article [Miotto et al., Phys. Rev. X **11**, 031002 (2021)], dealing with FnGD in glass-forming liquids, it is claimed that exponential tails of the displacement distribution are characterized by a *non-universal*

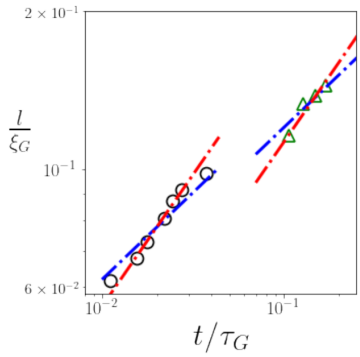

(a) 2HD

Figure 4.28. Rescaled decay length $l(t)/\xi_G$ of the tails of the displacement distribution as a function of t/τ_G, for experiments at two different area fractions,$\phi = 0.71$ (triangles) and 0.77 (circles). The red lines are local power-law fits $l(t) \propto t^{0.5}$, coinciding with those in Fig. 4.27 of the main text. The blue lines are local power-law fits $l(t) \propto t^{0.33}$.

time-dependence of the decay length $l(t)$.

Going in more detail, Miotto and co-workers claim that, in the FnGD of glass-forming liquids, $l(t)$ displays a behavior that is *non-universal*, but depends on system features, such as dimensionality d or the inter-particle potential. In the specific case of the paradigmatic Kob-Andersen model, they claim that $l(t) \propto t^{1/d}$, and further speculate that this behaviour can be generally extended to the whole class of glass-forming liquids with isotropic potential.

Concerning the time-dependence of $l(t)$, we have showed in the previous section that in our glass-formers $l(t) \propto t^{1/3}$ holds, not only for the 3d KALJ system, but also for both our 2d systems (which does not agree with the proposal by Miotto and co-workers), In this section, we try to reconcile such an apparent contrast, by re-analysing the KALJ data provided in that article.

We start by examining the data in Miotto et al. [65] for the displacement distributions $p(r,t)$ at various times, and at temperatures $T = 0.45$ for the $3d$ case and $T = 0.40$ for the $2d$ case, respectively[7]. (We notice

[7] We have normalized raw data from [65] of $p(r,t)$ in the usual way, $\int p(r,t) r^{d-1} dr =$

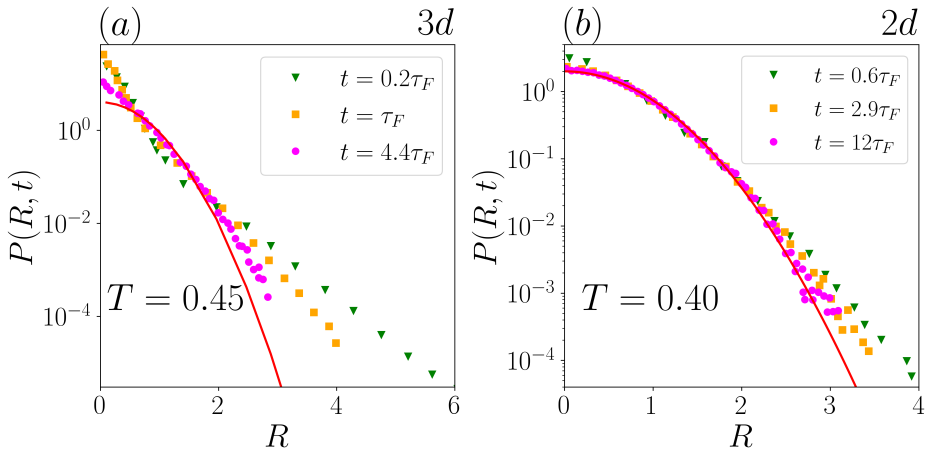

Figure 4.29. Non-dimensional distributions of particle displacements at different times, for $3d$ KALJ system at temperature $T = 0.45$ (a) and for $2d$ KALJ system at $T = 0.40$ (b). (Data from Fig. 1.c and d in Ref. [65].) The red lines are the universal Gaussian distribution $G(R)$. Times in legend are reported in units of the characteristic onset time of Fickian diffusion τ_F.

as an aside that the model studied in [65] is the standard KALJ, not the modified one considered in our work. Results for the two models do coincide at $T > 0.45$, i.e. the regime investigated by Miotto et al., while at lower temperatures the standard model presents crystallization at long times.) The adopted rescaling in Fig.4.29 allows to clearly highlight deviations from Gaussianity and their time-evolution, and also to compare displacement distributions pertaining to different systems [7, 6, 62]. Times are reported in units of $\tau_F(T) = \frac{\sigma^2}{2dD(T)}$, an estimate of the onset time of the Fickian regime, with σ the particle diameter,

The figure shows that, within the late sub-diffusive and early Fickian

1. In Fig. 4.29, we rescaled the data by defining $R = \frac{r}{\sqrt{\langle r^2(t)\rangle}}$, and $P(R,t) = p(r,t)\langle r^2(t)\rangle^{d/2}$, where $\langle r^2(t)\rangle = \int r^2 p(r,t) r^{d-1} dr$ is the mean square displacement. Notice that, with this rescaling, the standard Brownian-Gaussian distribution $g(r,t) = e^{-\frac{dr^2}{2\langle r^2(t)\rangle}} (\frac{d}{2\pi\langle r^2(t)\rangle})^{d/2}$ becomes a time-independent curve: $G(R) = (\frac{d}{2\pi})^{d/2} e^{-dR^2/2}$. We will not consider distributions at deep pre-Fickian times, either in the ballistic or in the early sub-diffusive regime shown in [65].

regime, the displacement distributions exhibit exponential tails $\propto e^{-R/L(t)}$ in both $3d$ and $2d$ systems (panels a and b, respectively), with a monotonic decrease of $L(t)$ in time. We emphasize that, under the adopted representation, the presence of tails with different slopes unequivocally implies that the dimensional decay-length $l(t) = L(t)\sqrt{\langle r^2(t)\rangle}$ does not scale as $t^{0.5}$, for both systems. This simple observation already questions the main conclusion by Miotto et al. on the $2d$-KALJ system.

A noticeable difference between the two panels of Fig. 4.29 is that all the distributions show clear exponential tails in the $3d$ system, whereas, in the $2d$ system, the displacement distribution at the longest available time, $t \simeq 10\tau_F$, seems to have reached the Gaussian limit, being in fact indistinguishable from the Gaussian mastercurve. This difference is simply due to the time-window spanned for the $3d$ system being smaller, in terms of t/τ_F, than for the $2d$ system.

As a direct consequence of the already completed Gaussian recovery for the $2d$ system at $t \simeq 10\tau_F$, any exponential fit to the tails of $p(r,t)$ for $t \geq 10\tau_F$ is definitely unreliable. All those fits in Ref. [65] should actually be considered as very local fits to what in fact are Gaussian distributions[8]. The conclusion that, for the $2d$ system at $T = 0.40$, the exponential fits to $p(r,t)$ for $t \geq 10\tau_F$ are definitely unreliable can certainly be extended to higher temperatures. By contrast, the same conclusion cannot be blindly extended to lower temperatures since, on cooling, the timescale for recovering Gaussianity grows more steeply than the time τ_F for the onset of Fickian diffusion, as we will discuss later on. Moreover, since the exponential-to-Gaussian crossover is a smooth process, exponential fits are expected to become inadequate *quite earlier* than the complete Gaussian recovery. Thus, the exponential fits at $T \geq 0.40$ cease to be reliable way before $t = 10\tau_F$: we can safely assume $t \simeq 10\tau_F$ as an indicative upper-boundary for meaningful exponential fits.

To quantitatively characterize the temporal evolution of the decay-length of the exponential fits, we now draw our attention on the behaviour of $l(t)$. Also in this case, we exclude the deep pre-Fickian regime and limit the range of considered times to the very late subdiffusive and the Fickian regimes. Firstly, we focus on the same two systems of Fig. 4.29: the

[8] Notice that, in figure 1d of Ref. [65], the impropriety of late exponential fits is partly hidden by the adopted scale.

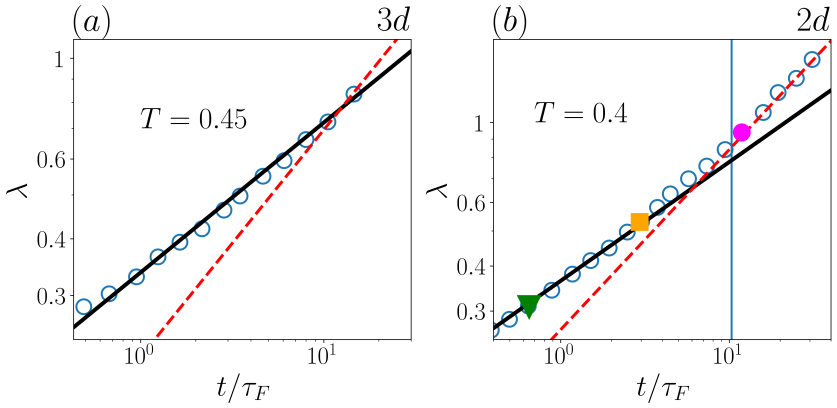

Figure 4.30. Decay length l as a function of t/τ_F in $3d$ (a) and $2d$ (b) KALJ systems, for different temperatures, as indicated in legends. (Data from Fig. 1.e, f in Ref. [65].) Black solid lines are power-law $\propto t^{0.33}$, red dashed lines are power-law $\propto t^{0.5}$. The vertical blue line indicates the time $t/\tau_F = 10$ at which the displacement distribution for $2d$ KALJ at $T = 0.40$ has already and clearly reached Gaussianity, as inferred from Fig.1b. The three points in panel b with different color and marker-style correspond to the distributions displayed Fig. 4.29.b.

exponential decay length is reported in Fig. 4.30, as a function of t/τ_F. $l(t)$ has the same behaviour in both $3d$ and $2d$ systems (panel a and b, respectively) over around the first decade in t/τ_F. In this range, including the early Fickian regime, the exponential tails of the displacement distributions are clear-cut, and the time-dependence of $l(t)$ is well captured by a $t^{0.33}$ power-law in both panels. We notice as an aside that this behaviour is already well established in the late sub-diffusive regime ($t/\tau_F < 1$).

For the $2d$ system (panel b), where data are available up to quite long time, $l(t)$ shows a clear crossover to a $t^{0.5}$ scaling around $t/\tau_F = 10$. As previously noticed, however, exponential fits for this system are definitely not reliable for $t/\tau_F \geq 10$, and therefore all data corresponding to this time-range in Fig. 4.30 must be disregarded. This consideration implies that the long-time "regime", $l(t) \propto t^{0.5}$, is an artifact arising from the fitting protocol adopted in Ref. [65], which does not take into account any time-boundaries for the presence of exponential tails. Incidentally, we notice that the missing identification of such boundaries is also evident on the short-time side: indeed, data for the exponential decay length $l(t)$ in Fig.1 e and f in [65] include the short-time ballistic regime, even though this latter is known to be characterized by Gaussian displacement distributions [37].

At variance with the $2d$ system (Fig. 4.30b), $3d$ simulations in Fig. 4.30a are too short-lasting to verify whether any clear deviation from the $l(t) \propto t^{0.33}$ behaviour emerges or not at long time. For this reason, in Fig. 4.31, we examine $l(t)$ for the $3d$ system at a temperature $T = 0.5$, slightly higher than the one considered in Fig. 4.30a. It is interesting to note, in fact, that comparing the dynamics in $3d$ at $T = 0.5$ with that in $2d$ at $T = 0.45$ is particularly appropriate, since these two systems are at similar "distance" from their respective Mode Coupling temperatures [167, 37, 168] and, therefore, similar dynamical features are expected. (An analogous consideration was made by Miotto et al. for choosing the temperature range displayed in their work.) For the $3d$ system at $T = 0.5$, the simulated dynamics is long enough (in terms of t/τ_F) to observe the same 0.33-to-0.5 power-law crossover in $l(t)$ found in $2d$ (Fig. 4.30.b), with the $t^{0.5}$ scaling stepping in charge at a similar time $t/\tau_F \simeq 10$.

Also in the $3d$ case, however, we argue that the long-time behaviour $l(t) \propto t^{0.5}$ is an artifact, again arising from exponential fits having been

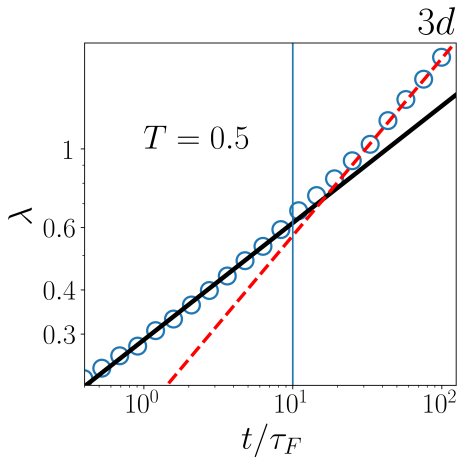

Figure 4.31. Decay length as a function of t/τ_F, in $3d$ KALJ system at temperature $T = 0.5$. (Data from figure 1e in Ref. [65].) Black solid line is a power-law $\propto t^{0.33}$; red dashed line is a power-law $\propto t^{0.5}$. The vertical line indicates the time $t/\tau_F = 10$.

performed in a (late) time-range, where Gaussianity of the displacement distributions has fully restored. This conclusion is supported by recent results on the non-Gaussian parameter for the same KALJ $3d$ system [27] at the same $T = 0.5$ temperature, showing that non-Gaussianity is already small at time $t/\tau_F \simeq 2$.

Performing the same analysis at different temperatures, both in $2d$ and $3d$, leads to similar conclusions (see Fig. 4.32 below for plots including all considered temperatures).

Overall, the same scenario emerges in $3d$ and $2d$: the only well-defined scaling for the decay length of the exponential tails is $l(t) \propto t^{0.33}$; both the crossover and the (apparent) ensuing scaling law $l(t) \propto t^{0.5}$ should be merely regarded as an indirect signal of the full restoring of Gaussianity.

The upper time limit of the $l(t) \propto t^{0.33}$ regime, in t/τ_F units, may in general depend on temperature. Indeed, in the emerging scenario, such time limit is controlled by the time for restoring of Gaussianity, whereas τ_F is a (lower) timescale related to onset of Fickianity: those two timescales do not necessarily have the same temperature dependence.

To address this issue, we re-analyzed the $l(t)$ datasets in $3d$ and $2d$ at

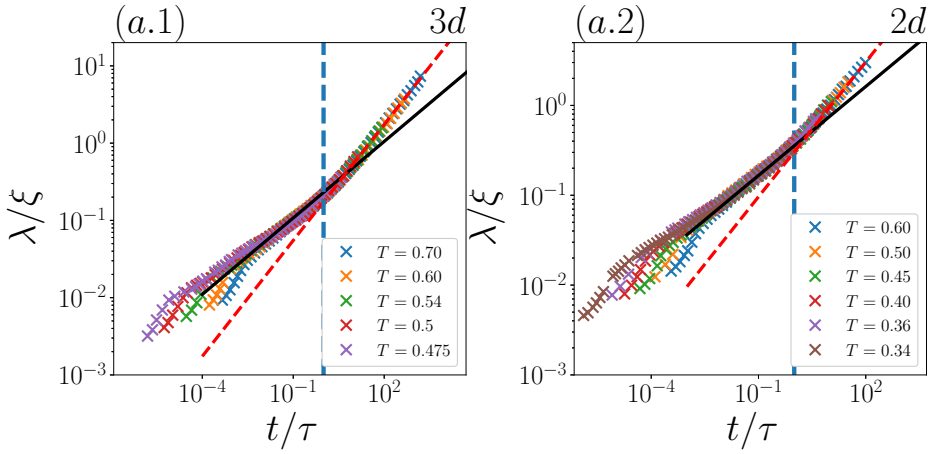

(a) KALJ

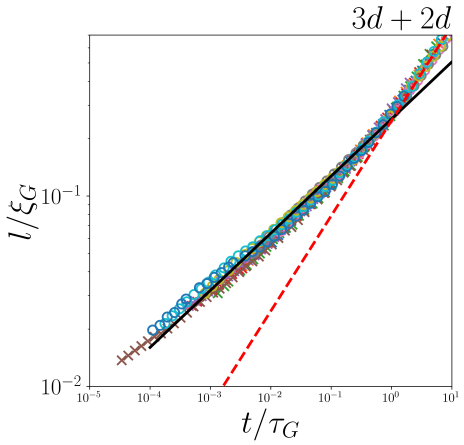

(b) KALJ

Figure 4.32. (a) Non-dimensional decay length l/ξ as function of non-dimensional time t/τ in $3d$ (a) and $2d$ (b) KALJ systems, and at different temperatures. (Data from figure 1 e and f of Ref. [65].) Black solid lines are power-law $\propto t^{0.33}$ and red dashed lines are power-laws $\propto t^{0.5}$. Vertical blue lines indicate $t/\tau = 1$. (c) Same data reported in the same plot.

many different temperatures included in Ref. [65]. In this case, we also consider short-time (very pre-Fickian) data. We rescale the abscissa of all l curves by a shifting factor τ. For each dataset, τ is selected so as to make the apparent crossover to occur at $t/\tau \simeq 1$. Once the τ values are identified, the vertical axis for each curve is rescaled by the *diffusion length* $\xi = \sqrt{2dD\tau}$ associated to the corresponding τ.

Using this rescaling, all data do collapse onto a single master-curve (apart from early-time deviations), as shown in Fig. 4.32 a and b, for the $3d$ and $2d$ system, respectively. These results clearly demonstrate that a common phenomenology - with a *unique* master-curve - arises for all systems, regardless not only of temperature, but also of space dimensionality, at odds with the main claim by Miotto et al. It is worth remarking that, by virtue of the τ-based rescaling procedure, the previously described power-laws become more clearly visible, now covering several time decades. Notice that early-time deviations from the master-curve are essentially limited to the very pre-Fickian regime, especially to the ballistic range, where they take a "comb-like" shape. As discussed above, measurement of an exponential decay length in this regime are likely artificial. Similarly, the long-time $t^{0.5}$ behaviour, present both in $3d$ and $2d$, comes from spurious late exponential fitting.

The *real* scaling characterizing exponential tails, $l(t) \propto t^{0.33}$, starts in the subdiffusive regime and persists in the early Fickian one (this latter being the true FnGD time-window), spanning more than four t/τ decades. In the emerging picture, the shifting factor $\tau(T)$ is the characteristic timescale for the disappearing of exponential tails and the recovering of Gaussianity (similarly to our τ_G). These findings are fully consistent with our results on 2d-systems (and, of course, on 3d-KALJ system).

The aforementioned similarities suggest the idea that the behaviour of the tails of the displacement distribution is universal near the glass transition, at least for systems with isotropic potential. Of course, other aspects of glassy dynamics, such as the caged particle motion, may show differences between $2d$ and $3d$, as indicated by a body of recent works, including Refs. [169, 170, 171, 172, 173]. However, the present results suggest that universal and non-universal behaviours may coexist, e.g. for different observables and/or on different timescales.

4.3.3 Mobile particles analysis

The formation of heavy tails in the displacement distribution is linked to the presence of a *certain amount* of particles that are markedly faster than the average. In this section, we precisely measure the extension (in terms of number of particles) of this sub-population[9].

When dealing with DHs in glass-formers, different definitions of fast (or *mobile*) particles have been proposed. In order to study the temporal evolution of this population, we set a threshold to identify particles that are faster than the average: we here define as *mobile* a particle that has moved more than δ times the root-MSD. This definition is well-grounded as long as δ is chosen in an appropriate way and large enough. A smart choice of this value can be readily made by inspecting the rescaled van Hove functions plotted as a function of $X = x/\sqrt{MSD}$ (Figs. 4.26 and 4.23). As previously noticed, it seems that "long"-time exponential behaviour is always at play for $X = x/\sqrt{MSD} > 2$ to 4 (and provided that $t \ll \tau_G$), thus a value of δ in this range might be a natural choice. Hence, this definition is different in spirit from other (time-independent) definitions of mobile particles present in literature [106].

The total number[10] of mobile particles is thus

$$N_{mm}(t) = \int_{\delta\sqrt{MSD}}^{\infty} p(x,t)\,dx = \int_{\delta}^{\infty} P(X,t)\,dX \tag{4.2}$$

In Fig. 4.33 we show $\tilde{N}_{mm}(t) \equiv N_{mm}(t)/N_G(t) - 1$, where N_G is the percentage of particles that has moved more than δ times the root-MSD in a Gaussian diffusion. In this case, the threshold is set to $\delta = 2$. The definition of $\tilde{N}_{mm}$ allows one to readily figure out the occurrence of rare events (large displacements) with respect to a Gaussian process.

It is not surprising that the behaviour of $\tilde{N}_{mm}$ closely resembles other DH indicators, as the NGP or the four-point correlation function χ_4: as glass transition is approached, $\tilde{N}_{mm}$ shows a higher and higher maximum at intermediate times, and decays to zero at very large times.

[9] This analysis has only been preliminarily performed on KALJ system, which is the largest available dataset in terms of number of particles, simulation length and explored temperature regimes. Hence, all data presented in this section pertain to this system.

[10] Since our distribution functions are normalized, we are, in fact, expressing N_{mm} in terms of percentages.

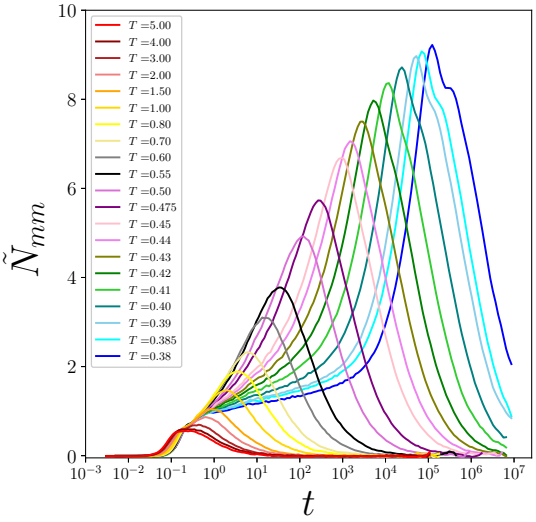

(a) 3KALJ

Figure 4.33. Rescaled number of mobile particle $\tilde{N}_{mm}$ as a function of time for KALJ system at different temperatures for a threshold $\delta = 2$.

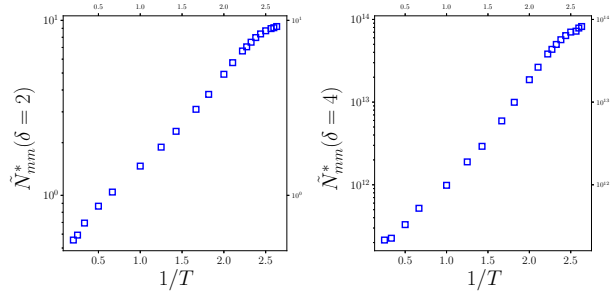

(a) 3KALJ **(b)** 3KALJ

Figure 4.34. Maximum $\tilde{N}^*_{mm}$ for KALJ system at different temperatures, for two different choices of the threshold, $\delta = 2$ (a) and $\delta = 4$ (b).

Intriguingly, the presence of a "shoulder" in $\tilde{N}_{mm}$ close to the maximum (and on its rightside) is recognized at very low temperature ($T < 0.42$). This latter feature indirectly indicates the appearance of some qualitative change in the shape of the displacement function for times close to the maximum of non-Gaussianity. However, this temporal regime is out of the central scope of our analysis.

In Fig. 4.34, we show the maximum N^*_{mm} of the rescaled number of mobile particles for two different choices of the threshold δ ($\delta = 2$ and $\delta = 4$). While showing rather similar temperature-dependence (this point is further clarified in Fig. 4.37), the two panels also indicate that the absolute value of N^*_{mm} increases by many orders of magnitude with increasing δ threshold. This effect might be primarily ascribed to the fact that $N_G \longrightarrow 0$ faster than N_{mm} as δ increases[11].

It is worth noticing that the growth of N^*_{mm} slows down at very low temperature $T < 0.42$. Further analysis are needed to determine whether this slowing corresponds to the approach of a saturation value (as it has been found also in this system for χ_4 [174]) on not (the NGP, conversely, does not show any saturation at low temperature, Fig. 4.35).

Finally, we investigate the connection with FnGD scales. In Fig. 4.36 we study the evolution of $\tilde{N}_{mm}$ as a function of the distance from the Gaus-

[11] The Gaussian function, indeed, decreases much more rapidly than the exponential decay that characterizes the tails.

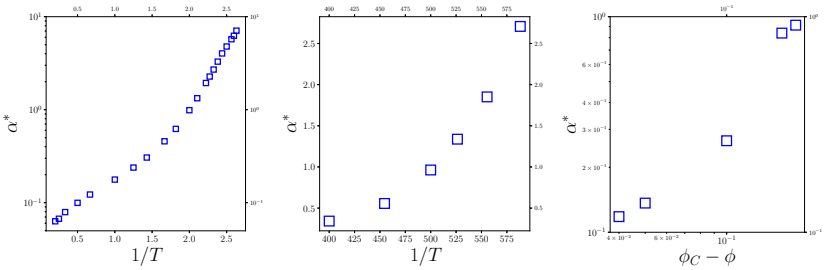

(a) 3KALJ **(b)** 2SD **(c)** 2HD

Figure 4.35. Maximum of the NGP α_2^* as a function of $1/T$ for numerical systems (a,b), and as a function of $\phi_C - \phi$ for experiments (c).

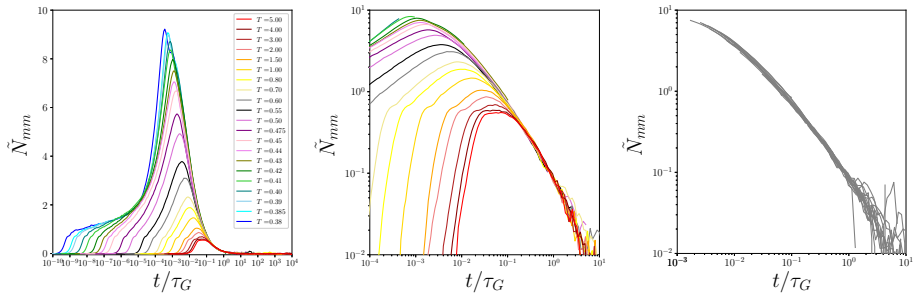

(a) 3KALJ **(b)** 3KALJ **(c)** 3KALJ

Figure 4.36. (a, b). Rescaled number of mobile particle $\tilde{N}_{mm}$ as a function of the rescaled time t/τ_G for KALJ system at different temperatures. (c) Mastercurve of $\tilde{N}_{mm}$ as a function of the rescaled time t/τ_G in the Fickian time-window $t > \tau_F$.

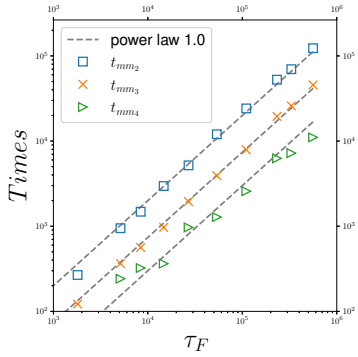

(a) 3KALJ

Figure 4.37. Scatter plot of the Fickian time τ_F vs the characteristic time of maximum extension of mobile clusters $t_{mm}(\delta)$, for various choices of the threshold: $\delta = 2, 3, 4$ (for $t_{mm2}, t_{mm3}, t_{mm4}$, respectively). Dashed lines are power-law guides to the eyes.

sian onset τ_G. It is emphasized that, the adopted time-rescaling leads to a clear data collapse in the long time tails of $\tilde{N}_{mm}$. This scaling, originally found for the NGP tails (see Figs. 4.10, **??** and 4.11), suggests that the long-time persistence of non-Gaussian deviations is mostly due to the presence of fast particles which, indeed, control higher moments of the displacement distribution (and, hence, the NGP).

By constrast, Fig. 4.37 instead demonstrates that the timescale to reach the maximum extension of mobile clusters $\tilde{N}^*_{mm}$ in the system, t_{mm}, is proportional to the Fickian timescale. This result agrees with the intuitive and widespread idea[35] that the onset of Fickian behaviour in glass-formers is controlled by faster particles. Fig. 4.37 also show that the absolute magnitude of t_{mm} depends on the chosen threshold. However, the temperature-dependence of t_{mm} depends on δ only weakly

4.4 Scaling laws and crossovers in single-particle long-time dynamics

In this section we compare all the investigated timescales, characterizing the early and late $\alpha-$relaxation of our glass-formers, and set them in

the framework of FnGD diffusion. Then, we summarize the scaling-laws identified in our study.

4.4.1 Comparison of fundamental timescales of long-time dyanmics

We start by showing all relevant timescales in Fig. 4.38 as a function of the thermodynamic control parameters in the investigated systems. The Gaussian timescale is the longest and, apparently, the steeply growing timescale in all investigated systems. We also confirm [142, 175, 33] that the Fickian timescale τ_F is always (and generally significantly) larger than the structural relaxation time τ_α. However, in both numerical systems data indicate an approach to a crossover at the lowest temperatures.

Indeed, the structural time is growing more than τ_F as glass transition is approached, as also shown in Fig. 4.39, which corresponds to a breakdown of Stokes Einstein relation (Fig. 4.40). Fig. 4.39 also shows that a power-law relation between the two times firmly holds for both numerical systems over the entire supercooled window. Deviations are of course present in KALJ system at very high temperature (*hot fluid* limit), where structural relaxation and self-diffusion are expected to be coupled and Stokes-Einstein relation holds. Experimental data are more lacking and scattered, but still compatible with the same power-law relation. However, the breakdown of Stokes-Einstein relation is not so evident (Fig. 4.40.c).

We compare, in Fig. 4.41, the structural relaxation timescale and the onset time of Gaussian diffusion τ_G. In KALJ system, two power-law regimes are clearly present: at higher temperatures, the Gaussian time markedly grows more steeply than τ_α, and $\tau_G \propto \tau_\alpha^{1.55}$; at $T = 0.50$ a crossover to a low-temperature $\tau_G \propto \tau_\alpha$ regime is present. Data on soft-disks system are compatible with the presence of such a crossover, while more experiments at different area fractions are necessary to clarify this point in the colloidal system.

The low temperature linear relation between τ_α and τ_G found in KALJ is not trivial since structural relaxation in supercooled liquids is often considered to be controlled by very slow particles [35, 176]. However, Fig.s 4.10, 4.36 and 4.27 indicate that the non-Gaussianity of the van Hove function is inherently linked to the presence of a number of fast particles, controlling higher moments of the displacement distribution (and, hence,

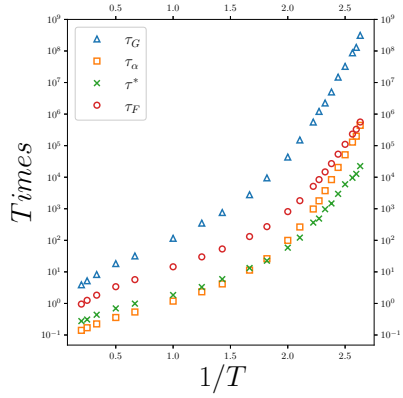

(a) 3KALJ

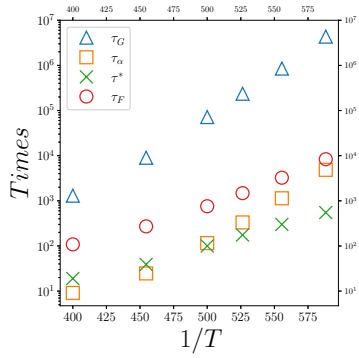

(b) 2SD

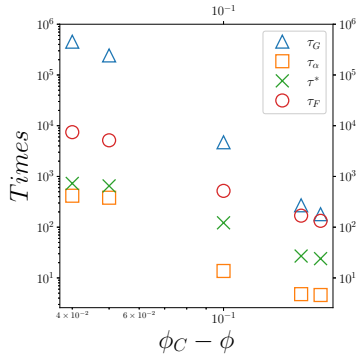

(c) 2HD

Figure 4.38. Characteristic timescales in the long-time dynamics as a function of $1/T$ for numerical systems (a,b), and as a function of $\phi_C - \phi$ for experiments (c).

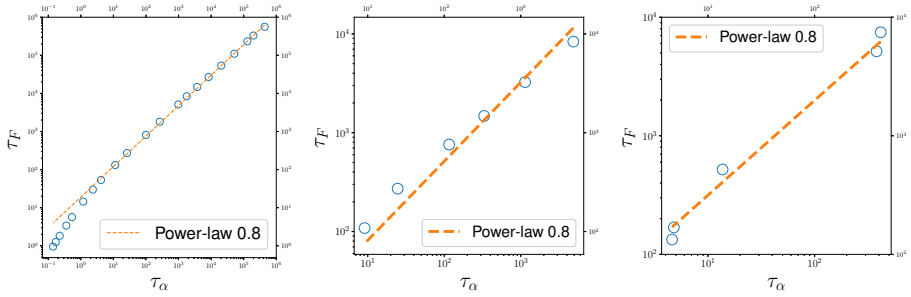

(a) 3KALJ **(b)** 2SD **(c)** 2HD

Figure 4.39. Scatter plot of τ_F VS τ_α for the three systems. Dashed lines are power-law fits.

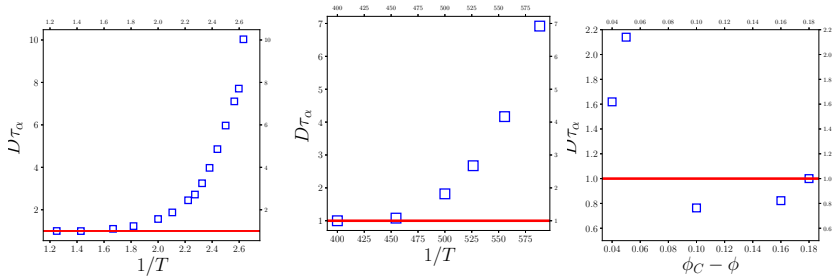

(a) 3KALJ **(b)** 2SD **(c)** 2SD

Figure 4.40. Product $D\tau_\alpha$ as a function of the thermodynamic control parameter, for the three systems. Data have been rescaled for the values at the highest temperature.

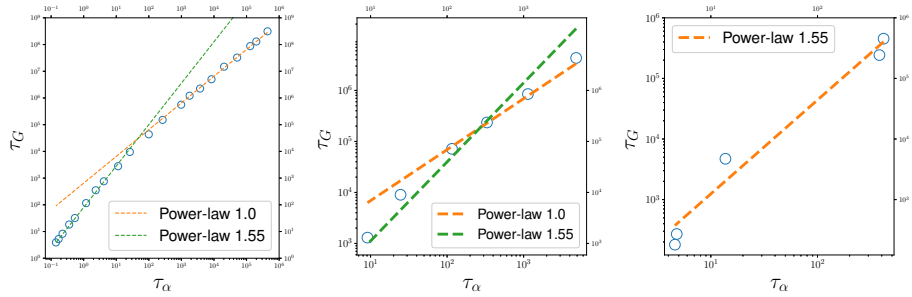

(a) 3KALJ **(b)** 2SD **(c)** 2HD

Figure 4.41. Scatter plot of τ_G VS τ_α for the three systems. Dashed lines are power-law fits.

the NGP). Thus, this picture suggests that also non-Gaussian deviations in the core of the van Hove functions are not completely erased in the long time regime and large enough to "compensate" tail deviations. We also notice that this result is at odds with some models and speculations [144, 143] on single-particle dynamics in supercooled liquids.

As already mentioned, the peak of non-Gaussian deviations is reached at τ^*, before the onset of Fickian diffusion at τ_F. Really surprisingly, Fig. 4.42 demonstrates that the two-timescales are always, and for whatever system, related through a power-law $\tau_F \propto \tau^{*1.16}$.

4.4.2 Analogy with critical phenomena

The large limit of a random walk process can be viewed as a critical phenomenon in which the displacement distribution function shows a scaling form characterized by a few relevant parameters corresponding to a "universality class" [103].

In this view, anomalous diffusion, as first suggested by Bouchaud and Georges [103], corresponds to *a* departure from mean-field behaviour [104] signalled by large-scale divergences.

It is tempting to consider Fickian non-Gaussian processes as *the first* departure from the mean field. Also in this case, scaling behaviours with critical-like exponents arise and a relation among those is likely encoded

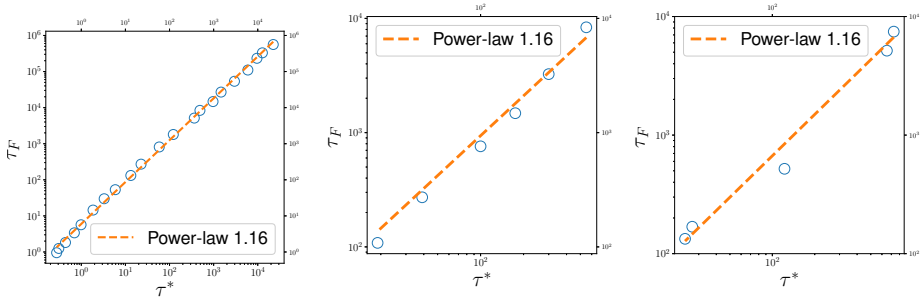

(a) 3KALJ **(b)** 2SD **(c)** 2HD

Figure 4.42. Scatter plot of τ_F VS τ^* for the three systems. Dashed lines are power-law fits.

	Scaling law	Exponents
Exponential tail decay length	$\frac{\lambda}{\xi_G} \propto (\frac{t}{\tau_G})^{\alpha}$	$\alpha \simeq 0.33 \pm 0.02$
Long-time NGP decay	$\alpha_2 \propto (\frac{t}{\tau_G})^{\delta}$	$\delta \simeq 0.55 - 1$
Fickian-Gaussian window	$\tau_G \propto \tau_F^{\gamma}$	$\gamma \simeq 1.40 - 1.80$
Relation Fickian time - maximum of NGP time	$\tau_F \propto \tau^{*\theta}$	$\theta \simeq 1.16$
Relation Fickian time - structural relaxation time	$\tau_F \propto \tau_{\alpha}^{\mu}$	$\mu \simeq 0.80$

Table 4.1. Scaling behaviours in long-time dynamics of glass-forming liquids

in the (unknown) scaling form of the displacement distribution, if any. In Table 4.1 we summarize the scaling behaviours and the exponents identified in our investigation.

CHAPTER 5

Conclusions

In this work, we investigated the connection between two major issues in soft matter, namely, glass transition, a very long-standing problem, and the recently discovered FnGD. Such a "hybrid" diffusion is, in fact, generically associated to some dynamical and/or structural heterogeneity of the environment. On the other hand, glass-forming liquids are considered the epitome of dynamical heterogeneity (which has been fairly well characterized in these systems) and, thus, represent a privileged stage to study FnGD.

Our study draws on experiments on hard-sphere colloidal suspensions and simulations of simple models of molecular liquids. In Section 4.1 we demonstrated that a FnGD regime exists in all investigated systems and spans increasingly larger time- and length-scales on approaching the glass transition. The timescales of the onset of a linearly increasing MSD (Fickian diffusion) and the recovery of Gaussian displacement distribution (Gaussian diffusion) are related by a power-law relation $\tau_G \propto \tau_F^{\gamma}$, with $\gamma > 1$, for all investigated systems. The here introduced timescale τ_G leads to the identification of novel scaling-laws for several dynamical indicators, as demonstrated throughout this work.

We further studied, in Section 4.2, the characteristic features of the

late relaxation in the reciprocal Fourier-space, when FnGD is at play in real space. Results indicate that recovery of the standard-Brownian features in Fourier space (i.e. exponentiality of the ISSF and the quadratic dependence of its relaxation time on wavelength) is exclusively related to the Gaussian scales in direct space, whereas the Fickian scales do not seem to play a major role. Moreover, on the Gaussian length-scale, Dynamic Heterogeneities are fully averaged out, and Stokes-Einstein relation is regained.

In Section 4.3, we focused on the study of the non-Gaussian deviations in the tails of the displacement distribution function. In the FnGD regime, in fact, such distribution displays exponential tails. We show that the time-dependent exponential decay lengths $l(t)$ at different temperatures all collapse onto a power-law master-curve, $l(t)/\xi_G \propto (l/\xi_G)^{\alpha}$ with $\alpha \simeq 0.33$. We also demonstrate that, in our glass-formers, this behaviour is independent from interaction potential and dimensionality [2], suggesting that this scaling is a universal hallmark of glassy dynamics, linked to some mean-field property.

Finally, in Section 4.4 we illustrated the connections between FnGD scales and other commonly adopted timescales identified in the early and late α-relaxation of glass-forming liquids, namely, the time τ^* of maximum of the NGP, and the structural relaxation time τ_α. We show that, for whatever systems, all timescales are related by the same power-law relations.

Overall, these results suggest that FnGD is the one-particle counterpart of long-time effects of Dynamical Heterogeneities. A number of "universal" scaling laws for single particle dynamics seem to emerge close to the glass transition, somehow in analogy to what occurs in critical phenomena.

We observe that all theoretical models of FnGD present in the literature are not able to capture the complete phenomenology described in this work. However, we must also notice that most of the scalings shown in this thesis are here reported for the first time. Thus, it is apparent that the validation of the here-proposed scalings largely relies on the availability of long-time data for other glass-formers, at many different values of the control parameter (temperature and concentration in our case) ruling the approach to glass transition.

In general terms, it would be interesting to examine in detail the precursors of FnGD, which build up in the subdiffusive regime. In our glass-

forming systems, strenghtening of FnGD corresponds to deepening of subdiffusion. How much such a connection between precursors in the subdiffusive time-window and FnGD is relevant on approaching glass transition is an intriguing open issue.

The idea that FnGD can be looked at as the "first" deviation from standard Brownian dynamics as a mean field representation of motion is tempting. In this direction, It seems interesting to study to what extent the Continuous Time Random Walk (which, of course, represents the simplest deviation from Einstein's model of random walk) can reproduce the rich phenomenology illustrated in this thesis. We have given some initial contributions (not reported in this thesis) in this vein [33, 51].

Finally, we stress that understanding the fundamental mechanisms of FnGD as a typical feature of glass-forming liquids, has deep practical implications. Firstly, this is demonstrated by the widespread presence of glassy materials and glass-formers in industry: optical fibers and photovoltaic cells are made of amorphous silica, most engineering plastics are in a glassy or supercooled state, liquid fabric softners are colloidal glassesk [177], metallic glasses and alloys are of great interest because of their soft magnetism [178]. Secondly, glasses provide a tunable model system to mimic the complex dynamics of a number of systems which are much more complicated from a physico-chemical point of view, such as biochemical systems or active matter. Indeed, many systems with FnGD often share also other features of glassy dynamics, such as intermittency, heterogenous dynamics or intermediate subdiffusion. Polymer adsorption on a solid surface from a bulk [78], diffusion of molecule in complex environments and cells [90, 6, 82] and chemical reactions are just a few examples of systems in which heterogeneous dynamics and the occurrence of rare events have deep consequences in the long-time behaviour before reaching an asymptotic state.

AVGVSTVS FRIDERICVS ROMANORVM IMPERATOR SEMPER

Bibliography

[1] Francesco Rusciano, Raffaele Pastore, and Francesco Greco. Fickian non-gaussian diffusion in glass-forming liquids. *Physical Review Letters*, 128(16):168001, 2022.

[2] Francesco Rusciano, Raffaele Pastore, and Francesco Greco. Is the time-evolution of the exponential tails in the fickian non-gaussian regime of glass-formers universal? *Physical Review X, under review.*

[3] A. Einstein. Über die von der molekularkinetischen theorie der wärme geforderte bewegung von in ruhenden flüssigkeiten suspendierten teilchen. *Annalen der Physik*, 322(8):549–560, 1905.

[4] Jean-Philippe Bouchaud and Antoine Georges. Anomalous diffusion in disordered media: statistical mechanisms, models and physical applications. *Physics reports*, 195(4-5):127–293, 1990.

[5] Yasmine Meroz and Igor M Sokolov. A toolbox for determining subdiffusive mechanisms. *Physics Reports*, 573:1–29, 2015.

[6] Bo Wang, Stephen M Anthony, Sung Chul Bae, and Steve Granick. Anomalous yet brownian. *Proceedings of the National Academy of Sciences*, 106(36):15160–15164, 2009.

[7] Juan Guan, Bo Wang, and Steve Granick. Even hard-sphere colloidal suspensions display fickian yet non-gaussian diffusion. *ACS nano*, 8(4):3331–3336, 2014.

[8] Jeongmin Kim, Chanjoong Kim, and Bong June Sung. Simulation study of seemingly fickian but heterogeneous dynamics of two dimensional colloids. *Physical review letters*, 110(4):047801, 2013.

[9] Kyriacos C Leptos, Jeffrey S Guasto, Jerry P Gollub, Adriana I Pesci, and Raymond E Goldstein. Dynamics of enhanced tracer diffusion in suspensions of swimming eukaryotic microorganisms. *Physical Review Letters*, 103(19):198103, 2009.

[10] Zahra Ghannad. Fickian yet non-gaussian diffusion in two-dimensional yukawa liquids. *Physical Review E*, 100(3):033211, 2019.

[11] Taejin Kwon, Ok-Seon Kwon, Hyuk-Jin Cha, and Bong June Sung. Stochastic and heterogeneous cancer cell migration: experiment and theory. *Scientific reports*, 9(1):1–13, 2019.

[12] Kai He, Firoozeh Babaye Khorasani, Scott T Retterer, Darrell K Thomas, Jacinta C Conrad, and Ramanan Krishnamoorti. Diffusive dynamics of nanoparticles in arrays of nanoposts. *ACS nano*, 7(6):5122–5130, 2013.

[13] Raphaël Jeanneret, Dmitri O Pushkin, Vasily Kantsler, and Marco Polin. Entrainment dominates the interaction of microalgae with micron-sized objects. *Nature communications*, 7(1):1–7, 2016.

[14] Fabio Giavazzi, Chiara Malinverno, Giorgio Scita, and Roberto Cerbino. Tracking-free determination of single-cell displacements and division rates in confluent monolayers. *Frontiers in Physics*, 6:120, 2018.

[15] Serge Mora and Yves Pomeau. Brownian diffusion in a dilute field of traps is fickean but non-gaussian. *Physical Review E*, 98(4):040101, 2018.

[16] Mykyta V Chubynsky and Gary W Slater. Diffusing diffusivity: a model for anomalous, yet brownian, diffusion. *Physical Review Letters*, 113(9):098302, 2014.

[17] Aleksei V Chechkin, Flavio Seno, Ralf Metzler, and Igor M Sokolov. Brownian yet non-gaussian diffusion: from superstatistics to subordination of diffusing diffusivities. *Physical Review X*, 7(2):021002, 2017.

[18] Eli Barkai and Stanislav Burov. Packets of diffusing particles exhibit universal exponential tails. *Physical review letters*, 124(6):060603, 2020.

[19] Vittoria Sposini, Aleksei V Chechkin, Flavio Seno, Gianni Pagnini, and Ralf Metzler. Random diffusivity from stochastic equations: comparison of two models for brownian yet non-gaussian diffusion. *New Journal of Physics*, 20(4):043044, 2018.

[20] Bo Wang, James Kuo, Sung Chul Bae, and Steve Granick. When brownian diffusion is not gaussian. *Nature materials*, 11(6):481–485, 2012.

[21] Ralf Metzler. Gaussianity fair: the riddle of anomalous yet non-gaussian diffusion. *Biophysical journal*, 112(3):413, 2017.

[22] Pinaki Chaudhuri, Ludovic Berthier, and Walter Kob. Universal nature of particle displacements close to glass and jamming transitions. *Physical review letters*, 99(6):060604, 2007.

[23] Raffaele Pastore, Antonio Coniglio, and Massimo Pica Ciamarra. From cage-jump motion to macroscopic diffusion in supercooled liquids. *Soft Matter*, 10(31):5724–5728, 2014.

[24] Eric R Weeks, John C Crocker, Andrew C Levitt, Andrew Schofield, and David A Weitz. Three-dimensional direct imaging of structural relaxation near the colloidal glass transition. *Science*, 287(5453):627–631, 2000.

[25] Ludovic Berthier, Giulio Biroli, Jean-Philippe Bouchaud, and Robert L Jack. Overview of different characterizations of dynamic heterogeneity. *Dynamical Heterogeneities in Glasses, Colloids, and Granular Media*, 150:68, 2011.

[26] N Lačević, Francis W Starr, TB Schrøder, and SC Glotzer. Spatially heterogeneous dynamics investigated via a time-dependent four-point density correlation function. *The Journal of chemical physics*, 119(14):7372–7387, 2003.

[27] Rajsekhar Das, Chandan Dasgupta, and Smarajit Karmakar. Time scales of fickian diffusion and the lifetime of dynamic heterogeneity. *Frontiers in Physics*, 8:210, 2020.

[28] Raffaele Pastore, Giuseppe Pesce, Antonio Sasso, and Massimo Pica Ciamarra. Many facets of intermittent dynamics in colloidal and molecular glasses. *Colloids and Surfaces A: Physicochemical and Engineering Aspects*, 532:87–96, 2017.

[29] Wolfgang Götze. *Complex dynamics of glass-forming liquids: A mode-coupling theory*, volume 143. OUP Oxford, 2008.

[30] Raphaël Candelier, Asaph Widmer-Cooper, Jonathan K Kummerfeld, Olivier Dauchot, Giulio Biroli, Peter Harrowell, and David R Reichman. Spatiotemporal hierarchy of relaxation events, dynamical heterogeneities, and structural reorganization in a supercooled liquid. *Physical review letters*, 105(13):135702, 2010.

[31] Aaron S Keys, Lester O Hedges, Juan P Garrahan, Sharon C Glotzer, and David Chandler. Excitations are localized and relaxation is hierarchical in glass-forming liquids [phys. rev. x 1, 021013 (2011)]. *Physical Review X*, 1(2):029901, 2011.

[32] Tomoshige Miyaguchi, Takuma Akimoto, and Eiji Yamamoto. Langevin equation with fluctuating diffusivity: A two-state model. *Physical Review E*, 94(1):012109, 2016.

[33] Giuseppe Porpora, Francesco Rusciano, Raffaele Pastore, and Francesco Greco. Comparing microscopic and macroscopic dynamics in a paradigmatic model of glass-forming molecular liquid. *International Journal of Molecular Sciences*, 23(7):3556, 2022.

[34] Salomon Bochner. *Harmonic analysis and the theory of probability*. Courier Corporation, 2005.

[35] Andrea Cavagna. Supercooled liquids for pedestrians. *Physics Reports*, 476(4-6):51–124, 2009.

[36] Pablo G Debenedetti and Frank H Stillinger. Supercooled liquids and the glass transition. *Nature*, 410(6825):259, 2001.

[37] Walter Kob and Hans C Andersen. Testing mode-coupling theory for a supercooled binary lennard-jones mixture i: The van hove correlation function. *Physical Review E*, 51(5):4626, 1995.

[38] C Patrick Royall and Stephen R Williams. The role of local structure in dynamical arrest. *Physics Reports*, 560:1–75, 2015.

[39] Raffaele Pastore, Massimo Pica Ciamarra, and Antonio Coniglio. Pacman percolation and the glass transition. *Fractals*, 21(03n04):1350021, 2013.

[40] Michael I Ojovan and Dmitri V Louzguine-Luzgin. Revealing structural changes at glass transition via radial distribution functions. *The Journal of Physical Chemistry B*, 124(15):3186–3194, 2020.

[41] Tina Hecksher, Albena I Nielsen, Niels Boye Olsen, and Jeppe C Dyre. Little evidence for dynamic divergences in ultraviscous molecular liquids. *Nature Physics*, 4(9):737–741, 2008.

[42] Massimo Pica Ciamarra, Raffaele Pastore, and Antonio Coniglio. Particle jumps in structural glasses. *Soft matter*, 12(2):358–366, 2016.

[43] Liesbeth MC Janssen. Mode-coupling theory of the glass transition: A primer. *Frontiers in Physics*, 6:97, 2018.

[44] R Yamamoto and A Onuki. Heterogeneous diffusion in highly supercooled liquids. *Phys. Rev. Lett.*, 81(22):4915–4918, 1998.

[45] Zane Shi, Pablo G Debenedetti, and Frank H Stillinger. Relaxation processes in liquids: Variations on a theme by Stokes and Einstein. *The Journal of Chemical Physics.*, 138(12):12A526, 2013.

[46] Shiladitya Sengupta, Smarajit Karmakar, Chandan Dasgupta, and Srikanth Sastry. Breakdown of the Stokes-Einstein relation in two, three, and four dimensions. *The Journal of Chemical Physics.*, 138(12):12A548, March 2013.

[47] Jennifer A Hodgdon and Frank H Stillinger. Stokes-einstein violation in glass-forming liquids. *Physical Review E*, 48(1):207, 1993.

[48] Gilles Tarjus and Daniel Kivelson. Breakdown of the stokes–einstein relation in supercooled liquids. *The Journal of Chemical Physics*, 103(8):3071–3073, 1995.

[49] Patrick Charbonneau, Yuliang Jin, Giorgio Parisi, and Francesco Zamponi. Hopping and the stokes–einstein relation breakdown in simple glass formers. *Proceedings of the National Academy of Sciences*, 111(42):15025–15030, 2014.

[50] Chandan K Mishra and Rajesh Ganapathy. Shape of dynamical heterogeneities and fractional stokes-einstein and stokes-einstein-debye relations in quasi-two-dimensional suspensions of colloidal ellipsoids. *Physical review letters*, 114(19):198302, 2015.

[51] Raffaele Pastore, Takuma Kikutsuji, Francesco Rusciano, Nobuyuki Matubayasi, Kang Kim, and Francesco Greco. Breakdown of the stokes–einstein relation in supercooled liquids: A cage-jump perspective. *The Journal of Chemical Physics*, 155(11):114503, 2021.

[52] Mark D Ediger. Spatially heterogeneous dynamics in supercooled liquids. *Annual review of physical chemistry*, 51(1):99–128, 2000.

[53] Luca Cipelletti and Laurence Ramos. Slow dynamics in glassy soft matter. *Journal of Physics: Condensed Matter*, 17(6):R253, 2005.

[54] Raffaele Pastore, Giuseppe Pesce, and Marco Caggioni. Differential variance analysis: a direct method to quantify and visualize dynamic heterogeneities. *Scientific reports*, 7(1):1–9, 2017.

[55] Marcus T Cicerone and Mark D Ediger. Enhanced translation of probe molecules in supercooled o-terphenyl: Signature of spatially heterogeneous dynamics? *The Journal of Chemical Physics*, 104(18):7210–7218, 1996.

[56] Raffaele Pastore, Marco Caggioni, Domenico Larobina, Luigi Santamaria Amato, and Francesco Greco. Concentrated suspensions of brownian beads in water: dynamic heterogeneities through a simple experimental technique. *Science China Physics, Mechanics & Astronomy*, 62(10):1–12, 2019.

[57] Jurgen Horbach, Walter Kob, and Kurt Binder. Molecular dynamics simulation of the dynamics of supercooled silica. *Philosophical magazine B*, 77(2):297–303, 1998.

[58] A. Einstein. Über die von der molekularkinetischen theorie der wärme geforderte bewegung von in ruhenden flüssigkeiten suspendierten teilchen. *Annalen der Physik*, 322(8):549–560, 1905.

[59] William Sutherland. Lxxv. a dynamical theory of diffusion for non-electrolytes and the molecular mass of albumin. *The London, Edinburgh, and Dublin Philosophical Magazine and Journal of Science*, 9(54):781–785, 1905.

[60] Karl Pearson. The problem of the random walk. *Nature*, 72(1867):342–342, 1905.

[61] Paul Langevin. Sur la théorie du mouvement brownien. *Compt. Rendus*, 146:530–533, 1908.

[62] Raffaele Pastore, Antonio Ciarlo, Giuseppe Pesce, Francesco Greco, and Antonio Sasso. Rapid fickian yet non-gaussian diffusion after subdiffusion. *Physical Review Letters*, 126(15):158003, 2021.

[63] Mpumelelo Matse, Mykyta V Chubynsky, and John Bechhoefer. Test of the diffusing-diffusivity mechanism using near-wall colloidal dynamics. *Physical Review E*, 96(4):042604, 2017.

[64] Matteo Brizioli, Tatjana Sentjabrskaja, Stefan U Egelhaaf, Marco Laurati, Roberto Cerbino, and Fabio Giavazzi. Reciprocal space study of brownian yet non-gaussian diffusion of small tracers in a hard-sphere glass. *Frontiers in Physics*, page 408, 2022.

[65] José M Miotto, Simone Pigolotti, Aleksei V Chechkin, and Sándalo Roldán-Vargas. Length scales in brownian yet non-gaussian dynamics. *Physical Review X*, 11(3):031002, 2021.

[66] Bhanu Prasad Bhowmik, Indrajit Tah, and Smarajit Karmakar. Non-gaussianity of the van hove function and dynamic-heterogeneity length scale. *Physical Review E*, 98(2):022122, 2018.

[67] Simona Hapca, John W Crawford, and Iain M Young. Anomalous diffusion of heterogeneous populations characterized by normal diffusion at the individual level. *Journal of the Royal Society Interface*, 6(30):111–122, 2008.

[68] Hüseyin Kurtuldu, Jeffrey S Guasto, Karl A Johnson, and Jerry P Gollub. Enhancement of biomixing by swimming algal cells in two-dimensional films. *Proceedings of the National Academy of Sciences*, 108(26):10391–10395, 2011.

[69] Wei He, Hao Song, Yun Su, Ling Geng, Bruce J Ackerson, HB Peng, and Penger Tong. Dynamic heterogeneity and non-gaussian statistics for acetylcholine receptors on live cell membrane. *Nature communications*, 7:11701, 2016.

[70] Yang Liu, Xu Zheng, Dongshi Guan, Xikai Jiang, and Guoqing Hu. Heterogeneous nanostructures cause anomalous diffusion in lipid monolayers. *ACS nano*, 16(10):16054–16066, 2022.

[71] Chundong Xue, Xu Zheng, Kaikai Chen, Yu Tian, and Guoqing Hu. Probing non-gaussianity in confined diffusion of nanoparticles. *The journal of physical chemistry letters*, 7(3):514–519, 2016.

[72] Daniel S Banks, Charmaine Tressler, Robert D Peters, Felix Höfling, and Cécile Fradin. Characterizing anomalous diffusion in crowded polymer solutions and gels over five decades in time with variable-lengthscale fluorescence correlation spectroscopy. *Soft Matter*, 12(18):4190–4203, 2016.

[73] Sukanya Bhattacharya, Dharmendar Kumar Sharma, Saumya Saurabh, Suman De, Anirban Sain, Amitabha Nandi, and Arindam Chowdhury. Plasticization of poly (vinylpyrrolidone) thin films under ambient humidity: Insight from single-molecule tracer diffusion dynamics. *The Journal of Physical Chemistry B*, 117(25):7771–7782, 2013.

[74] Indrani Chakraborty and Yael Roichman. Disorder-induced fickian, yet non-gaussian diffusion in heterogeneous media. *Physical Review Research*, 2(2):022020, 2020.

[75] Fang Zhou, Huaguang Wang, and Zexin Zhang. Diffusion of anisotropic colloids in periodic arrays of obstacles. *Langmuir*, 36(40):11866–11872, 2020.

[76] Partho S Goohpattader and Manoj K Chaudhury. Diffusive motion with nonlinear friction: apparently brownian. *The Journal of chemical physics*, 133(2):024702, 2010.

[77] Changqian Yu, Juan Guan, Kejia Chen, Sung Chul Bae, and Steve Granick. Single-molecule observation of long jumps in polymer adsorption. *ACS nano*, 7(11):9735–9742, 2013.

[78] Michael J Skaug, Joshua Mabry, and Daniel K Schwartz. Intermittent molecular hopping at the solid-liquid interface. *Physical review letters*, 110(25):256101, 2013.

[79] A Christian Silva, Richard E Prange, and Victor M Yakovenko. Exponential distribution of financial returns at mesoscopic time lags: a new stylized fact. *Physica A: Statistical Mechanics and its Applications*, 344(1-2):227–235, 2004.

[80] Dmitri O Pushkin and Julia M Yeomans. Fluid mixing by curved trajectories of microswimmers. *Physical review letters*, 111(18):188101, 2013.

[81] Jiwei Wang. Anomalous diffusion of active brownian particles in crystalline phases. In *IOP Conference Series: Earth and Environmental Science*, volume 237, page 052005. IOP Publishing, 2019.

[82] Carlo Manzo, Juan A Torreno-Pina, Pietro Massignan, Gerald J Lapeyre Jr, Maciej Lewenstein, and Maria F Garcia Parajo. Weak ergodicity breaking of receptor motion in living cells stemming from random diffusivity. *Physical Review X*, 5(1):011021, 2015.

[83] Alice L Thorneywork, Dirk GAL Aarts, Jürgen Horbach, and Roel PA Dullens. On the gaussian approximation in colloidal hard sphere fluids. *Soft Matter*, 12(18):4129–4134, 2016.

[84] Maiko Kofu, Antonio Faraone, Madhusudan Tyagi, Michihiro Nagao, and Osamu Yamamuro. Two inherent crossovers of the diffusion process in glass-forming liquids. *Physical Review E*, 98(4):042601, 2018.

[85] Raffaele Pastore, Antonio Ciarlo, Giuseppe Pesce, Antonio Sasso, and Francesco Greco. A model-system of fickian yet non-gaussian diffusion: light patterns in place of complex matter. *Soft Matter*, 18(2):351–364, 2022.

[86] Jack Deodato C Jacob, Kai He, Scott T Retterer, Ramanan Krishnamoorti, and Jacinta C Conrad. Diffusive dynamics of nanoparticles in ultra-confined media. *Soft Matter*, 11(38):7515–7524, 2015.

[87] Sayantan Acharya, Ujjwal Kumar Nandi, and Sarika Maitra Bhattacharyya. Fickian yet non-gaussian behaviour: A dominant role of the intermittent dynamics. *The Journal of chemical physics*, 146(13):134504, 2017.

[88] Heejin Jeon, Hyun Woo Cho, Jeongmin Kim, and Bong June Sung. Non-gaussian rotational diffusion in heterogeneous media. *Physical Review E*, 90(4):042105, 2014.

[89] Alejandro Cuetos, Neftalí Morillo, and Alessandro Patti. Fickian yet non-gaussian diffusion is not ubiquitous in soft matter. *Physical Review E*, 98(4):042129, 2018.

[90] Gyemin Kwon, Bong June Sung, and Arun Yethiraj. Dynamics in crowded environments: is non-gaussian brownian diffusion normal? *The Journal of Physical Chemistry B*, 118(28):8128–8134, 2014.

[91] Suman Dutta and J Chakrabarti. Anomalous dynamical responses in a driven system. *EPL (Europhysics Letters)*, 116(3):38001, 2016.

[92] Rajsekhar Das, Chandan Dasgupta, and Smarajit Karmakar. Time scales of fickian diffusion and the lifetime of dynamic heterogeneity. *Frontiers in Physics*, 8:210, 2020.

[93] Zijian Zheng, Fanzhu Li, Jun Liu, Raffaele Pastore, Guido Raos, Youping Wu, and Liqun Zhang. Effects of chemically heterogeneous nanoparticles on polymer dynamics: insights from molecular dynamics simulations. *Soft matter*, 14(7):1219–1226, 2018.

[94] Eiji Yamamoto, Takuma Akimoto, Antreas C Kalli, Kenji Yasuoka, and Mark SP Sansom. Dynamic interactions between a membrane binding protein and lipids induce fluctuating diffusivity. *Science advances*, 3(1):e1601871, 2017.

[95] Jianjin Wang, Yong Zhang, and Hong Zhao. Non-gaussian normal diffusion induced by delocalization. *Physical Review E*, 93(3):032144, 2016.

[96] K Białas, J Łuczka, Peter Hänggi, and J Spiechowicz. Colossal brownian yet non-gaussian diffusion induced by nonequilibrium noise. *Physical Review E*, 102(4):042121, 2020.

[97] Karol Białas and Jakub Spiechowicz. Colossal brownian yet non-gaussian diffusion in a periodic potential: Impact of nonequilibrium noise amplitude statistics. *Chaos: An Interdisciplinary Journal of Nonlinear Science*, 31(12):123107, 2021.

[98] Govind Paneru, Jin Tae Park, and Hyuk Kyu Pak. Transport and diffusion enhancement in experimentally realized non-gaussian correlated ratchets. *The Journal of Physical Chemistry Letters*, 12(45):11078–11084, 2021.

[99] Gennaro Tucci, Andrea Gambassi, Shamik Gupta, and Édgar Roldán. Controlling particle currents with evaporation and resetting from an interval. *Physical Review Research*, 2(4):043138, 2020.

[100] Leon B Lucy. An iterative technique for the rectification of observed distributions. *The astronomical journal*, 79:745, 1974.

[101] Jagannathan T Kalathi, Umi Yamamoto, Kenneth S Schweizer, Gary S Grest, and Sanat K Kumar. Nanoparticle diffusion in polymer nanocomposites. *Physical review letters*, 112(10):108301, 2014.

[102] Raffaele Pastore, Antonio Coniglio, and Massimo Pica Ciamarra. Dynamic phase coexistence in glass–forming liquids. *Scientific reports*, 5:11770, 2015.

[103] Jean-Philippe Bouchaud and Antoine Georges. Anomalous diffusion in disordered media: statistical mechanisms, models and physical applications. *Physics reports*, 195(4-5):127–293, 1990.

[104] BV Gnedenko, AN Kolmogorov, BV Gnedenko, and AN Kolmogorov. Limit distributions for sums of independent. *Am. J. Math*, 105, 1954.

[105] W Götze. The essentials of the mode-coupling theory for glassy dynamics. *Condensed Matter Physics*, 1998.

[106] Pinaki Chaudhuri, Ludovic Berthier, and Walter Kob. Universal nature of particle displacements close to glass and jamming transitions. *Physical review letters*, 99(6):060604, 2007.

[107] T Odagaki and Y Hiwatari. Gaussian–to–non-gaussian transition in supercooled fluids. *Physical Review A*, 43(2):1103, 1991.

[108] Takashi Odagaki. Non-ergodicity and non-gaussianity in vitrification process. *Progress of Theoretical Physics Supplement*, 126:9–12, 1997.

[109] T Odagaki. Glass transition singularities. *Physical review letters*, 75(20):3701, 1995.

[110] T Odagaki and Y Hiwatari. Stochastic model for the glass transition of simple classical liquids. *Physical Review A*, 41(2):929, 1990.

[111] Adolf Fick. Ueber diffusion. *Annalen der Physik*, 170(1):59–86, 1855.

[112] Nicolaas Godfried Van Kampen. *Stochastic processes in physics and chemistry*, volume 1. Elsevier, 1992.

[113] Crispin Gardiner. *Stochastic methods*, volume 4. Springer Berlin, 2009.

[114] MM Hurley and Peter Harrowell. Non-gaussian behavior and the dynamical complexity of particle motion in a dense two-dimensional liquid. *The Journal of chemical physics*, 105(23):10521–10526, 1996.

[115] Takashi Uneyama, Tomoshige Miyaguchi, and Takuma Akimoto. Fluctuation analysis of time-averaged mean-square displacement for the langevin equation with time-dependent and fluctuating diffusivity. *Physical Review E*, 92(3):032140, 2015.

[116] Rohit Jain and Kizhakeyil L Sebastian. Diffusion in a crowded, rearranging environment. *The Journal of Physical Chemistry B*, 120(16):3988–3992, 2016.

[117] Eli Barkai and Stanislav Burov. Packets of diffusing particles exhibit universal exponential tails. *Physical review letters*, 124(6):060603, 2020.

[118] Christian Beck and Ezechiel GD Cohen. Superstatistics. *Physica A: Statistical mechanics and its applications*, 322:267–275, 2003.

[119] LC Evans. Partial differential equations (1998) graduate studies in mathematics, 19. *Amer. Math. Soc., Providence, Rhode*.

[120] SH Strogatz. Nonlinear dynamics and chaos: With applications to physics, biology, chemistry and engineering (cambridge, ma: Westview). 1994.

[121] Takuma Akimoto and Eiji Yamamoto. Distributional behaviors of time-averaged observables in the langevin equation with fluctuating diffusivity: Normal diffusion but anomalous fluctuations. *Physical Review E*, 93(6):062109, 2016.

[122] Tomoshige Miyaguchi, Takashi Uneyama, and Takuma Akimoto. Brownian motion with alternately fluctuating diffusivity: Stretched-exponential and power-law relaxation. *Physical Review E*, 100(1):012116, 2019.

[123] Matthias Fuchs, Wolfgang Götze, and Matthias R Mayr. Asymptotic laws for tagged-particle motion in glassy systems. *Physical Review E*, 58(3):3384, 1998.

[124] J Helfferich, J Brisch, H Meyer, O Benzerara, F Ziebert, J Farago, and J Baschnagel. Continuous-time random-walk approach to supercooled liquids: Self-part of the van hove function and related quantities. *The European Physical Journal E*, 41(6):71, 2018.

[125] Rohit Jain and KL Sebastian. Lévy flight with absorption: A model for diffusing diffusivity with long tails. *Physical Review E*, 95(3):032135, 2017.

[126] Rohit Jain and KL Sebastian. Diffusing diffusivity: Rotational diffusion in two and three dimensions. *The Journal of chemical physics*, 146(21):214102, 2017.

[127] Rohit Jain and KL Sebastian. Diffusing diffusivity fractional brownian oscillator model for subdiffusion and its solution. *Physical Review E*, 98(5):052138, 2018.

[128] Neha Tyagi and Binny J Cherayil. Non-gaussian brownian diffusion in dynamically disordered thermal environments. *The Journal of Physical Chemistry B*, 121(29):7204–7209, 2017.

[129] Neha Tyagi and Binny J Cherayil. Brownian motion under dynamic disorder: effects of memory on the decay of the non-gaussianity parameter. *Journal of Statistical Mechanics: Theory and Experiment*, 2018(3):033211, 2018.

[130] J Helfferich, J Brisch, H Meyer, O Benzerara, F Ziebert, J Farago, and J Baschnagel. Continuous-time random-walk approach to supercooled liquids: Self-part of the van hove function and related quantities. *The European Physical Journal E*, 41:1–14, 2018.

[131] J Helfferich, F Ziebert, S Frey, H Meyer, J Farago, A Blumen, and J Baschnagel. Continuous-time random-walk approach to supercooled liquids. ii. mean-square displacements in polymer melts. *Physical Review E*, 89(4):042604, 2014.

[132] Elliott W Montroll and George H Weiss. Random walks on lattices. ii. *Journal of Mathematical Physics*, 6(2):167–181, 1965.

[133] Wanli Wang, Eli Barkai, and Stanislav Burov. Large deviations for continuous time random walks. *Entropy*, 22(6):697, 2020.

[134] Raymond E Goldstein. Green algae as model organisms for biological fluid dynamics. *Annual review of fluid mechanics*, 47:343–375, 2015.

[135] Francisco J Sevilla. Diffusion of active chiral particles. *Physical Review E*, 94(6):062120, 2016.

[136] Sidney Goldstein. On diffusion by discontinuous movements, and on the telegraph equation. *The Quarterly Journal of Mechanics and Applied Mathematics*, 4(2):129–156, 1951.

[137] RC Bourret. Turbulent diffusion in two and three dimensions by the random-walk model with memory. *Canadian Journal of Physics*, 39(1):133–140, 1961.

[138] R Bourret. An hypothesis concerning turbulent diffusion. *Canadian Journal of Physics*, 38(5):665–676, 1960.

[139] Sanggeun Song, Seong Jun Park, Minjung Kim, Jun Soo Kim, Bong June Sung, Sangyoub Lee, Ji-Hyun Kim, and Jaeyoung Sung. Transport dynamics of complex fluids. *Proceedings of the National Academy of Sciences*, 116(26):12733–12742, 2019.

[140] Pinaki Chaudhuri, Yongxiang Gao, Ludovic Berthier, Maria Kilfoil, and Walter Kob. A random walk description of the heterogeneous glassy dynamics of attracting colloids. *Journal of Physics: Condensed Matter*, 20(24):244126, 2008.

[141] Grzegorz Szamel and Elijah Flenner. Time scale for the onset of fickian diffusion in supercooled liquids. *Physical Review E*, 73(1):011504, 2006.

[142] Francesco Rusciano, Raffaele Pastore, and Francesco Greco. Supercooled liquids are fickian yet non-gaussian. *arXiv preprint arXiv:2212.09679*, 2022.

[143] Ludovic Berthier, David Chandler, and Juan P Garrahan. Length scale for the onset of fickian diffusion in supercooled liquids. *Europhysics Letters*, 69(3):320, 2004.

[144] Ludovic Berthier, Elijah Flenner, and Grzegorz Szamel. Are supercooled liquids fickian yet non gaussian? *arXiv preprint arXiv:2210.07119*, 2022.

[145] Benoit Charbonneau, Patrick Charbonneau, Yuliang Jin, Giorgio Parisi, and Francesco Zamponi. Dimensional dependence of the stokes-einstein relation and its violation. *The Journal of chemical physics*, 139(16):164502, 2013.

[146] George David Joseph Phillies. In complex fluids the gaussian diffusion approximation is generally invalid. *Soft matter*, 11(3):580–586, 2015.

[147] John C Crocker and David G Grier. Methods of digital video microscopy for colloidal studies. *Journal of colloid and interface science*, 179(1):298–310, 1996.

[148] Eric Jones, Travis Oliphant, and Pearu Peterson. {SciPy}: open source scientific tools for {Python}. *http://www.scipy.org*, 2014.

[149] Fernando Pérez and Brian E Granger. Ipython: a system for interactive scientific computing. *Computing in Science & Engineering*, 9(3), 2007.

[150] Steve Plimpton. Fast parallel algorithms for short-range molecular dynamics. *Journal of computational physics*, 117(1):1–19, 1995.

[151] Wataru Shinoda, Motoyuki Shiga, and Masuhiro Mikami. Rapid estimation of elastic constants by molecular dynamics simulation under constant stress. *Physical Review B*, 69(13):134103, 2004.

[152] Søren Toxvaerd and Jeppe C Dyre. Communication: Shifted forces in molecular dynamics. *The Journal of Chemical Physics*, 134(8):081102, 2011.

[153] Thomas B Schrøder and Jeppe C Dyre. Solid-like mean-square displacement in glass-forming liquids. *The Journal of Chemical Physics*, 152(14):141101, 2020.

[154] Walter Kob and Hans C Andersen. Scaling behavior in the β-relaxation regime of a supercooled lennard-jones mixture. *Physical review letters*, 73(10):1376, 1994.

[155] Ulf R Pedersen, Thomas B Schrøder, and Jeppe C Dyre. Phase diagram of kob-andersen-type binary lennard-jones mixtures. *Physical review letters*, 120(16):165501, 2018.

[156] Michael P Allen and Dominic J Tildesley. *Computer simulation of liquids*. Oxford university press, 2017.

[157] Trond S Ingebrigtsen, Jeppe C Dyre, Thomas B Schrøder, and C Patrick Royall. Crystallization instability in glass-forming mixtures. *Physical Review X*, 9(3):031016, 2019.

[158] Masao Doi, Samuel Frederick Edwards, and Samuel Frederick Edwards. *The theory of polymer dynamics*, volume 73. oxford university press, 1988.

[159] Jeppe C Dyre and Thomas B Schrøder. Universality of ac conduction in disordered solids. *Reviews of Modern Physics*, 72(3):873, 2000.

[160] M Schmiedeberg, J Roth, and H Stark. Brownian particles in random and quasicrystalline potentials: How they approach the equilibrium. *The European Physical Journal E*, 24(4):367–377, 2007.

[161] Matthias Fuchs, Wolfgang Götze, and Matthias R Mayr. Asymptotic laws for tagged-particle motion in glassy systems. *Physical Review E*, 58(3):3384, 1998.

[162] MM Hurley and Peter Harrowell. Non-gaussian behavior and the dynamical complexity of particle motion in a dense two-dimensional liquid. *The Journal of chemical physics*, 105(23):10521–10526, 1996.

[163] Carsten FE Schroer and Andreas Heuer. Anomalous diffusion of driven particles in supercooled liquids. *Physical review letters*, 110(6):067801, 2013.

[164] T Odagaki, Jun Matsui, and Y Hiwatari. Trapping diffusion model for glass transition and slow dynamics in supercooled liquids. *Physica A: Statistical Mechanics and its Applications*, 204(1-4):464–481, 1994.

[165] Elijah Flenner and Grzegorz Szamel. Relaxation in a glassy binary mixture: Comparison of the mode-coupling theory to a brownian dynamics simulation. *Physical Review E*, 72(3):031508, 2005.

[166] David R Reichman and Patrick Charbonneau. Mode-coupling theory. *Journal of Statistical Mechanics: Theory and Experiment*, 2005(05):P05013, 2005.

[167] Ralf Brüning, Denis A St-Onge, Steve Patterson, and Walter Kob. Glass transitions in one-, two-, three-, and four-dimensional binary lennard-jones systems. *Journal of Physics: Condensed Matter*, 21(3):035117, 2008.

[168] Giuseppe Porpora, Francesco Rusciano, Raffaele Pastore, and Francesco Greco. Comparing microscopic and macroscopic dynamics in a paradigmatic model of glass-forming molecular liquid. *International Journal of Molecular Sciences*, 23(7):3556, 2022.

[169] Elijah Flenner and Grzegorz Szamel. Fundamental differences between glassy dynamics in two and three dimensions. *Nature communications*, 6(1):1–6, 2015.

[170] Hayato Shiba, Yasunori Yamada, Takeshi Kawasaki, and Kang Kim. Unveiling dimensionality dependence of glassy dynamics: 2d infinite fluctuation eclipses inherent structural relaxation. *Physical review letters*, 117(24):245701, 2016.

[171] Bernd Illing, Sebastian Fritschi, Herbert Kaiser, Christian L Klix, Georg Maret, and Peter Keim. Mermin–wagner fluctuations in 2d amorphous solids. *Proceedings of the National Academy of Sciences*, 114(8):1856–1861, 2017.

[172] Skanda Vivek, Colm P Kelleher, Paul M Chaikin, and Eric R Weeks. Long-wavelength fluctuations and the glass transition in two dimensions and three dimensions. *Proceedings of the National Academy of Sciences*, 114(8):1850–1855, 2017.

[173] Gilles Tarjus. Glass transitions may be similar in two and three dimensions, after all. *Proceedings of the National Academy of Sciences*, 114(10):2440–2442, 2017.

[174] Pallabi Das and Srikanth Sastry. Crossover in dynamics in the kob-andersen binary mixture glass-forming liquid. *Journal of Non-Crystalline Solids: X*, 14:100098, 2022.

[175] Daniele Coslovich, Misaki Ozawa, and Walter Kob. Dynamic and thermodynamic crossover scenarios in the kob-andersen mixture: Insights from multi-cpu and multi-gpu simulations. *The European Physical Journal E*, 41(5):1–11, 2018.

[176] Ludovic Berthier. Time and length scales in supercooled liquids. *Physical Review E*, 69(2):020201, 2004.

[177] G Porpora, F Rusciano, V Guida, F Greco, and R Pastore. Understanding charged vesicle suspensions as wigner glasses: dynamical aspects. *Journal of Physics: Condensed Matter*, 33(10):104001, 2020.

[178] A Lindsay Greer. Metallic glasses. *Science*, 267(5206):1947–1953, 1995.

AVGVSTVS FRIDERICVS ROMANORVM IMPERATOR SEMPER

Author's Publications

[1] Rusciano, F., Pastore, R., and Greco, F. (2022). *Fickian non-Gaussian diffusion in glass-forming liquids.* Physical Review Letters, 128(16), 168001.

[142] Rusciano, F., Pastore, R., and Greco, F. (2022). *Supercooled liquids are Fickian yet non-Gaussian.* arXiv preprint arXiv:2212.09679.

[2] Rusciano, F., Pastore, R., and Greco, F. *Is the time-evolution of the exponential tails in the Fickian non-Gaussian regime of glass-formers universal?.* Under review.

[33] Porpora, G., Rusciano, F., Pastore, R., and Greco, F. (2022). *Comparing microscopic and macroscopic dynamics in a paradigmatic model of glass-forming molecular liquid.* International Journal of Molecular Sciences, 23(7), 3556.

[51] Pastore, R., Kikutsuji, T., Rusciano, F., Matubayasi, N., Kim, K., and Greco, F. (2021). *Breakdown of the Stokes–Einstein relation in supercooled liquids: A cage-jump perspective.* The Journal of Chemical Physics, 155(11), 114503.

[177] Porpora, G., Rusciano, F., Guida, V., Greco, F., and Pastore, R. (2020). *Understanding charged vesicle suspensions as Wigner glasses: dynamical aspects.* Journal of Physics: Condensed Matter, 33(10), 104001.

AVGVSTVS FRIDERICVS ROMANORVM IMPERATOR SEMPER